POLITECNICO DI TORINO

Corso di Laurea Magistrale in Ingegneria Aerospaziale

Numerical Investigation of the impact of Geometric Variations on Hydrogen Micromix Combustion Performance

AUTHOR:

Francesco Carbonara

SUPERVISORS:

Prof. D. Pastrone (PdT)

Dr. V. Sethi (CU)

Dr. D. Abbott (CU)

Dr. P. Gauthier (CU)

Dr. X. Sun (CU)

Academic Year 2019-2020

Abstract

Over the years, pollution has become a main concern and more stringent emissions legislations have been introduced to reduce the influence of aviation on environmental and human health. Despite the development of numerous low emissions combustion technologies, it is necessary to switch to more sustainable fuels to replace fossil fuels to meet long term emissions targets. Liquid hydrogen has been identified as one of the most promising alternative fuels. However, its introduction in civil aviation has been slowed down by issues of different nature. Due to its properties, in particular high flame speed and stoichiometric flame temperature, a significant redesign of the combustion system is required. Cranfield University, as partner of ENABLEH2 project, is directly involved in the development of a micromix combustion system for aero engines. This novel technology allows to burn hydrogen in numerous miniaturised diffusion-based flames and enhance fuel mixing injecting fuel in cross-flow, in order to reduce the occurrence of local hotspots and, thus, NO_x emissions. In this context, the improvement of the single injector geometry in such a way to deliver a desirable flame dynamic plays a fundamental role. Because of the transition in the design, a potential occurrence of other risks, such as thermoacoustic instabilities, has to be considered to avoid the occurrence of dangerous combustion oscillations.

The present research work aims to investigate the impact of geometric variations on micromix flame structure, fuel mixing and time delay through a CFD analysis and establish key trends of combustion performance parameters, in order to identify relevant design parameters to minimise NO_x emissions. The effects of two geometry parameters variations have been investigated: the air gate shape and the hydrogen injector angle. The variation of the first design parameter has shown potential to significantly modify the flame dynamics and minimise the emissions by redistributing the incoming air flow, whereas the injection angle by improving the fuel mixing.

Keywords:

Hydrogen; Micromix; CFD; Jet in Cross-Flow; NO_x; Thermoacoustic.

Acknowledgement

È dura. È davvero dura poter gioire per il raggiungimento di un traguardo così importante davanti a quello che sta succedendo adesso in Italia e nel mondo. Questo momento dovrebbe rappresentare il trampolino di lancio verso mille altre esperienze, invece siamo costretti a rimanere in casa, laurearci per via telematica e festeggiare con amici e parenti tramite uno schermo. Ma supereremo anche questa, ne sono convinto. Piuttosto, la mia più grande speranza è che tutto ciò possa aver destato alcune coscienze sul valore della vita umana, troppo spesso messa in secondo piano in favore di interessi personali ed economici. Penso ai milioni di innocenti e bambini che devono pagare per guerre che non hanno scelto di combattere. Alle milioni di persone che vivono nella povertà assoluta alle quali viene negato il diritto ad una vita dignitosa. A tutte le ingiustizie del mondo. Penso alla nostra Terra, che stiamo distruggendo e calpestando senza alcun rispetto e che probabilmente avremo negato alle future generazioni per il nostro egoismo.

Ma voglio pensare positivo. Ho cercato di sfruttare il tempo a disposizione per riflettere sull'importanza di alcuni valori e la necessità di rivedere le proprie priorità. Troppo spesso siamo così impegnati a costruirci un'identità e progettare il futuro da trascurare il presente e le cose che realmente contano. In fondo, "in questo mondo terrificante, ci restano solo i legami che creiamo".

Per questo, un ringraziamento speciale va alla mia famiglia, che mi ha sempre trasmesso sicurezza, supporto e amore incondizionato, ma in questo periodo complicato più che mai. Ho riscoperto il piacere di stare in famiglia.

A tutti i miei amici, torneremo alle vecchie abitudini, torneremo ad abbracciarci, a viaggiare, a condividere esperienze, momenti ed emozioni insieme. E tutto ciò lo apprezzeremo molto di più. Ciò che prima ci sembrava scontato avrà un sapore diverso, più dolce. Mai quanto adesso mi rendo conto della vostra importanza.

A tutti coloro stanno lottando in prima fila per restituirci la libertà.

Table of Contents

List of Figures

List of Tables

List of Abbreviations

AGP   Air Guiding Panel
CFD   Computational Fluid Dynamics
CO   Carbon monoxide
CO_2 Carbon dioxide
CVP   Counter-rotating Vortex Pair
DNS   Direct Numerical Simulation
FAR   Fuel/Air Ratio
FDF   Flame Describing Function
FGM   Flamelet Generated Manifold
FTF   Flame Transfer Function
H_2 Hydrogen
H_2O Water
JICF   Jet In Cross-Flow
LBO   Lean Blowout
LES   Large Eddy Simulation
LH_2 Liquid Hydrogen
NO_x Nitrogen Oxides
OH   Hydroxyl radical
OPR   Overall Pressure Ratio
OSCILOS   Open Source Combustion Instability Low Order Simulator
PDF   Probability Density Function
ppmV   Volumetric Parts Per Million
RANS   Reynolds-Averaged Navier-Stokes
TET   Turbine Entry Temperature
TRL   Technology Readiness Level
UHC   Unburned Hydrocarbons
URANS   Unsteady Reynolds-Averaged Navier-Stokes

1 Introduction

1.1 Project Background

In the last decades, an increased interest in environmental impact of the gas turbine engines led to a significant redesign of the combustor concept and the development of low emissions combustion technologies, in order to reduce emissions. Over the years, most of the worldwide organizations have worked to establish regulations that limit the production of greenhouse gases and other compounds harmful to human and environmental health, resulting in pollutant emissions legislations more stringent. In this context, the reduction of emissions has become one of the main requirements in the combustor design.

Historically, gas turbine engines are well-known for their characteristic low specific fuel consumption. In terms of thermodynamic cycle, it is possible to achieve this by increasing Overall Pressure Ratio (OPR) and Turbine Entry Temperature (TET), resulting in improvement in thermal efficiency. In recent decades, thanks to the introduction of new materials and cooling technologies in gas turbine industry, engines with these features have been developed. It has led to higher temperatures and pressures at the combustor inlet [1] and consequent problems associated with the production of NO_x emissions, which is a function of flame temperature and residence time at high temperature, because its mechanism of formation is based on the dissociation of nitrogen molecules present in the air.

In order to face these increasingly elevated temperatures and reduce emissions, particularly NO_x, a first action was the development of several low emissions combustion technologies. These technologies are based on the concept of moving from stoichiometric conditions in order to reduce flame temperature and, consequently, NO_x emissions.

Despite the significant improvements in terms of NO_x emissions introduced by these novel technologies, it is vital to move from kerosene to alternative fuels to meet long term emissions targets and one of the most promising alternative fuels is liquid hydrogen [2]. In this context, a large amount of research work has been

conducted to investigate novel and promising hydrogen combustor technologies. This research work is part of ENABLEH2 project, which involves several R&D organizations across the Europe to promote research about the introduction of liquid hydrogen (LH_2) as fuel in civil aviation, in order to achieve zero mission-level CO_2 and ultra-low NO_x emissions. In this way, it could be possible to meet Flightpath 2050 targets: 75% reduction in CO_2 emissions and 90% reduction in NO_x emissions, relative to year 2000. The aim of the project is to tackle key challenges, i.e. safety, infrastructure development, economic sustainability, community acceptance, and explore key opportunities through improved combustor design and fuel system heat management to further minimise NO_x emissions, improve energy efficiency and reduce the required volumes of LH_2 [46]. The project is divided in 6 Work Packages, as shown in Figure 1.1, and Cranfield University, as leader partner of Work Package 3, is required to conduct experimental and analytical work on a single injector, an injector array and a full scale annular combustor segment, in order to mature hydrogen micromix combustion technology to TRL4. The present research study performed simplified RANS CFD on a single injector geometry to support the down-selection of the designs able to offer good mixing and emissions characteristics for experimental evaluation.
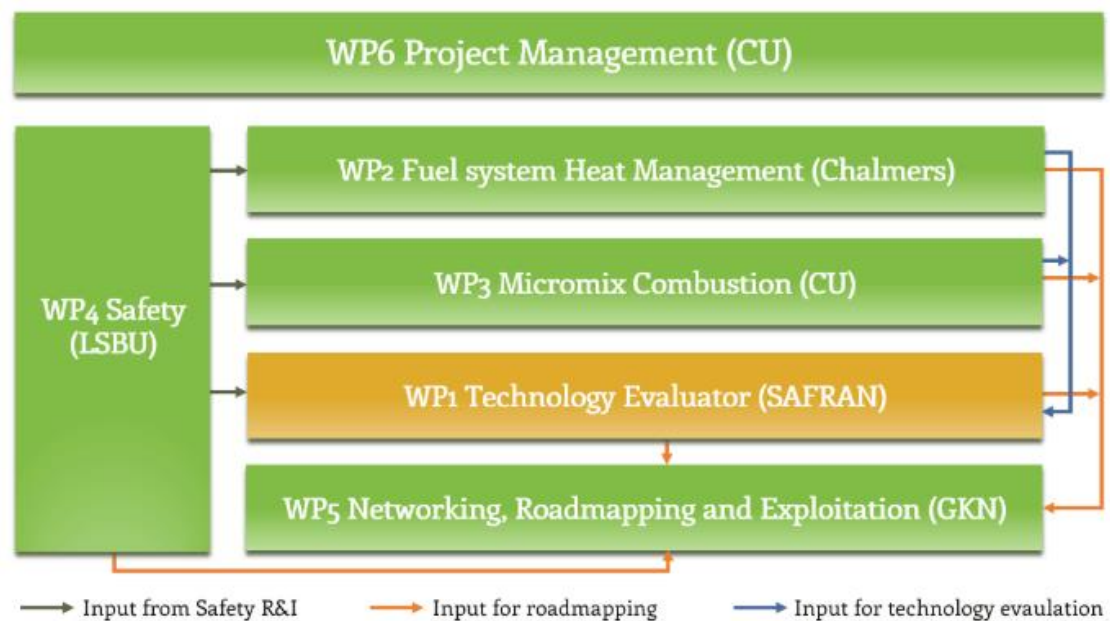
Figure 1.1: project structure and interconnections between Work Packages [46]

Although hydrogen is a free-carbon fuel which allows to delete carbon-based emissions, it is also affected by several issues which imply a significant redesign of the aircraft and the combustion chamber, due to differences between hydrogen and kerosene properties. Additionally, it is necessary to consider that molecular hydrogen H_2 is not present naturally in this configuration on Earth and it needs to be produced. The common method used to produce hydrogen is the steam reforming of natural gas, which uses fossil sources. For this reason, it is necessary to be sure that manufacturing processes do not increase the overall carbon footprint.
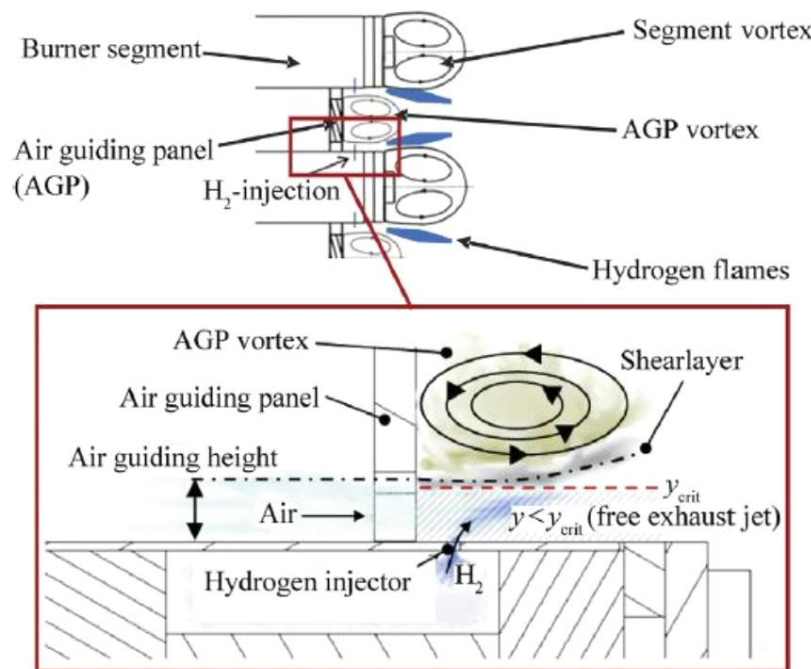
Figure 1.2: Schematic of a jet in cross-flow structure and flame anchoring between recirculation vortices [3]

In order to overcome these problems, lean non-premixed micromix combustion concept has shown high potential. A micromix combustor is composed by a large number of micro-diffusion flames to enhance mixing and reduce the potential for local stoichiometric pockets. The micromix combustion concept is based on the replacement of the conventional big flame with several smaller flames to reduce residence time at high temperature and, ideally, to reduce peak temperatures by good local mixing. In this new concept, the fuel is not premixed with the air, but it

3

is introduced perpendicularly to the direction of the air stream, like a jet in cross-flow. As illustrated in Figure 1.2, the fuel jet is injected in cross-flow and the micromix flame is anchored within the shear layer between two recirculating vortices. For this reason, it is essential to optimise the hydrogen jet penetrating into the air cross-flow to achieve a better fuel mixing and an optimal flame shape and position within the combustion zone. The typical structure of a single injector geometry is depicted in Figure 1.3, in which the main design parameters are identified. Their variation can significantly affect flow dynamics and the behaviour of the micromix flame. They are listed as follow:

- Hydrogen injector diameter, which directly influences the energy density and the momentum flux ratio, due to the impact on the fuel jet velocity;
- Air gate shape, which can be modified in two ways: keeping the area constant and varying the ratio between height and width, or modifying the area. The last option will influence the momentum flux ratio;
- H_2 injector angle;
- H_2-air offset distance, i.e. the distance between the air gate outlet plane and the injector hole;
- Mixing distance, i.e. the distance between the injector hole and the step;

Other design parameters are associated to the injector array geometry, such as the spacing between injectors, which governs the flames interaction. It is also necessary to consider the behaviour of the micromix combustor at different operating conditions and equivalence ratios, in order to ensure a reasonable response during each phase of the engine lifecycle.
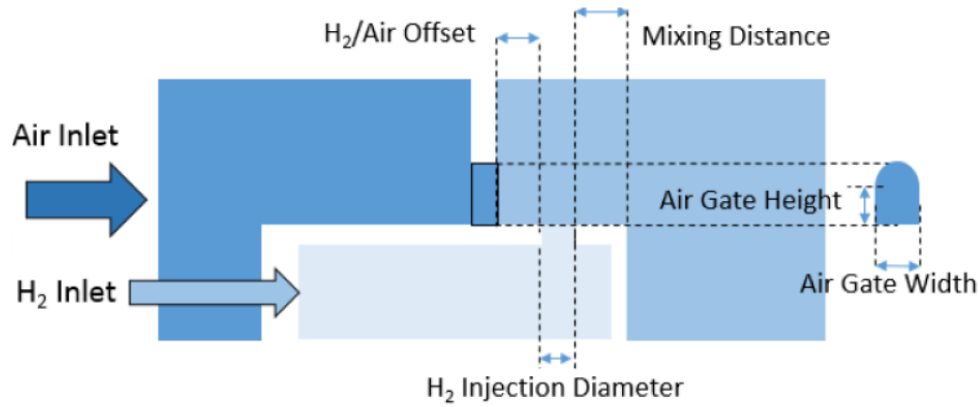
Figure 1.3: Geometry parameters of a single injector configuration. Image courtesy of P. Agarwal

When the combustor design is subject to changes or a new combustor design is introduced, it is necessary to consider the occurrence of other potential risks, such as thermoacoustic instabilities. They are mainly due to the presence of noise sources within the combustor, such as heat release rate and entropy fluctuations, which can be amplified under some circumstances and lead to destructive pressure oscillations. Usually, the incidence of thermoacoustic problems is relatively low for conventional combustors, whereas they have been seriously taken into account since the introduction of lean-premixed combustors because the pressure oscillations have caused dangerous incidents. A diffusion combustion system is characterized by several sources of acoustic losses and, therefore, the pressure oscillations are rarely amplified, whereas, in a premixed combustion system, the sources of acoustic losses are low. In addition, a premixed flame is typically more intense and compact than a diffusion flame. In theory, a micromix combustion system should be less prone than a premixed system to suffer thermoacoustic instabilities due to the diffusion-based nature of its flames. Nevertheless, micromix flames are more compact and intense than conventional diffusion flames. In addition, one of the main sources of acoustic losses are the dilution holes because the noise passes out of the combustor to be lost elsewhere. In a micromix combustion system, the dilution is likely to be lower than conventional combustors and similar to lean premixed systems. This leads to a higher risk of thermoacoustic instabilities. Additionally, there are several factors which influence thermoacoustic properties, such as ambient

conditions, fuel composition, fuel scheduling, gas turbine maintenance, firing temperature. In a gas turbine engine for aero applications, operating conditions could significantly affect the thermoacoustic properties of the combustor because of the wide range of conditions in which the engine has to operate. For these reasons, it is essential to investigate this possible risk since the first design stages, in order to avoid a complete redesign of the combustor during last stages.

This design investigation is carried out using CFD tools, in particular Simcenter STAR-CCM+, a software produced by CD-Adapco. The outcome of this research work is to establish key trends of combustion performance parameters, in order to support the down-selection of a promising single injector geometry which offers the possibility to minimise NO_x emissions without compromising other combustion performance. Since the main objective of the research in Cranfield University is to introduce the micromix technology in aero applications, one of the main issues is related to the several operating conditions at which the combustor has to be tested in order to satisfy all the phases of the engine lifecycle. The aim of the present research project is to investigate the behaviour of the micromix combustor at high-pressure condition (15 bar), which is the most critical condition in terms of NO_x emissions.

1.2 Aim and Objectives

The aim of this research project is to numerically investigate the impact of geometric variations on micromix combustion performance and thermoacoustic properties of the flame. Two different geometric parameters have been analysed: the air gate shape and the hydrogen injector angle. In the first part of the work, the micromix combustion performance in terms of mixing characteristics and NO_x emissions have been evaluated and compared, showing benefits and drawbacks associated with the geometric change. In the second part, the focus has been put on the determination of characteristic flame delay times for several single injector geometries. Their comparison has enabled to establish key trends representative of the flame response to acoustic perturbations. The estimation of time delays is necessary to estimate a series of Flame Transfer Functions (FTF) using analytical

formulations described in Section 3.8, in order to promote a further thermoacoustic assessment. The outcome of the project is to provide a set of key trends of NO_x emissions, mixing properties and FTF for each geometric variation.

The objectives are as follow:

- Investigate numerically the effects of geometric variations on the aerodynamic features of a single injector geometries, particularly the jet in cross-flow and the recirculation vortices which stabilize the flame
- Provide a series of key trends of NO_x emissions and fuel mixing characteristics in order to assess qualitatively the impact of geometric variations
- Estimate time delay and time delay spread using different approaches from RANS simulations and compare the results achieved, underlying discrepancies between the different methods
- Provide a series of FTFs for different geometries, in order to enable a future assessment of thermoacoustic instabilities

Research questions:

- How can the air gate shape and injection angle be modified in such a way to minimise NO_x emissions and improve the fuel mixing?
- How and to which degree these geometric variations can affect the acoustic properties of a micromix flame?

1.3 Project Methodology
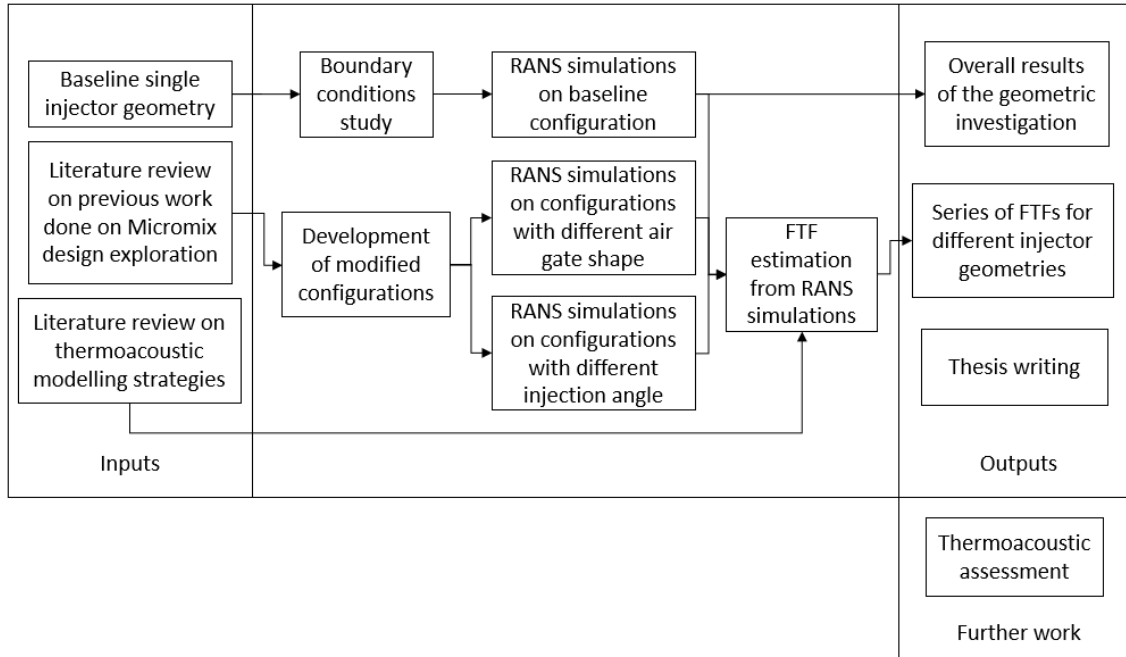
Figure 1.4: Overall methodology

The overall methodology of the project is presented in Figure 1.4. In the first stage of the project, significant literature review on the project background has been conducted, with a particular focus on the basic principles of micromix combustion concept and design space exploration carried out by previous research works in Cranfield University, Aachen University of Applied Sciences and other authors, in order to obtain a relevant understanding of the work done so far and the necessity for further research. In addition, literature review on thermoacoustic instabilities which can occur in the combustion system has allowed an understanding of the necessity of a preliminary thermoacoustic assessment in the first stages of the combustor design.

After this first stage, starting from a baseline single injector geometry, several CFD simulations have been performed using the software developed by CD-Adapco, STAR-CCM+. First of all, a boundary condition study has allowed the determination of the type of boundary condition which better reproduce the periodicity of the computational domain without influencing the typical structure of the micromix flame. After choosing the physical models which are able to

8

represent and capture all the relevant flow phenomena, RANS simulations have been run on the baseline configuration to provide the aerodynamic features of the jet in cross-flow and its combustion performance. After that, several configurations characterized by different air gate shape and injection angle have been created, in order to investigate the sensitivity of combustion performance parameters to these geometry variations. The comparison between all the different configurations have enabled to obtain the results of the numerical investigation in terms of key trends of NO_x emissions, mixing properties and time delays. For each configuration, a series of Flame Transfer Functions have been achieved using different methods from RANS simulations.

1.4 Thesis Structure

This thesis is structured in such a way to provide a fluent and clear reading. The first chapter aims to introduce the reader in a scenario in which it is unavoidable to move to alternative fuels in order to reduce emissions and address long term emissions targets. A brief description of the advantages associated with hydrogen and the challenges behind the ENABLEH2 project is provided. Once the reader is introduced in the project context, thesis objectives and research questions are set. In Chapter 2, a relevant literature review is supplied, in order to emphasise the fundamental aspects of hydrogen micromix combustion and thermoacoustic issues associated with it. The basic concept of micromix technology is furnished, with a particular focus on the jet in cross-flow structure and the design parameters which is possible to vary in order to modify the flame shape in such a way to reduce NO_x emissions. A summary of the most relevant investigation works on jet in cross-flow and previous work done at Cranfield University is provided. In Chapter 3, the description of the CFD set-up is furnished, comprising the single injector geometry, the meshing strategy, the boundary conditions and the main physic models employed to reproduce the flow phenomena. In Chapters 4 and 5, the discussion of the results obtained is provided, emphasising the influence of the geometry variations on the combustion performance parameters. The results are initially provided by looking at the separate effect of both air gate shape and injector angle variations, and then looking at the combined effect of both geometry variations. Finally, the most promising geometry have been simulated for a range of equivalence ratio, in order to have a complete view of the single injector behaviour at that condition. All the relevant conclusions achieved from this work are summarized in Chapter 6, whereas the suggestions for further work are collected in Chapter 7.

2 Literature Review

2.1 Hydrogen Combustion

Hydrogen represents one of the most promising alternative fuels in order to reduce aviation emissions and address future emissions targets, but its introduction in gas turbine applications is slowed down due to some issues associated with its properties, which are significantly different compared with those of kerosene. The biggest advantage of hydrogen is that it is a free-carbon fuel and allows to delete all the carbon-based emissions: CO, CO_2, UHC and soot. Hydrogen is the most abundant element in the universe, but most of the hydrogen on Earth react with numerous elements to form water and organic compounds. However, molecular hydrogen H_2 is not present naturally in this configuration and needs to be produced from other compounds, i.e. water or hydrocarbon molecules. The conventional methods to produce hydrogen are the steam reforming of natural gas ($CH_4+H_2O=CO+3H_2$), partial oxidation of methane ($2CH_4+O_2=2CO+4H_2$), or coal gasification ($C+H_2O=CO+H_2$) [38]. For this reason, it is necessary to ensure that manufacturing processes do not increase the overall carbon footprint. Electrolysis of water is the most sustainable approach, but it is necessary to consider that its sustainability depends on the electricity source. Only if the electricity is delivered through a renewable process such as hydropower, wind power, solar power or nuclear power, the hydrogen production can be considered completely sustainable and characterized by zero lifecycle carbon footprint.
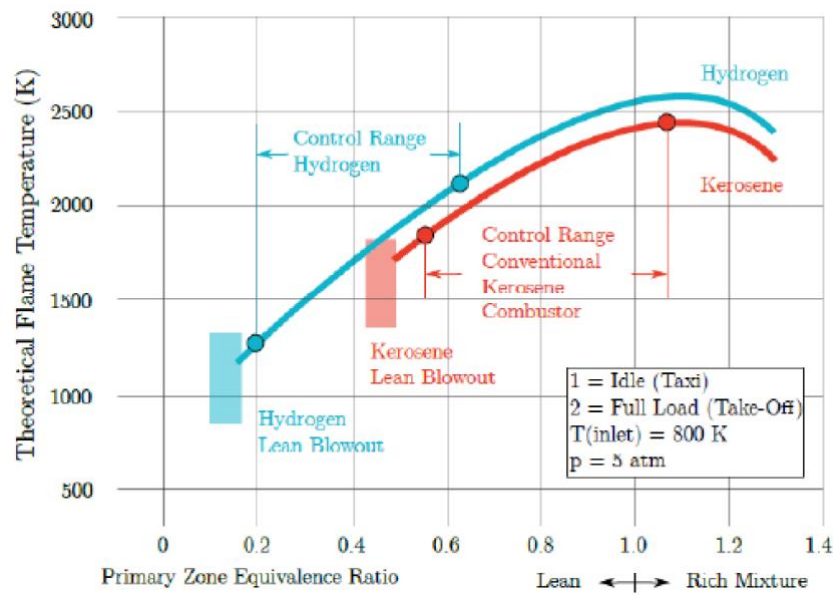
Figure 2.1: Hydrogen and kerosene stability loops [40]

As shown in Figure 2.1, hydrogen is characterized by a higher heat release rate and flame temperature at stoichiometric condition, but it has wider stability limits, compared to kerosene stability loop. For this reason, it is possible to burn hydrogen at leaner condition and, consequently, reduce flame temperature, without approaching lean blowout. Considering that hydrogen is characterized by high flame speed, which results in shorter flames, it is possible to achieve a reduction in NO_x emissions due to the short residence time at high temperature. However, it is necessary to mention a significant increase in H_2O emissions, which could result in additional contrail production and have negative implications on global warming. Thanks to its properties, liquid hydrogen as fuel is also beneficial from a combustor design perspective. Due to high flame speed and shorter flames, it is possible to realize a smaller combustor, which allows to save weight and length. Additionally, the liner durability can be significantly increased due to the absence of carbon content, which results in lower luminous radiation. The main hydrogen properties are compared to those of kerosene in Table 2.1.

Property	Hydrogen	Kerosene
Combustion		
Spontaneous Ignition Temperature (K)	847	483
Specific Energy (MJ/kg)	120.2	43.4
Energy Density (liquid) (MJ/L)	8.4	34.7
Energy Density (vapour) (MJ/m^3)	10.22	-
Stoichiometric Fuel/Air ratio (-)	0.0292	0.0680
Flammability Limits (% volume in air)	4-74	1-5.5
Minimum Ignition Energy (MJ)	0.02	0.25
Laminar Flame Speed (in air) (m/s)	3.5	0.6
Carbon Content (% mass)	0	86.0
Specific Heat Capacity (kJ/kg)	8.7	1.94
Handling and Storage		
Density (liquid @ 288K) (kg/L)	0.07	0.80
Density (Vapour @ 273K) (kg/L)	0.090	-
Boiling Point (K)	20.1	423-533
Freezing Point(K)	13.9	226

Table 2.1: Comparison between hydrogen and kerosene properties [2], [39]

Nevertheless, the introduction of hydrogen as fuel in aero gas turbine applications is limited by several problems associated with its properties and public acceptance issues. One of the biggest problems is the fuel storage. Hydrogen is characterized by a much lower density at both vapour and liquid state compared to kerosene, resulting in the necessity of much larger fuel tanks. Considering the same amount of energy, hydrogen requires a volumetric storage 4 times bigger than gasoline. The only practical way to store hydrogen is by taking advantage of the cryogenic nature of liquid hydrogen LH_2, which must be stored below -253°C. Because of its low atomic weight, the hydrogen storage could be affected by leakages and the fuel tanks require to be well insulated. For this reason, the wing fuel tanks used on current civil aircraft are unsuitable for hydrogen storage and a significant redesign of the aircraft is required [2]. Several research projects have analysed this aspect, particularly the CRYOPLANE project, in which a consortium of 35 partners from 11 European countries have collaborated in order to develop a number of configurations for short, mid and long range hydrogen-fuelled aircraft [4].

In addition, the implementation of hydrogen requires also a significant redesign of the combustor because burning hydrogen in a conventional combustion system would imply an extremely high NO_x production. The main challenge is to burn hydrogen keeping emissions low.

2.2 Micromix Combustion Technology

The micromix combustion technology has been developed in order to meet the requirement of pollutant emissions reduction while burning hydrogen at dry conditions. As described in Section 2.1, hydrogen flames are characterized by very high stoichiometric temperatures and it could drastically affect the production of NO_x emissions. Thus, it is necessary to move from the stoichiometric condition and burn leaner. The micromix combustion concept is based on burning the fuel in several small micro-diffusion flames, rather than one bigger flame. These small flames allow a better redistribution of the heat release, which results in much shorter flames compared to the standard case. This flame configuration and the high flame speed allow a reduction of the flame residence time by 10 to 15 times and it offers potential to reduce NO_x emissions. Due to the high flammability of hydrogen, which increases the risk of auto ignition, it is extremely hazardous to premix the hydrogen with the air, therefore the fuel is injected in a cross-flow jet perpendicular to the air stream in order to improve the mixing characteristics of the two reacting jets. A representation of a micromix combustion system is illustrated in Figure 2.2.

For several years, Cranfield University has been interested in micromix combustion research, especially with the aim of introducing this technology into aero applications. The combustor configuration under investigation is composed by linear arrays of micromix injectors. A different configuration composed by annular fuel supply rings is illustrated in Figure 2.3.
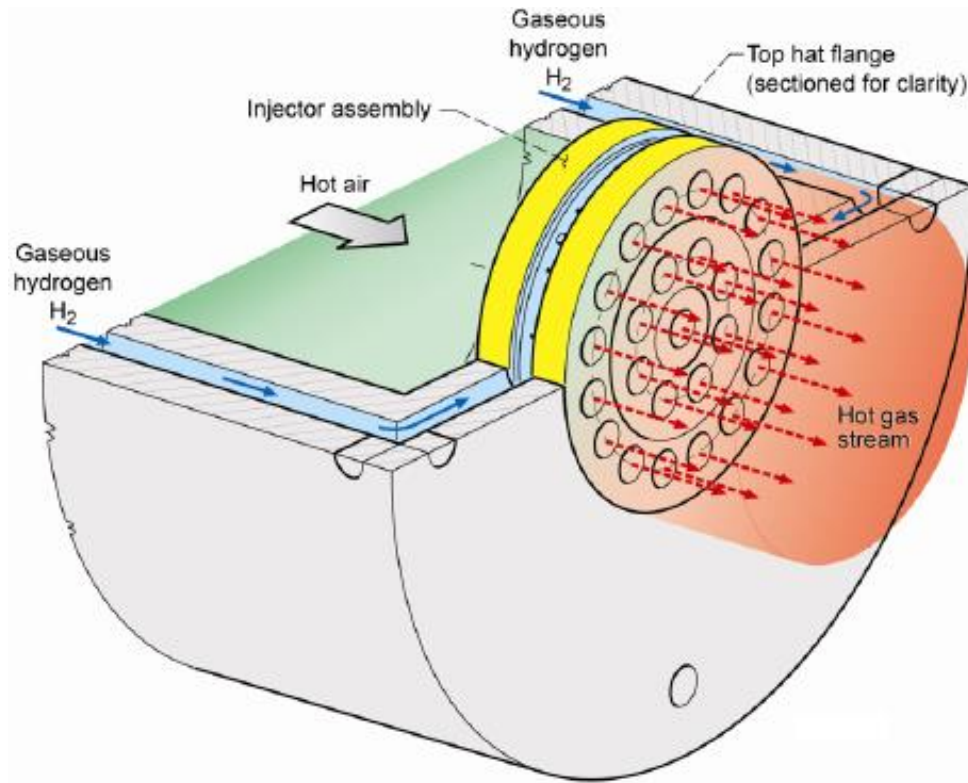
Figure 2.2: Schematic of a micromix combustion system [41]

Other research work on hydrogen micromix combustion systems for industrial gas turbines has been conducted at Aachen University of Applied Sciences in partnership with B&B-AGEMA GmbH and Kawasaki Heavy Industries [2]. Thanks to this research work, a micromix combustion chamber composed by around 1600 miniature injectors was designed and implemented in a small size Auxiliary Power Unit APU GTCP 36–300. It is illustrated in Figure 2.3. In order to achieve a distributed combustion and establish small micro-diffusion flames in the combustor, this micromix combustor is composed by annular fuel supply rings and small fuel injectors, which are circumferentially arranged along the fuel supply rings from both sides, in order to establish one micromix flame on each fuel injector.

- Micromix H$_2$ jet in air cross-flow
- 0.30 mm H$_2$ injector diameter
- 1600 H$_2$/air injector couples
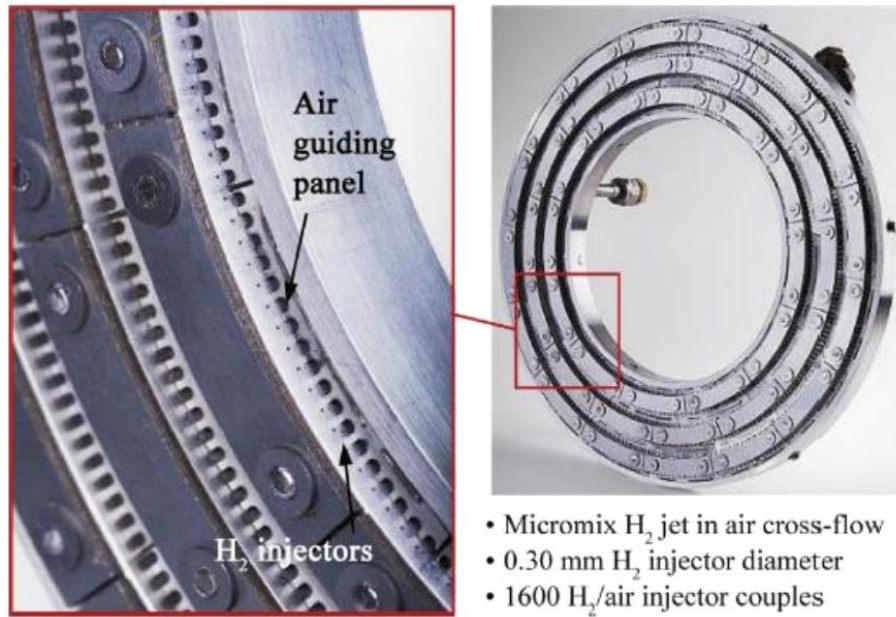
Figure 2.3: Micromix prototype combustor for gas turbine Honeywell/ Garrett Auxiliary Power Unit APU GTCP 36-300 [5]

More in detail, this micromix burner structure is composed by fuel supply rings and air guiding panels to guide the air into the burner. The fuel injectors are arranged on the fuel supply rings and the micromix flames are intended to establish and stabilise downstream of the injectors. Typical values for fuel injector diameter are about 0.3 mm. The air stream flows in the burner passing through the air guiding panels, which have small openings called air gates. These small air gates are used to contract the air stream and this air contraction allows to establish vortices in the wake of air guiding panel. These vortices are called inner recirculation vortices or inner vortices and are intended to recirculate fresh cold air in the wake of air guiding panel. Hydrogen fuel is injected perpendicularly to the main air stream, so a jet in-cross flow is established and aims to enhance mixing of fuel in air.

Downstream the fuel injector, the fuel and air mixture flows in the combustion chamber and, in the wake of fuel supply rings, larger recirculation vortices, called outer vortices, are created. This aerodynamic structure of small inner vortices and larger outer vortices is essential for the flame anchoring of the micromix flame and allows to ensure that the flames are stable and separated from each other in radial direction, in order to maintain the micromix flame structure and to keep

16

small flames burning independently from each other. Flame merging should be avoided because it would lead to an enlarged flame zone and longer residence time of nitrogen at high temperature [6]. The fuel and air mixture flows between this system of vortices, where ignition takes place and flames are intended to be stabilized along the inter-vortex shear layer. Figure 2.4 shows the fuel injection in cross-flow and the flame anchoring and stabilization between the recirculating vortices.
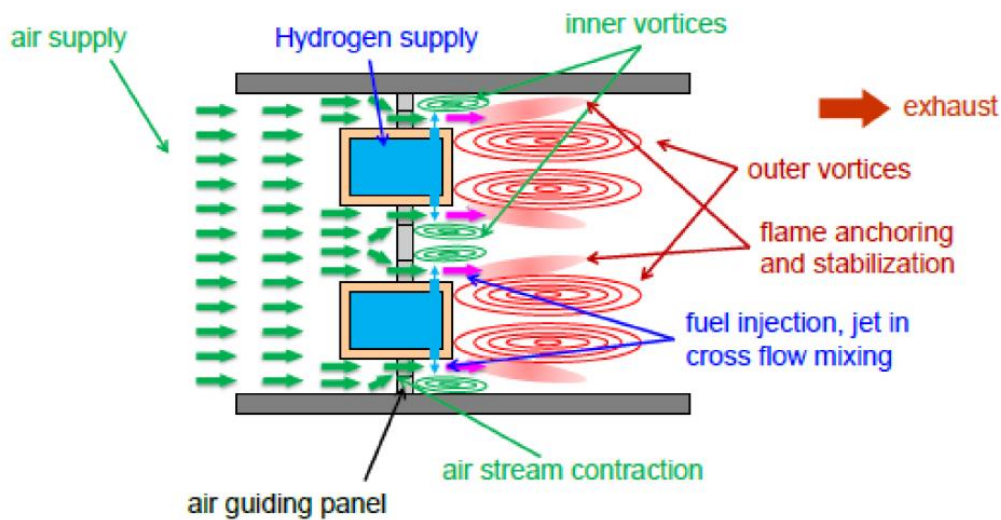
Figure 2.4: Principle of micromix combustion system [6]

One of the main issues is related to the low energy density of this technology because the hydrogen injectors are very small and, therefore, the energy density per fuel injector is low. For this reason, the integration in real gas turbine combustor requires several hundreds of fuel injectors to be arranged in the fuel supply rings. This leads to high manufacturing efforts and costs and a complexity of the burner system, which is not appreciated in the gas turbine industry. A further issue is that small injectors are susceptible to blockage with time. A numerical investigation has been conducted by Ayed et al. [7] to explore the possibility to increase the injector size, which consequently means reducing the manufacturing efforts and increasing energy density of the combustor. It has demonstrated the feasibility of increasing the injector diameter from 0.3 to 1 mm, which means increasing the energy density more than 11 times, without compromising the low NO_x ability.

2.2.1 Jet in Cross-Flow

As previously described, the micromix combustion concept is based on the choice to burn hydrogen in several small flames instead of one bigger flame in order to reduce NO_x emissions. In this context, the role assumed by the mixing process is critical. A jet in cross-flow (JICF) is an efficient mechanism which allows to improve the mixing process thanks to three-dimensional and unsteady vortical structures generated during the interaction between the jet and the cross-flow [9]. It has several practical applications, particularly in the gas turbine industry. As illustrated in Figure 2.5, a jet in cross-flow is featured by the formation of some vortical structures: the horseshoe vortex, the leading-edge and lee-side vortices, the wake vortices and the counter-rotating vortex pair (CVP). The horseshoe vortex is generated upstream of the jet hole and develops all around the jet stream. Along the jet boundary, some vortices form at the leading-edge and at the lee-side, merge and create ring-like vortices surrounding the jet column. The wake vortices are generated downstream of the jet stream, starting from the jet shear layer. The counter-rotating vortex pair is produced from the jet stream, when it is deflected in the cross-flow direction. These structures are liable for the entrainment of the cross-flow fluid by the jet: in the near-field, the entrainment is governed by the leading-edge and lee-side vortices, also known as ring-like vortices, whereas the far-field entrainment is influenced by the counter-rotating vortex pair [10].
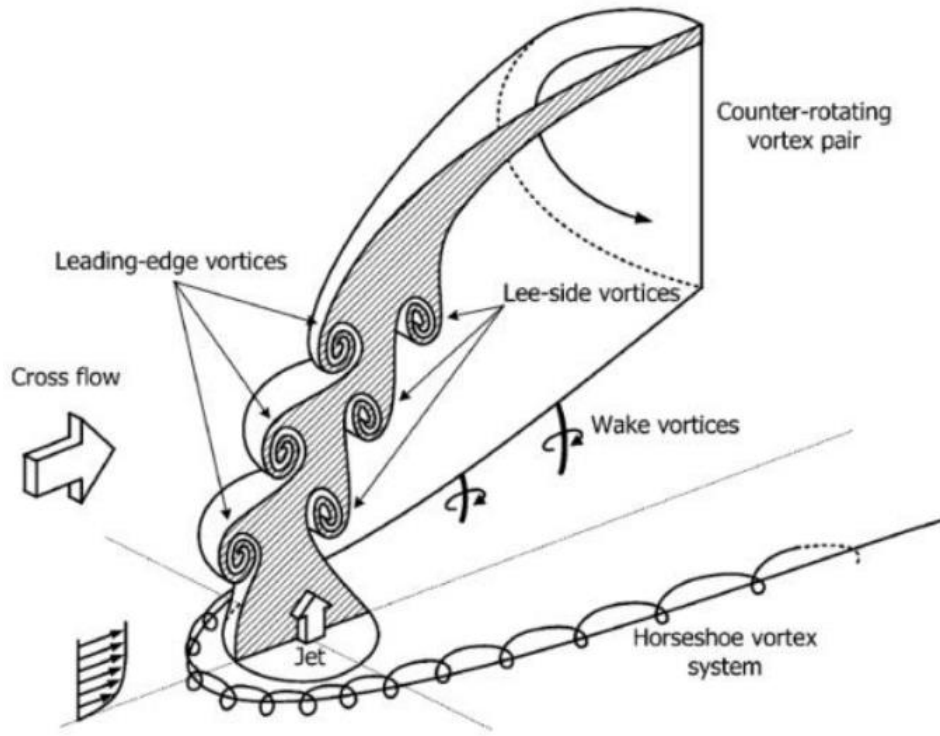
Figure 2.5: Sketch of typical vortex structures in a Jet in Cross-Flow [10]

Viscous effects, such as entrainment and separations, are essential to allow the bending of the jet, in their absence the jet would act like a free jet. Particularly entrainment is a crucial phenomenon, responsible of the development of the JICF [11]. The shape and trajectory of the jet is influenced by the momentum flux ratio, which relates densities and velocities of the two reacting jets. Depending on the intensity of the two streams, the jet is deflected in the axial direction and flows simultaneously with the cross-flow. Several correlations are described in the literature, which allow to predict the jet trajectory. One of these is known as Holdeman correlation and provided by several papers [12]. It is defined as follow:

$$\frac{z}{d} = 0.76 \left(\frac{\rho_j}{\rho_m}\right)^{0.15} J^{0.52} \left(\frac{x}{d}\right)^{0.27} \qquad \textbf{(2-1)}$$

Where d is the hole's diameter, J is the momentum flux ratio, ρ_j and ρ_m are the jet and cross-flow densities. The definition of momentum flux ratio is provided in Section 2.3.3.

2.2.2 Previous work at Cranfield University

Cranfield University, as leader partner of the Work Package 3 in ENABLEH2 project, has been conducting a significant amount of analytical work on the development of a micromix combustor, which allows the introduction of liquid hydrogen (LH2) as fuel in the civil aviation. The next step will be to carry out the experimental work and validate the numerical results obtained from the simulations.

Murthy [13] carried out a research investigation on the potential to reduce NO_x emissions by comparing four configurations of hydrogen micromix combustors, which differ for the injector module design. This work has showed the main advantages associated with each model in terms of NO_x reduction, mixing capabilities and other combustion performance. In addition, an equivalence ratio study has allowed to evaluate the potential to reduce the equivalence ratio and burn leaner. Karakurt [14] investigated a propane fuelled combustor can with a single injector and compared it with some cases in which he replaced the single injector with micromix injectors. He highlighted the importance of interaction between injectors and the necessity to rearrange their positions, in order to improve the mixing properties and avoid local stoichiometric pockets. The model developed by Karakurt is illustrated in Figure 2.6.
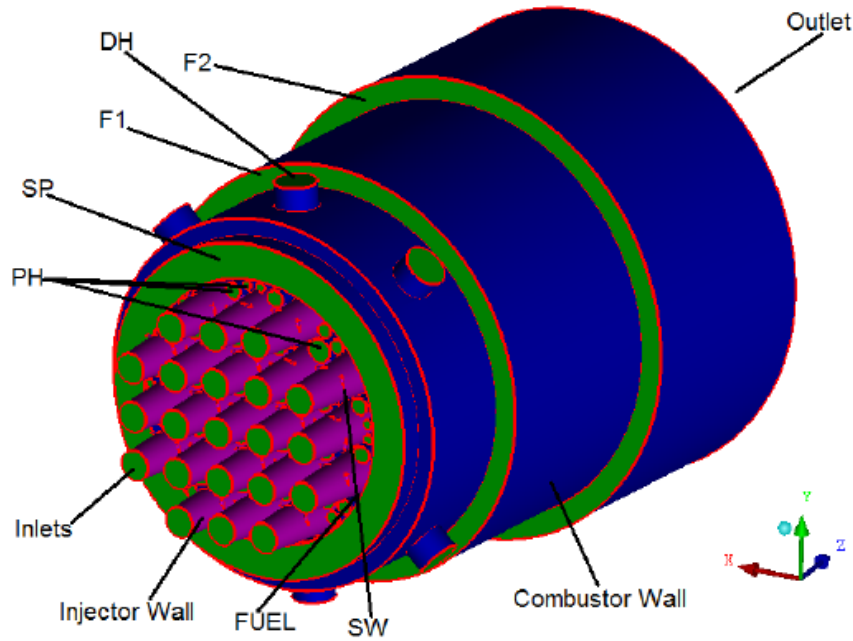
Figure 2.6: Geometry and boundary conditions of the model developed by Karakurt [14]

Degroote [15] investigated on the capability of different turbulence models to assess micromix combustion, comparing LES, URANS and RANS approaches. LES approach has shown to be more appropriate to simulate the micromix flame and to predict NO_x emissions and hydrogen mixing. In the second part of his work and in Asanitthong's work [16], a research on the possibility to control the combustor outlet temperature distribution have been performed. Petit de Bantel [17] conducted a comparative study to evaluate the most suitable combustion model to address the hydrogen properties, which concluded that the model combining both laminar and eddy-dissipation models is more appropriate. Sabin [18] continued to investigate this aspect, comparing two species models: the non-premixed combustion model and the species transport model. The second model has shown better capabilities to capture the mass transport mechanism which governs the micromix flame shape. He put particular emphasis on the species diffusion, stating that it is not accurate to consider a homogeneous diffusion for all the species involved in the reacting process. The species transport model is promising in order to simulate a micromix flame, but the diffusion coefficients of all the species have to be assessed.
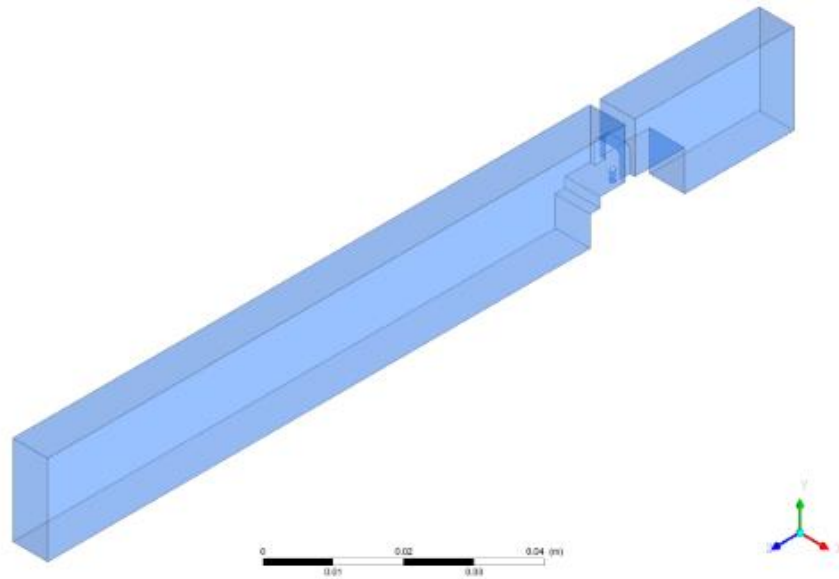
Figure 2.7: Single injector geometry developed by Ramzi Ben Abdallah

Abdallah's work [19] represents an important progress in micromix combustion research at Cranfield University because he delivered a single injector geometry and an injector-array conceptually similar to the actual configuration. The single injector geometry developed by R. B. Abdallah is illustrated in Figure 2.7. He carried out sensitivity studies on the models and diffusion parameters. In order to achieve a reasonable prediction of species transport, he suggested to use the Flamelet Generated Manifold model due to the fast chemistry of hydrogen. He noticed a significant influence of the Schmidt number on the flame shape and highlighted the necessity of a sensitivity study to obtain a reasonable evaluation of the thermal and momentum diffusion processes for hydrogen combustion. Instead, the FGM model is not sensitive to changes in the Prandtl number, probably because it is not present in the species transport equations. A value of 0.85 for the Prandtl number has been selected. G. Babazzi [20] focused her work on the importance of the turbulence-chemistry interaction, conducting a study to address the coupling between the Flamelet model and different hydrogen combustion mechanisms. It concluded that the turbulence-chemistry interaction is not affected by the choice of the reduced chemistry on the flow field prediction and all the hydrogen combustion mechanisms investigated in this work can be used to properly model a micromix flame. In addition, two methods to predict NO_x

emissions have been compared: a post-processing technique from RANS simulations and a Reactor Network model coupled with a detailed hydrogen combustion mechanism, which provides good forecast, even in terms of absolute values. J. McClure [2] carried out a thermoacoustic analysis of the hydrogen micromix combustor. Two different modelling strategies have been investigated to estimate the flame response to acoustic excitations from RANS and LES simulations. The thermoacoustic analysis has been conducted using a low order acoustic combustor model and it revealed that the hydrogen micromix combustors is more prone to higher frequency instabilities than conventional combustion systems and that the risk of thermoacoustic instabilities should not be neglected.

2.2.3 State of the Art Summary

Several research on micromix combustion system and jet in cross-flow has been conducted in the last decades, which led to an appreciable amount of numerical and experimental investigations present in the literature.
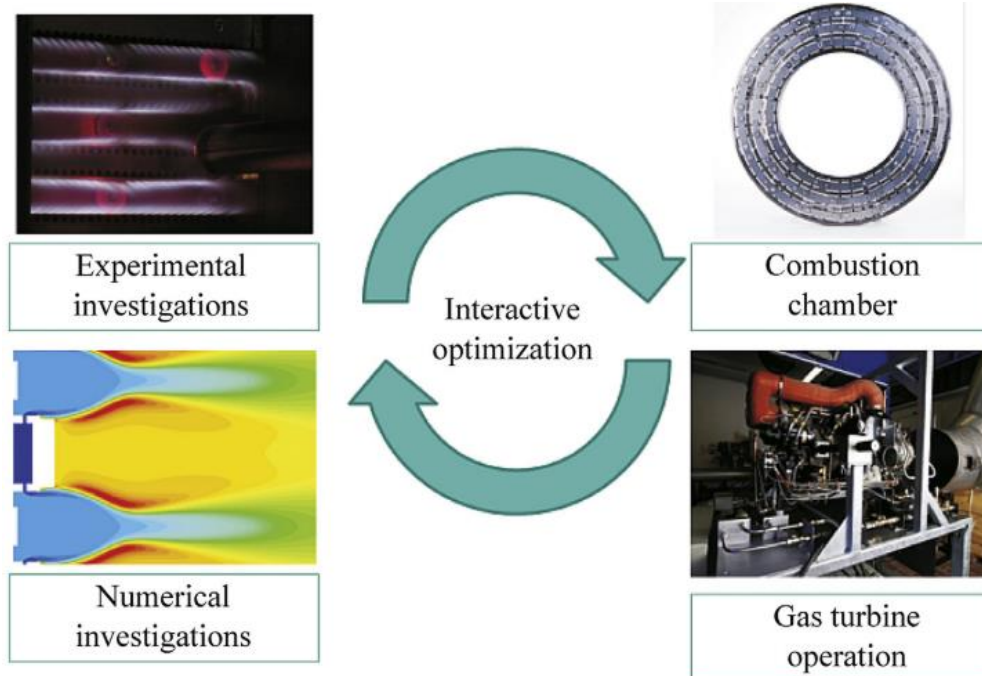
Figure 2.8: Interactive optimization cycle of micromix combustor research and development [3]

In this context, a primary role is assumed by a consortium of three partners: Aachen University for applied sciences, B&B-AGEMA GmbH and Kawasaki Heavy Industries, which collaborate to develop a micromix combustor for industrial applications. The Micromix combustor research has been conducted following an interactive optimization cycle shown in Figure 2.8, in which the numerical results obtained from simulations are validated on test burners and then implemented in a combustion chamber to observe the real capabilities. Numerical simulations represent an important step in this optimization cycle because they allow to understand how the hydrogen Micromix flame responds to geometric variations and develop important key trends.
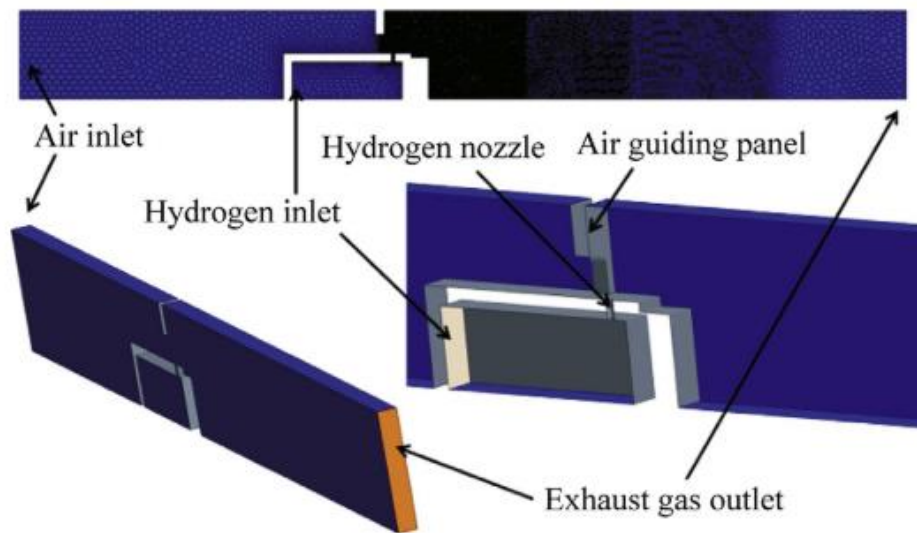
Figure 2.9: Computational domain of the single injector geometry investigated by A.H. Ayed et al. [3]

Considerable part of the work has been done on the single injector geometry illustrated in Figure 2.9, where the fuel is introduced through an injector with a diameter of 0.3 mm at 300 K, whereas the air is preheated at 550 K. The operating pressure has been set to atmospheric condition (1 bar). Firstly, different combustion models have been compared to characterize the micromix flame structure, its interaction with the flow field and its emissions. Three combustion models have been investigated: the Eddy Dissipation Model (EDM) where the reaction is controlled by the turbulence mixing, the Eddy Dissipation – Finite Rate (ED-FR) and the Eddy Dissipation Concept (EDC) which combine the turbulent

mixing driven reaction rate and the chemical kinetic reaction rate. The results obtained using the EDC model have shown good agreement with the experimental results, particularly in NO_x prediction.

Another investigation has been carried out by Ayed et al. [7] in order to increase the energy density of the micromix combustor. To do this, the power per injector has to increase and, consequentially, also the fuel flow. Since it is required to keep the fuel velocity constant, the injector size must increase. The increase in the injector diameter has a positive impact from the manufacturability perspective because it is possible to reduce the number of injectors by increasing the power per injector. In addition, the risk of hole's blockage is reduced. The injector size has been increased gradually: two configurations with injector diameter of 0.45 and 0.55 have been tested. For these two cases the energy density is increased by 2.5 and 3.36 times respectively. Despite the increased flame length, thickness and flame temperatures of the two burners, they have shown good response in terms of NO_x production. This is mainly due to the scaling of the injector distance, which has a direct influence on NO_x emissions because more cold air surrounds the flame and reduce the temperature in the outer recirculation vortex. These results led to a further scaling of the burner. An injector diameter of 1 mm allows to increase the energy density around 11 times than the baseline configuration. This investigation has revealed that the 1 mm injector is able to produce low NO_x emissions in a wide range of equivalence ratio, but at equivalence ratio higher than 0.55, the NO_x production starts to increase quickly. The measured and calculated NO_x emissions have been plotted and are available in Figure 2.10.
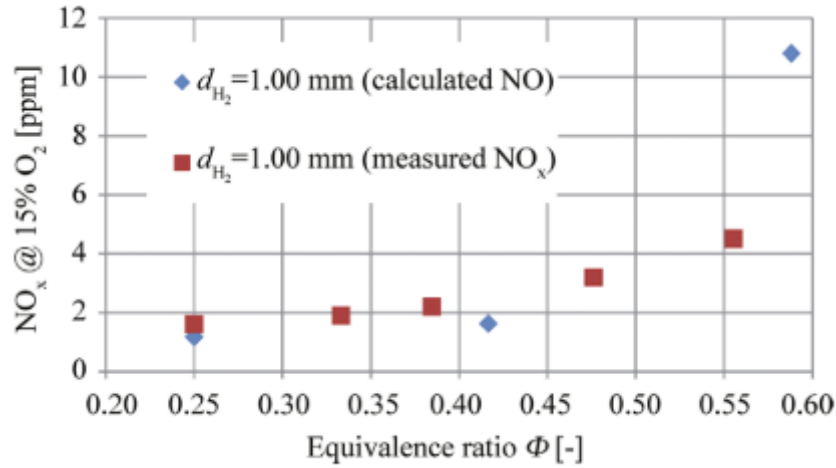
Figure 2.10: Measured and calculated NO$_x$ emissions at different equivalence ratios for the 1 mm injector burner [7]

Further work has been conducted by Ayed et al. [8] in order to investigate the influence of different geometry parameter variations on the flame structure and the NOx emission and to identify the most relevant design parameters. This investigation has been done on the micromix combustor at elevated energy density, achieved by increasing the injector diameter to 1 mm. Starting from the baseline configuration, two geometry parameters have been varied: the variation of the mixing distance in order to increase the fuel-air mixing before the flame is establish and the air guiding panel height to increase the dimension of the inner recirculation vortex and reduce the risk of flames merging. The variation of these two geometry parameters is illustrated in Figure 2.11 and Figure 2.12.
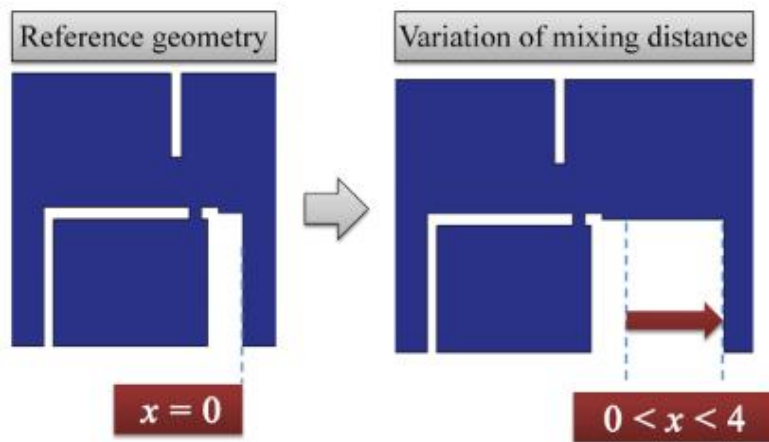
Figure 2.11: Variation of the mixing distance [8]

The variation of the mixing distance has shown interesting results: increasing the air-fuel mixing is beneficial in terms of NO_x emissions because there is a reduction in the formation of local hotspots, which are the main sources of NO_x production.
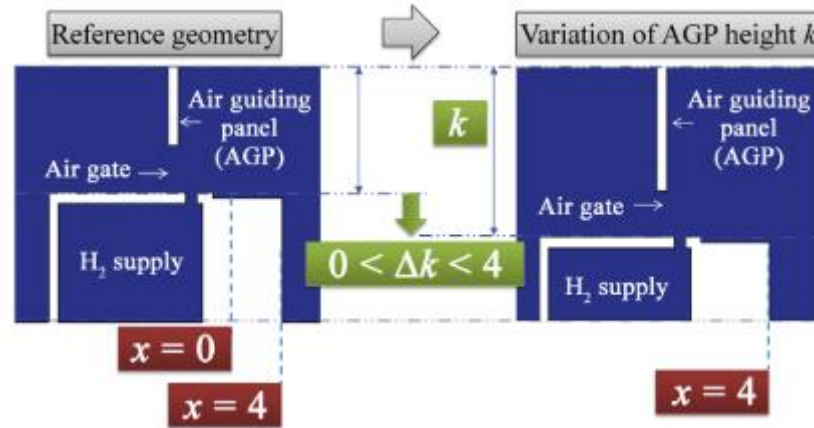
Figure 2.12: Variation of air guiding panel height [8]

As previously anticipated, the aim of increasing the AGP height is to increase the size of the inner recirculation vortex. Due to this bigger inner vortex, it is possible to achieve a change in the flame structure, providing a longer shear layer. In this way, it is possible to burn all the fuel in the first flame fragment, limit the flame in the shear layer zone and significantly reduce the "post shear layer" flame, which promotes NO_x production.

Thanks to the research work on hydrogen micromix combustion, a micromix combustion chamber composed by around 1600 miniature injectors was designed and implemented in a small size Auxiliary Power Unit APU GTCP 36–300.

Other research works have focused their attention on the effects of different jet's hole shapes on combustion performance parameters. S. R. Gollahalli and D. Pardiwalla [21] have compared the properties of turbulent propane jet flames from circular and elliptic burners. Both configurations with the major and minor axis aligned with the crossflow have been analysed and an aspect ratio of 3 has been chosen. All the geometry analysed are characterized by an equivalent exit area. These configurations have been compared in terms of flame stability and

structure and emissions. Both elliptic burners have shown lower CO production, but higher NO than circular burner.

B. A. Haven and M. Kurosaka [22] have conducted experimental works to analyse the effect of different hole shapes on the near-field characteristics of JICF. Round, elliptical, square and rectangular hole shapes have been investigated, all of them with the same cross-sectional area. This investigation has revealed that the hole geometry has a significant impact on the near-field feature of the kidney vortices. These vortices, depending how they develop in the crossflow, are critical in order to increase or reduce the jet lift-off. By manipulating the hole geometry without varying the cross-sectional area it is possible to modify the structure of the vortices and influence the jet lift-off. The fuel injected from high-aspect-ratio holes, characterized by increased distance between the sidewall vortices, tends to remain attached to the wall, while from low-aspect-ratio holes is more prone to blow off.
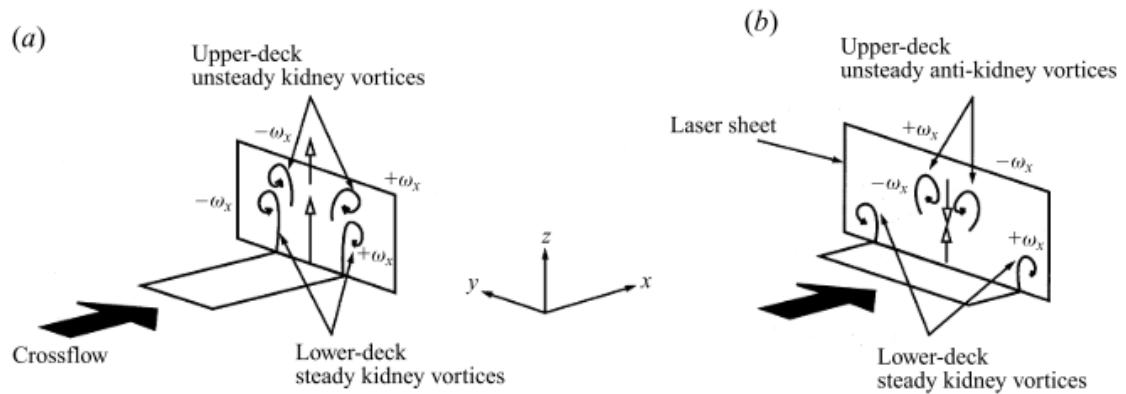
Figure 2.13: Double-decked structure showing (a) unsteady kidney vortices in the upper deck and (b) unsteady anti-kidney vortices [22]

In addition, the analysis of square and rectangular shapes has allowed to distinguish between the vorticity generated from the leading and trailing edges and that from the sidewall. As shown in Figure 2.13, the leading-edge and the sidewall boundary layers combine to form the steady lower deck of kidney vortical structure. Instead, the central part of the leading-edge boundary layer is periodically shed and generates the unsteady kidney vortices which arise in the upper deck of kidney structure. Depending on the hole geometry, these unsteady

vortices can be kidney or anti-kidney pair: unsteady kidney vortices are associated with low-aspect-ratio holes, the anti-kidney vortices with high-aspect-ratio holes.

2.3 Design parameters

2.3.1 Penetration depth

As described before, the air stream reaches the air guiding panel, is contracted by passing through the air gate and mixed with the hydrogen jet in cross-flow. Downstream the air guiding panel, there is the formation of the inner vortex. A critical penetration depth y_{crit} is defined by Ayed [6] and it is equal to the air guiding height. Figure 2.14 clearly illustrates the formation of the inner recirculation vortex downstream the air guiding panel and the limit imposed by the critical penetration depth. As long as the penetration depth y remains lower than this critical value, the hydrogen jet mixes with air stream and the micromix flame is regularly formed downstream the fuel supply system and stabilized along the shear layer between the inner and outer vortices. When the penetration depth exceeds the critical value, the hydrogen jet enters within the inner vortex and mixes with air, drastically increasing the risk of ignition here and the residence time of nitrogen at high temperature. It is important to design the jet penetration depth in such a way to avoid recirculation of fuel within the inner vortices to delete risk of ignition in this zone [6].
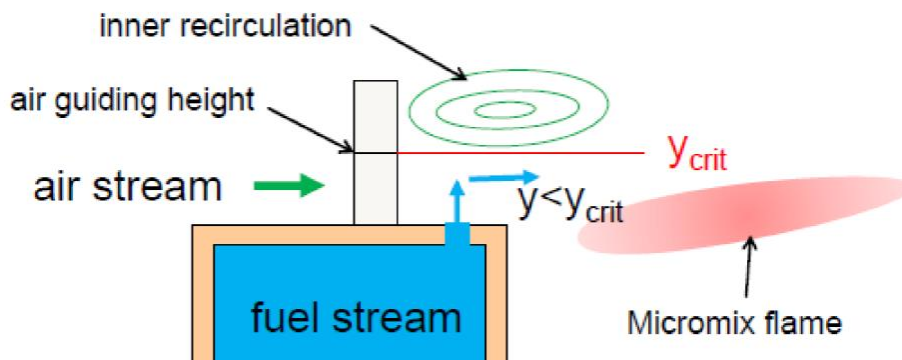
Figure 2.14: Penetration depth of a jet in cross-flow [6]

The penetration depth is proportional to the momentum flux ratio J, which is a function of the air and fuel densities and air and fuel velocity.

$$J = \frac{\rho_{H_2} \cdot U_{H_2}^2}{\rho_{air} \cdot U_{air}^2} \qquad \text{(2-2)}$$

2.3.2 Energy density

A general definition of the combustor's energy density relates the required thermal energy in a combustor with the combustion chamber size and the operational parameters of the gas turbine [6]. The energy density ED for a single micromix combustor element is defined as:

$$ED_n = \frac{E_{ref}}{A_{ref} \cdot p_{ref}} \left[\frac{MW}{m^2 \cdot bar} \right] \qquad \text{(2-3)}$$

Where E_{ref} is the amount of energy associated with this element, characterized by the reference section A_{ref}, and p_{ref} is the operating pressure of the combustor.

The injector energy density ED_i corresponds to the amount of energy associated with a single fuel injector and is defined as the fuel flow rate injected in a single fuel injector. Therefore, this parameter is directly proportional to the diameter of the fuel injector and to the operating pressure [6].

2.3.3 Momentum Flux Ratio

One of the main parameters which characterize the behaviour of a jet in cross-flow (JICF) is the momentum flux ratio. It is defined as follow:

$$J = \frac{\rho_{H_2} U_{H_2}^2}{\rho_{air} U_{air}^2} \qquad \text{(2-4)}$$

This parameter allows to combine the density and velocity of both jet and cross-flow and understand how they interact each other. Typically, the maximum flux ratio identifies three flow regimes. For J<1, the intensity of the jet is weak and it flows along the wall after being injected. For J>100, the jet is extremely intense and it is not affected by the cross-flow. For this reason, it behaves like a free jet in static flow [23]. The most interesting regime in industrial applications is 1<J<100. In this range, the jet is deflected by the cross-flow at a certain distance from the wall and it flows downstream describing a jet trajectory.

2.3.4 Other geometric parameters

Alternatively, there is the possibility to vary a significant number of geometric parameters, in order to modify the position, size and intensity of the stabilization vortices. The Micromix flames anchor along the shear layer between the outer and inner vortices, therefore a variation in this structure will result in a different shape and orientation of the Micromix flame and it will cause in turn a change in NO_x emissions.

It is possible to vary the air gate size, in terms of both width and height. It is important to consider that an increase in the air gate size means a reduction in the air stream velocity, and it will result in a change in the momentum flux ratio and a change in the air gate height will affect the critical penetration depth. Alternatively, it could be possible to analyse changes in the hydrogen/air offset distance (space between the air gate exit and the hydrogen injector), the mixing distance and the angle of the hydrogen injector, in order to enhance fuel mixing, and the blockage ratio, which is the ratio between the air gate height and the height of the air guiding panel and influences shape, position and size of the inner vortex [8].

2.4 Turbulence-Chemistry Interaction

Turbulent combustion is characterized by the interaction between turbulence and combustion. It is a very complex phenomenon because different physical processes are involved and each of them characterized by time and length scales. The understanding of how these different length and time scales interact and influence each other is fundamental in order to model properly the flame behaviour. A representation of a generic flame front is depicted in Figure 2.15, which highlights the interaction between different chemical and turbulent length scales.
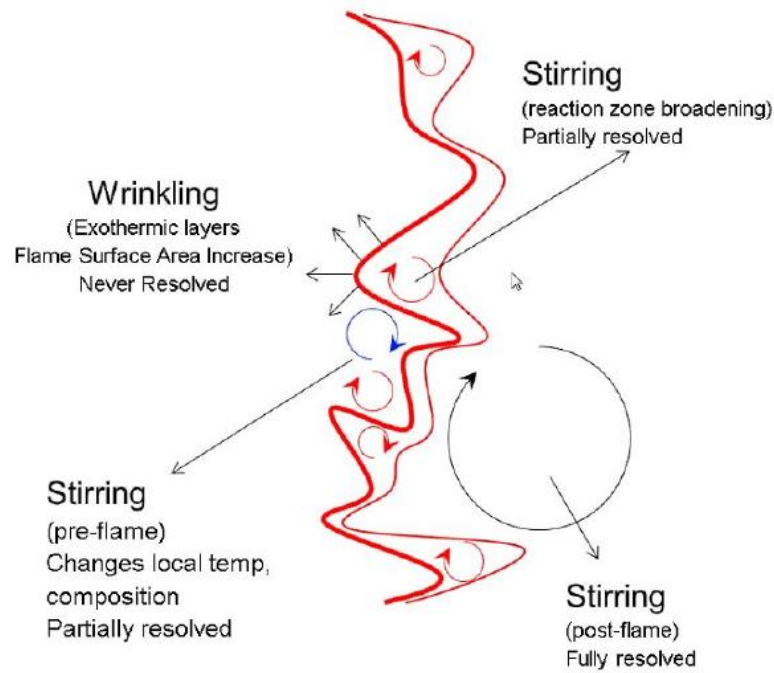
Figure 2.15: Schematic of a generic flame front, in which different chemical and flow length scales interact each other [42]

A turbulent flow is characterized by several length scales from the largest l_t to the smallest, called Kolmogorov length scale η_k, which is a function of the viscosity of the flow v and the dissipation rate of the kinetic energy ε

$$\eta_k = \left(\frac{v^3}{\varepsilon}\right)^{1/4} \qquad \textbf{(2-5)}$$

In Figure 2.16, a schematic of a non-premixed turbulent flame is represented. In this sketch, the main chemical length scales are illustrated: the diffusion layer thickness l_d, where the mixture fraction change from 0 to 1, and the reaction zone thickness l_r, in correspondence of the stoichiometric mixture fraction, where the reaction takes place.
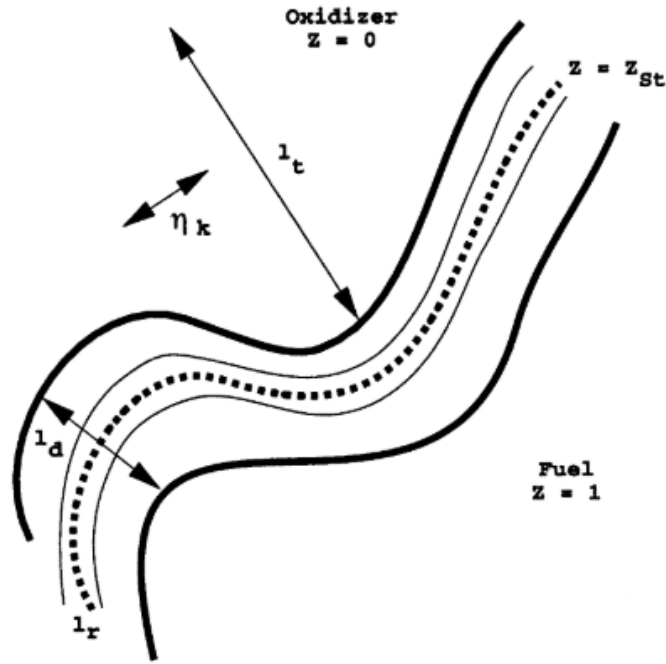
Figure 2.16: Schematic of a non-premixed turbulent flame [24]

In order to characterize the turbulent combustion, these chemical scales need to be compared with characteristic scales of the flow field. Some non-dimensional quantities allow to relate chemical and turbulent scales to characterize the turbulent flame behaviour. The Reynolds number characterizes the flow turbulence intensity and it is defined as follow:

$$Re = \frac{u' \cdot l_t}{\nu} \tag{2-6}$$

where u' is the turbulence intensity and l_t is the largest length scale. The turbulent Damkoler number relates the chemical and flow time scales, but it can also be defined in terms of laminar flame speed S_L and laminar flame thickness l_F.

$$Da = \frac{t_t}{t_F} = \frac{S_L \cdot l_t}{u' \cdot l_F} \tag{2-7}$$

The Karlovitz number describes the flame front straining by comparing the laminar flame time scale t_F to the Kolmogorov time t_k.

$$Ka = \frac{t_F}{t_k} = \frac{l_F}{t_k \cdot S_L} \tag{2-8}$$

33

Usually, these parameters are grouped in diagrams and allow to identify different regimes. Several diagrams are proposed in the literature. In this chapter, the phase diagram developed by Peters [25] for non-premixed turbulent flames is proposed.

Turbulent flows with combustion are mainly divided in two classes: diffusion and premixed combustion systems. The main difference between them is that, in diffusion system, fuel and oxidizer are introduced separately in the combustor and they need to mix together before burning, whereas, in premixed system, fuel and oxidizer are already mixed at the molecular level before being injected. For this reason, non-premixed combustion is highly dependent on the mixing process. In a diffusion combustion system, time scales for convection, diffusion and reaction are involved, premixed system removes the diffusion process [25].

- **Non-premixed combustion**

Non-premixed combustion systems are associated with diffusion flames, in which the diffusion process is considered the rate controlling step. The structure of a diffusion flame is strictly related to the amount of mixing between the fuel and the oxidizer and the combustion is treated as a mixing problem. Thus, the thermochemistry is represented by the mixture fraction, which is the local mass fraction of burnt and unburnt elements of the fuel stream.

Non-premixed flames are not characterized by intrinsic length scales because the flame front is wrinkled and strictly related to the turbulent flow conditions. For this reason, it is difficult to identify regimes on a diagram for non-premixed flames because the local flame scale depends on the local flow conditions [24].
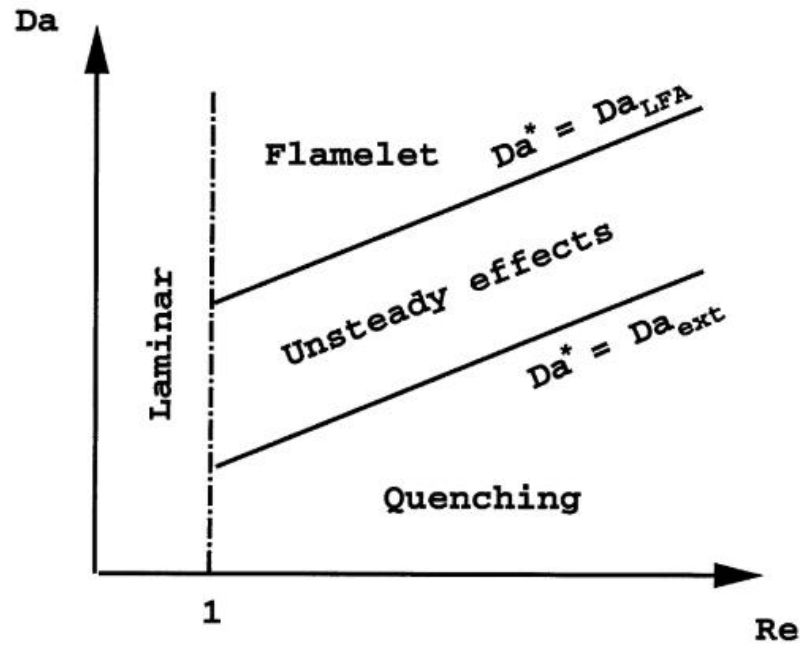
Figure 2.17: Phase diagram for non-premixed flames developed by Peters [24]

In the diagram illustrated in Figure 2.17, turbulent non-premixed combustion regimes are represented. The part of the chart in which the turbulent Reynolds number is lower than 1 is not of interest because related to laminar flames. For higher Reynolds number and Damkoler number sufficiently high to allow the assumption of fast chemistry, the flame front is thin and can be considered as a series of laminar flame elements defined as flamelets. When the chemical time scale starts to increase in such a way that it is not still possible to assume fast chemistry, the laminar flame behaviour disappears and it is replaced by unsteady effects. For lower Damkoler numbers, which correspond to large chemical times, extinctions may occur.

- **Flamelet concept**

The Flamelet concept is based on the idea that the flame front is composed by a series of flame elements which have the structure of a laminar flame and is embedded in a turbulent flow. The Flamelet model assumes a fast chemistry, which means that it is unable to capture non-equilibrium effects and slow chemistry processes such as NO_x production [2]. For this reason, a specific thermal NO_x model is used to predict NO_x emissions, which is described in Section 3.7. This method has been developed in order to reduce the

35

computational cost compared to complex chemistry models. Instead of solve the equations for each species involved in the combustion, the chemistry is pre-calculated in 0D or 1D laminar flames using detailed chemical mechanisms and tabulated in such a way to be used during the simulation. The concentration of species and the temperature field is parametrized by two or more variables.

2.5 Thermoacoustic Instabilities

Thermoacoustic instabilities are the result of interactions between combustion process and acoustic properties of the combustion chamber under certain conditions [1]. In a gas turbine combustor, there are several noise sources which can trigger pressure oscillations, such as perturbations in the inlet flow velocity. High amplitude pressure oscillations in combustion systems are mainly due to acoustic feedback because perturbations in inlet flow can cause fluctuations in the equivalence ratio and, consequently, in the unsteady heat release rate. This perturbation will generate a pressure oscillation, which will propagate through the combustion chamber and will be reflected back to combustion zone, minus the acoustic losses in the chamber, with a time delay dependant on the combustor geometry. A schematic of the acoustic feedback is depicted in Figure 2.18. Acoustically, the flame acts as an amplifier and, if the degree of amplification due to the flame is greater than the acoustic losses, growth of the oscillation will occur [1].
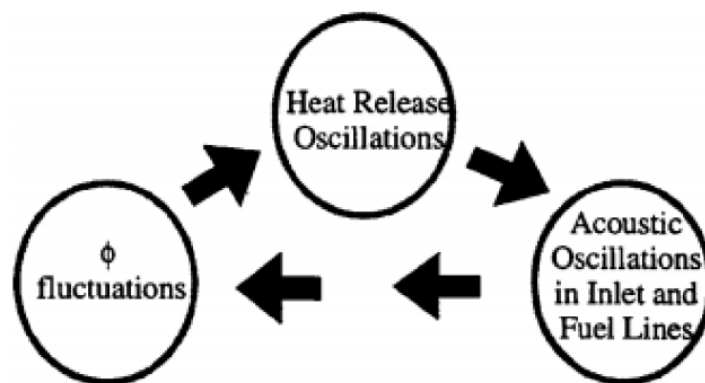
Figure 2.18: Schematic of the acoustic feedback responsible for combustion instabilities [26]

These heat release oscillations may be due to perturbations of the velocity, pressure, temperature, and reactants composition in the combustion system [26]. This mechanism is called self-excited because it does not require an external source to be activated. For these self-excited oscillations to occur, two conditions must be met. Firstly, the unsteady heat release rate must be in phase with the fluctuating acoustic pressure, in order to add that energy to the unsteady process. Secondly, the amount of energy addition must exceed the amount of energy dissipation [26].

For industrial gas turbines, environmental noise does not represent a big concern because of the presence of heavy and resistant casing, enclosures, inlet and outlet silencing, but thermoacoustic problems are a major issue because they can lead to significant vibrations and component cracking [35]. Generally, diffusion flames are less likely than premixed flames to suffer thermoacoustic problems, but it is important to consider it from the early stage of design to avoid a significant redesign of the combustor in later stages. Micromix combustion is inherently diffusion-based, and often assumed to be less prone to thermoacoustic problems than lean premixed systems. However, the flames are more compact and intense than conventional diffusion flames, thus more like lean premixed flames. Furthermore, micromix combustors are likely to have less dilution and cooling air than conventional diffusion systems. This leads to lower acoustic damping and thus increased risk of instabilities.

3 CFD Modelling

CFD approach is increasingly assuming a primary role in the representation of physical phenomena in order to obtain an understanding of the flow field behaviour and improve the quality of a design. This is a powerful tool to simulate the flow field because it is low cost and time consuming, particularly with the increasing computational power. However, it is fundamental to bear in mind that CFD is not an exact method and it is affected by some discrepancies compared to reality because very complex physics phenomena are modelled by different methods. Although the increasing use of CFD approach, experimental results are still required and necessary in order to collect appreciable data and information of the phenomena and validate the numerical solution. The problem is that experiments are very expensive and a long set-up time is required. In this case, experiments on the micromix combustor are not started yet and it is still not possible to validate the numerical results. Nevertheless, the physical models employed to set-up the flow field have been selected after a series of studies, in which some models have been tested, compared with LES results and the prediction of physical phenomena, as result of the literature review about experiments done on Micromix combustors. Most of these studies have been conducted by M. Lopez Juarez and described in his research work [44].

3.1 Single Injector Geometry

In this numerical analysis, a single injector geometry has been investigated. A single injector analysis is able to provide a characterization of the flow dynamics and the flame behaviour, however this analysis is limited by the impossibility to assess the flames interaction. Taking advantage of the symmetric nature of the injector array, a single injector volume is obtained from the whole combustor design in order to reduce the size of the domain and, hence, the computational cost. In Figure 3.1, a representation of the whole injector array, composed by 52 injectors, allows to understand where the single injector geometry comes from.
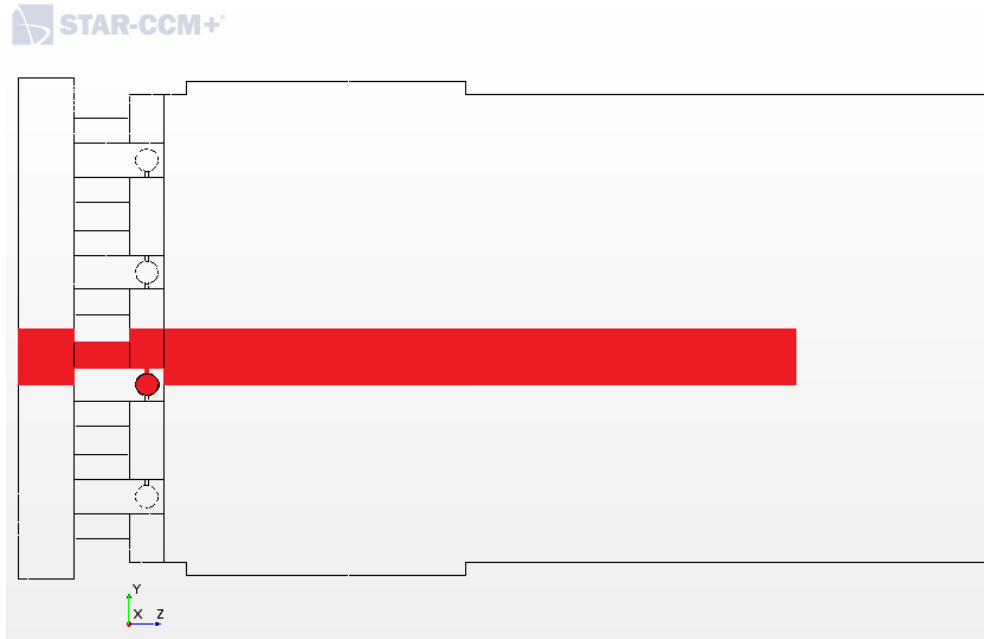
Figure 3.1: Layout of the injector array and the single injector geometry in red

As shown in Figure 3.4, the air and the hydrogen streams are introduced separately, in order to maintain the non-premixed characteristics of hydrogen micromix injectors, and perpendicularly, to represent the jet in cross-flow behaviour. The air is introduced through a square gate and then is accelerated passing in a channel. The shape of this channel is one of the parameters which has been varied in this work. In order to maintain the non-dimensional mass flow constant and consider the same operating conditions for all the simulations, the air gate area has been kept unchanged. In this context, several configurations of air gate have been tested and compared, each of them characterized by a different height and width. They are illustrated in Figure 3.2.
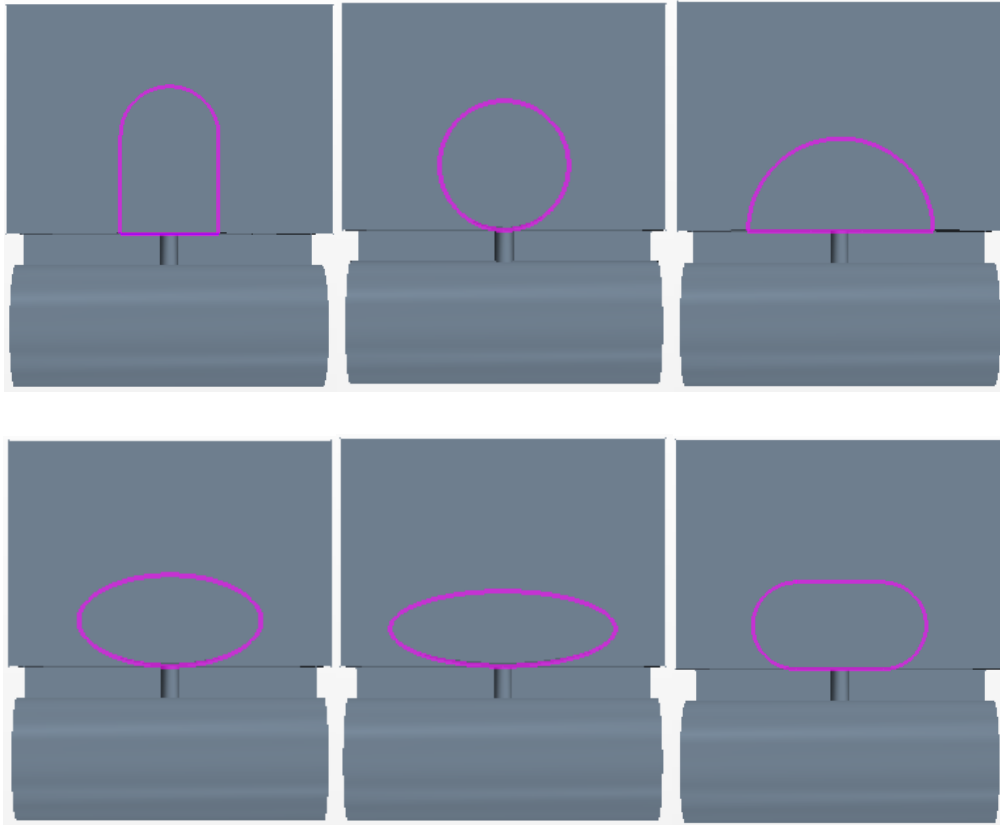
Figure 3.2: Representation of air gate shapes

The hydrogen is introduced through two separated inlets with the same mass flow, as illustrated in Figure 3.4. These two streams are gathered in a cylindrical tank and the whole hydrogen mass flow is accelerated in a pipe with a diameter of 0.3 mm before being injected. Downstream the step where the outer recirculation vortex is generated, the domain develops for 100 mm, maintaining a constant area.

3.2 Meshing Strategy

The meshing procedure is a fundamental process in a CFD simulation because it is responsible of the division of the fluid dynamic domain in cells where the transport equations will be solved. For this reason, it is fundamental to create a mesh with enough cells to capture all the relevant flow phenomena and, at the same time, not too fine to reduce as much as possible the computational cost. In order to estimate a good value for the cell size, it is necessary to carry out a mesh independence study. It has been done by M. Lopez Juarez [44], analysing three

different mesh sizes: 0.08, 0.1 and 0.125 mm. The intermediate cell size has shown to be appropriate, but in this project it has been used the finest mesh (0.08 mm) because the computational domain is small and a fine mesh ensures to capture all the significant length scales, particularly in the flame zone and in the field near the jet in cross-flow. Since STAR-CCM+ solver is able to generate automatic meshes, a polyhedral mesh has been chosen instead of a hexahedral mesh because of its advantages. One of this is a better approximation of gradients because each cell has a big number of adjacent cells. Additionally, a polyhedral mesh is particularly appropriate to simulate recirculating flows. It can be explained because a hexahedral cell has three optimal flow directions, whereas a polyhedral cell has more optimal flow directions depending on the number of faces. These advantages lead to an accurate solution with a lower number of cells [27]. A prism layer mesh has been used for the hydrogen injector and for the plane where the hydrogen hole is located because it is necessary to capture the near-wall behaviour of the two streams in order to estimate properly their interaction and the jet in cross-flow structures. In detail, 10 prism layers have been placed, each of them characterized by a thickness 50% higher than the previous one.
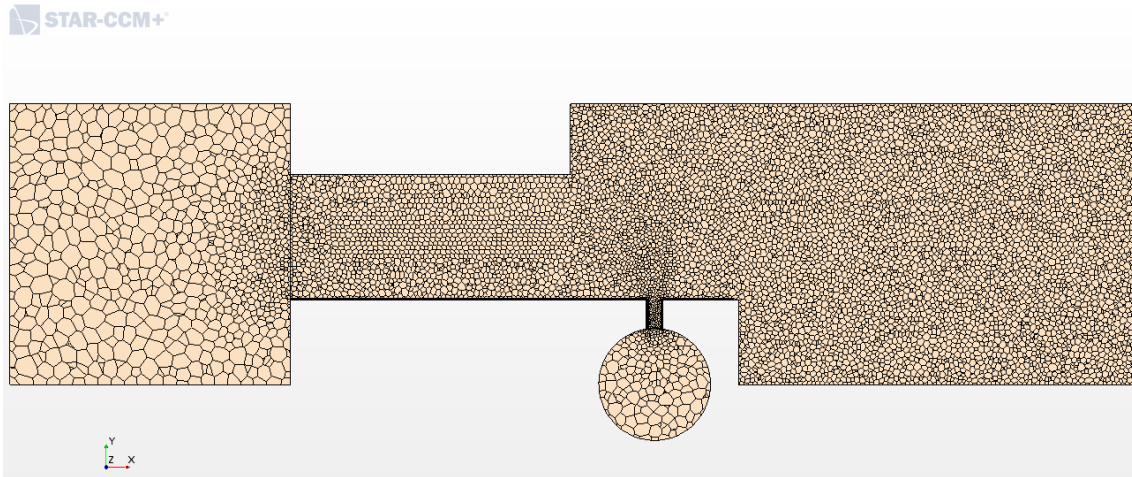
Figure 3.3: Polyhedral mesh of the flame zone at the symmetry plane

As shown in Figure 3.3, in order to reduce the computational cost, the fine mesh with a base size of 0.08 mm has been assigned to the flame region, where complex phenomena such as the jet in cross-flow and the combustion process

require a fine mesh to capture all the relevant length scales. In the regions where the air and the fuel are introduced is not required a fine mesh and the base size has been set four times higher (0.24 mm). The same mesh properties have been applied for the final volume of the domain, where the reacting flow is completely developed and stabilized downstream the recirculation vortices and a coarse mesh is acceptable. In correspondence of all the interfaces between these regions characterized by different mesh properties, the mesh has been customized to make the transition as smooth as possible and have a better approximation of gradients. The total number of cells produced is around 1.5 million.

3.3 Boundary Conditions

In Figure 3.4, a representation of the single injector allows to identify the boundary conditions of the computational domain. The air is introduced through the air inlet with a temperature of 600 K, in order to reproduce the air conditions downstream the combustor at the operating conditions considered in this study.
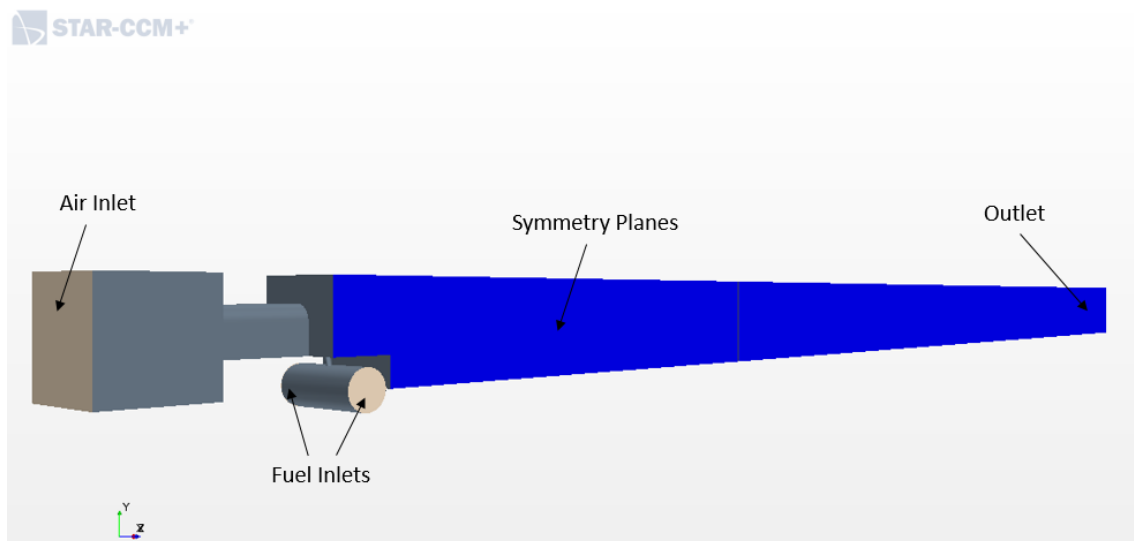
Figure 3.4: Three-dimensional model showing boundary conditions

A set of operating conditions for the test combustor, depicted in Figure 3.5, has been identified, for each of them considering a wide range of equivalence ratio in the lean combustion zone. In this study, only one operating condition has been selected, in order to compare the geometric variations effects at the same

43

conditions. In detail, the high-pressure condition has been used for all the geometries, characterized by 15 bar and an equivalence ratio equal to 0.4. A matrix comprising all the cases have been developed, in which are grouped several combinations of different pressure, air temperature and equivalence ratio. For each case, the fuel and the air mass flows for the whole injector array have been calculated.

Proposed tests for baseline design

	P (bar)	T_air (K)	Φ	W_air (g/s)	W_fuel (g/s)
Case1		300	0.50	9.48	0.086
Case2			LBO		
Case3	1		0.50		0.070
Case4		450	0.40	7.74	0.056
Case5			0.30		0.042
Case6			LBO		
Case7			0.50		0.350
Case8	5	450	0.40	38.68	0.280
Case9			0.30		0.210
Case10			LBO		
Case11			0.50		0.699
Case12	10	450	0.40	77.36	0.559
Case13			0.30		0.419
Case14			LBO		
Case15			0.50		1.284
Case16		300	0.40	142.13	1.027
Case17			0.30		0.771
Case18			LBO		
Case19			0.50		1.049
Case20		450	0.40	116.05	0.839
Case21			0.30		0.629
Case22	15		LBO		
Case23			0.50		0.908
Case24			0.45		0.817
Case25			0.40		0.727
Case26		600	0.35	100.50	0.636
Case27			0.30		0.545
Case28			0.25		0.454
Case29			0.20		0.363

Figure 3.5: Matrix comprising the proposed test cases for the baseline configurations

In order to accomplish that equivalence ratio of 0.4, the fuel mass flow has been calculated. As shown in Figure 3.4, the fuel stream is introduced through two separated inlets, flowing in opposite direction until they mix together and enter the fuel injector. Both fuel and air inlets have been set as mass flow inlet and their properties are summarized in the table below. All the boundary condition settings are gathered in Table 3.1.

Boundary	*Variable*	*Value*
Operating Conditions	Pressure	15 bar
	Equivalence Ratio Φ	0.4
Air Inlet	Type	Mass Flow Inlet
	Fluid	Air (23.3% O_2+ 76.7% N_2)
	Mass Flow Rate	1.9327 g/s
	Temperature	600 K
	Turbulence Intensity	5%
Fuel Inlet	Type	Mass Flow Inlet
	Fluid	Hydrogen (100% H_2)
	Mass Flow Rate	0.02272 g/s
	Temperature	300 K
	Turbulence Intensity	5%

Table 3.1: Boundary condition settings

The outlet surface has been set as pressure outlet and all the other surfaces as wall, except the four surrounding the combustion zone. Several simulations have been run in order to identify an appropriate boundary type which simulates properly the periodicity of the combustion domain. Some configurations have been compared, combining in different ways symmetry planes and walls. The best solution is to set all the four surfaces as symmetry plane, as shown in Figure 3.4, where they are represented in blue. The other cases were not able to capture the aerodynamic structures typical of the micromix combustion concept, described previously in Chapter 2. In particular, the results obtained using wall as boundary type has shown several fluctuations in the solution, which does not reach convergence. In Figure 3.6, the two vector plots refer to the single injector model with surfaces surrounding the flame zone set as wall and symmetry

respectively. As shown, the symmetry planes are able to generate the inner and outer recirculation vortices described in the literature, whereas the presence of the wall favours the formation of several smaller vortices throughout the domain, generating an unstable solution. For this reason, all the surfaces surrounding the flame zone have been set as symmetry plane.
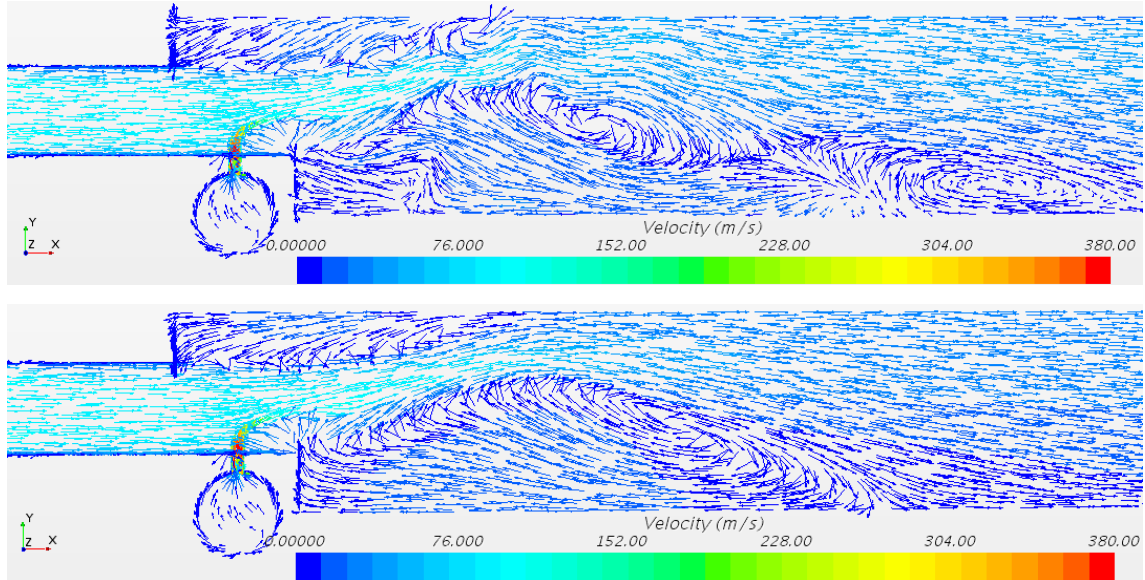
Figure 3.6: Vector plots of single injector model with surfaces surrounding the flame zone set as wall and symmetry respectively

3.4 Turbulence Model

Turbulence is an extremely complex phenomenon characterized by the formation of unsteady vortices in a wide range of length scales. This is mainly due to a high amount of kinetic energy present in some regions of the fluid flow, where the intensity of the fluid's viscosity is not enough to damp the turbulent effect. Because of this extremely irregular flow field, flow quantities are characterized by several local fluctuations of different scales. The turbulence of a fluid flow is generally represented by the dimensionless Reynolds number, which relates the kinetic energy to the fluid's viscosity. It is defined as follow:

$$Re = \frac{\rho U L}{\mu} = \frac{U L}{\nu} \qquad \text{(3-1)}$$

Where ρ is the fluid's density, U is the velocity of the flow field, L is the characteristic length, μ and ν are respectively the dynamic and kinematic viscosities of the fluid.

Due to the prohibitive computational cost required to solve the governing equations of a turbulent flow, some modelling strategies have been developed to capture the main turbulent phenomena in CFD. The main approaches are three and differ each other for their complexity and computational cost: Reynolds-Averaged Navier-Stokes (RANS) approach, Large Eddy Simulation (LES) and Direct Numerical Simulation (DNS). In Figure 3.7, the turbulence energy spectrum as a function of wave number and a local temperature evolution over time have been included to highlight the computational complexity of the different approaches.
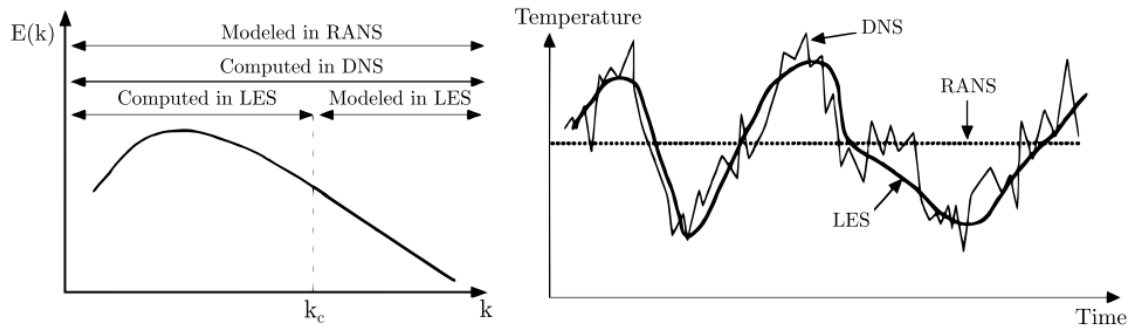
Figure 3.7: Turbulence energy spectrum as a function of wave number (a) and local temperature evolution over time (b) [28]

Direct Numerical Simulation (DNS)

This approach is the most computationally expensive because the governing equations of the turbulent flow are directly solved. It allows to capture all the fluctuating quantities, even those characterized by the smallest scales which are resolved in time and space. Due to the extremely high computational cost required, it is unfeasible to consider this approach for most of the industrial applications. Therefore, the introduction of alternative methods in which the Navier-Stokes equations are not solved for all the time and length scales was deemed indispensable.

Large Eddy Simulation (LES)

In order to reduce the computational cost compared to the DNS, Large Eddy Simulation is a transient technique in which the large scales of the turbulence are directly resolved in time and space everywhere in the flow field, whereas the small scales are modelled [33]. The difference between large and small scales is identified by the cut-off length scale k_c. In this case, the Navier-Stokes equations which govern the flow field evolution are subject to a spatial filtering.

Although the computational cost of LES is not prohibitive, it is still excessive, particularly for applications characterized by large computational domain.

Reynolds-Averaged Navier-Stokes (RANS) Turbulence Models

This approach allows a further reduction in computational cost by applying a time-averaging process. This method is based on a simple concept: all the flow quantities present in the governing equations are decoupled in a mean value and its fluctuating component

$$\phi = \bar{\phi} + \phi' \qquad\qquad \textbf{(3-2)}$$

$$\bar{\phi} = \frac{1}{\Delta t} \int_{t_0}^{t_0 + \Delta t} \phi(t) dt \qquad\qquad \textbf{(3-3)}$$

Where $\bar{\phi}$ and ϕ' are respectively the mean value and the fluctuating component of a general flow quantity and t is the time. The RANS equations are formally equal to the Navier-Stokes equations, but the instantaneous values are replaced by the time-averaged values. Moreover, in the momentum transport equation an additional term appears, the Reynolds stress tensor, which accomplishes the system of governing equations. The different RANS turbulent models differ each other depending how this Reynolds stress tensor is modelled in terms of mean flow quantities [33]. The eddy viscosity models are the most common and are based on the concept that the derivation of the turbulent eddy viscosity μ_t allows to model the Reynolds stress tensor in terms of mean flow quantities. The turbulent eddy viscosity is obtained by solving additional transport equations for scalar quantities.

In this research work, the k-ω model has been used. This method solves transport equations for the turbulent kinetic energy k and the specific dissipation rate ω. The main reason why it was chosen is its ability to better predict the presence of vortices and model swirling flows than other models available, such as k-ε [2].

3.5 Chemistry and Turbulence-Chemistry Interaction Models

When reacting flows are treated, certainly the governing equations are influenced and modified to account for the reaction process. Unlike the continuity equation and the conservation equation for the momentum which are not affected, the conservation equation for the energy is adjusted to account for the heat released during the reaction and a source term is added to the equation. In addition, the governing equations are completed by the conservation equations for species mass fractions. In order to calculate the source term, the estimation of the rates of all the reactions involved in the chemical mechanism is necessary. The reaction rate is dependent upon rate constants and the concentration of the species. Reaction constants take into account the energy required to activate a reaction and are generally calculated using the Arrhenius equation:

$$k = AT^{\beta} e^{\left(-\frac{E_a}{RT}\right)} \qquad \text{(3-4)}$$

Where A is the frequency factor, E_a is the activation energy, β is the temperature exponent and R is the universal gas constant [33].

In Simcenter STAR-CCM+, two different approaches to handle reacting flows are available: reacting species transport and flamelet. In reacting species transport models, a conservation equation is solved for each species involved in the combustion. Particularly in complex reactions, this approach represents a significant increase in terms of computational cost. In Flamelet models, instead of solving a transport equation for each species, the thermo-chemistry of the reaction is parametrized by two or more parameters, depending on the specific model used. In this way it is possible to reduce the number of transport equations and the chemistry in the reaction mechanism is solved before the run-time [33].

In the present study, the Flamelet Generated Manifold model was employed, considering previous work [19] already conducted at Cranfield University to select a chemistry model suitable for the properties of hydrogen combustion. It is appropriate to model premixed and partially-premixed flames. The hydrogen flame can be considered as a partially-premixed flame due to its particular nature between a diffusion and a premixed flame. This allows to model it as a diffusion flame and, at the same time, capture the partial-premixing effects of the jet in cross-flow [2]. The FGM model assumes that the thermo-chemical state of a turbulent flame is similar to that in a laminar flame and it is parameterized by three variables: the mixture fraction Z, the progress variable c and the enthalpy h. The mixture fraction represents the elemental mass fraction that originates from the fuel stream and assumes a value of 1 for the fuel stream and 0 for the oxidizer stream. In STAR-CCM+, a transport equation for the mixture fraction is solved to achieve species mass fractions [33]. The progress variable is the only one reacting variable which defines the reaction progress and assumes a value of 0 for the unburnt condition and 1 for the burnt condition. This variable can vary between these two values to identify intermediate conditions, which leads to a non-zero flame thickness. However, this zone is restricted in a thin layer where the combustion takes place. Within the Flamelet table, the enthalpy is parameterized by the heat loss ratio, which describes the normalized enthalpy difference between the cell enthalpy and its adiabatic state. In the transport equation for the progress variable, a term which refers to the progress variable source appears. Depending on the model chosen, the source term is calculated in different ways. In this case study, the FGM Kinetic Rate is used, in which the progress variable source is derived from the chemical kinetic reaction rate.

Within the FGM model, it is required to import a combustion mechanism, in which the species involved and the reactions are specified. For each reaction, the activation energy E_a, the temperature exponent β and the pre-exponent coefficient A necessary to calculate the rate constants from the Arrhenius equation are indicated. Several hydrogen combustion mechanisms characterized by different levels of complexity were published over the last decade. G. Babazzi carried out a hydrogen combustion mechanisms comparative study in her

research project [20] in order to identify the reaction mechanism that could accurately predict hydrogen/air kinetics over a range of operating conditions, particularly at high pressure conditions. She concluded that all the reaction mechanisms analysed, apart from one, are suitable to model the hydrogen Micromix flame. In the present study, the hydrogen combustion mechanism developed by Naik in 2009 and composed by 21 reactions was employed. All the reactions and coefficients used in this mechanism are grouped in Table 3.2.

#	Reaction	A	β	E_a [J/kmol]
1	$H+O_2=O+OH$	3.55e15	-0.4	6.94544e7
2	$O+H_2=H+OH$	50800	2.7	2.631736e7
3	$H_2+OH=H_2O+H$	2.16e8	1.5	1.435112e7
4	$O+H_2O=OH+OH$	2970000	2	5.60656e7
5	$H_2+M=H+H+M$	4.58e19	-1.4	4.35136e8
6	$O+O+M=O_2+M$	6.16e15	-0.5	0
7	$O+H+M=OH+M$	4.71e18	-1	0
8	$H+OH+M=H_2O+M$	3.8e22	-2	0
9	$H+O_2(+M)=HO_2(+M)$	6.37e20	-1.72	2196600
10	$HO_2+H=H_2+O_2$	1.66e13	0	3443432
11	$HO_2+H=OH+OH$	7.08e13	0	1234280
12	$HO_2+O=O_2+OH$	3.25e13	0	0
13	$HO_2+OH=H_2O+O_2$	2.89e13	0	-2079448
14	$HO_2+HO_2=H_2O_2+O_2$	4.2e14	0	5.0208e7
15	$HO_2+HO_2=H_2O_2+O_2$	1.3e11	0	-6819920
16	$H_2O_2(+M)=OH+OH(+M)$	1.2e17	0	1.90372e8
17	$H_2O_2+H=H_2O+OH$	2.41e13	0	1.661048e7
18	$H_2O_2+H=HO_2+H_2$	4.82e13	0	3.32628e7
19	$H_2O_2+O=OH+HO_2$	9550000	2	1.661048e7
20	$H_2O_2+OH=HO_2+H_2O$	1e12	0	0
21	$H_2O_2+OH=HO_2+H_2O$	5.8e14	0	4e7

Table 3.2: Hydrogen combustion mechanism developed by Naik

The FGM model described in the previous section depicts the flame as a set of laminar flamelets embedded in the turbulent flow, but not influenced by the turbulence. In reality, the reaction rate is affected by both turbulence and chemistry and this phenomenon is known as turbulence-chemistry interaction. In order to take into account this interaction in Flamelet models, it is common to apply probability density functions PDFs for the Flamelet variables, which allow to create a local distribution of temperature and species mass fractions.

3.6 Diffusion Coefficients

The combustion is characterized by several diffusion processes. Generally, they are modelled by some non-dimensional parameters which relate different diffusion processes. One of these is the Lewis number, which identifies the diffusion coefficient of each species involved in the reaction D_k and compares it with the heat diffusivity coefficient D_{th}. The Lewis number is defined as follow:

$$Le_k = \frac{D_{th}}{D_k} = \frac{\lambda}{\rho c_p D_k}$$

(3-5)

Where λ is the heat diffusion coefficient, c_p is the specific heat and ρ is the flow density. This value is very low for hydrogen (around 0.2), which means that thermal diffusivity is negligible compared to the diffusion of hydrogen molecules. However, it has been set to calculate the thermal conductivity directly from the Flamelet table, instead of specifying the Lewis number.

The Prandtl number describes how much the momentum is diffused through the flow compared to the heat transfer. It compared the viscous and thermal diffusion rates and it defines as follow:

$$Pr = \frac{\nu}{\alpha} = \frac{\mu c_p}{\lambda}$$

(3-6)

Where ν and α represent the momentum and thermal diffusivity. In order to find an accurate value of Prandtl number for hydrogen, a sensitivity study was carried out by R. B. Abdallah [19]. The results of this study show that a value of 0.85 correctly predict the relationship between the momentum and heat diffusion.

The turbulent Schmidt number relates the turbulent momentum transport and the turbulent mass transport. It is defined as:

$$Sc_t = \frac{\mu_t}{\rho D_t}$$

(3-7)

Where μ_t is the turbulent viscosity of the flame and D_t is the turbulent diffusivity. A sensitivity study on the turbulent Schmidt number has been performed by M. Lopez Juarez [44] and it has led to a value of 0.2.

3.7 Thermal NOₓ Model

The prediction of key trends of NOₓ emissions is one of the main outcomes of this research project. In order to obtain a quantitative estimation of NOₓ production, a CFD approach has been employed. Since NOₓ concentration is relatively low compared to other species concentrations, NOₓ chemistry is decoupled from the main combustion and flow field calculations and a specific model for the calculation of nitric oxide concentration is available in STAR-CCM+. Thermal NOₓ is the only source of NOₓ taken into account in this analysis, whereas Fuel and Prompt NOₓ are respectively absent and very low, for this reason can be neglected. This NOₓ formation is based on the Zeldovich mechanism.

The transport equation is the same for all NOₓ models, with the addition of reacting source terms to account for each NOₓ source [33].

$$\rho \frac{\partial Y_{NO_x}}{\partial t} + \nabla \cdot \left[\rho \boldsymbol{v} Y_{NOX} - [\rho D_f + \frac{\mu_t}{\sigma_t}] \nabla Y_{NO_x} \right] = \dot{\omega}_{NOX,therm} + \dot{\omega}_{NOX,prompt} + \dot{\omega}_{NOX,fuel}$$

(3-8)

Thermal NOₓ is produced by oxidation of atmospheric nitrogen at elevated temperature because a high activation energy is required to break strong bonds of molecular nitrogen. This NOₓ emissions model considers the following three reactions for the nitric oxide formation:

$$N_2 + O \leftrightarrow NO + N$$

(3-9)

$$N + O_2 \leftrightarrow NO + O \tag{3-10}$$

$$N + OH \leftrightarrow NO + H \tag{3-11}$$
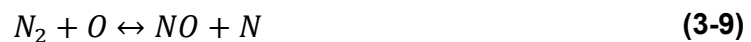
Depending on the temperature, each reaction tends to move in a preferred direction and it is indicated by forward and backward rate constants, experimentally measured and critically evaluated by Baulch et al. [34].

$$k_{f1} = 1.8 \cdot 10^{11} \cdot e^{-\left(\frac{38370}{T}\right)} \qquad k_{b1} = 3.8 \cdot 10^{10} \cdot e^{-\left(\frac{425}{T}\right)} \tag{3-12}$$

$$k_{f2} = 1.8 \cdot 10^{7} \cdot T \cdot e^{-\left(\frac{4680}{T}\right)} \qquad k_{b2} = 3.8 \cdot 10^{6} \cdot T \cdot e^{-\left(\frac{20820}{T}\right)} \tag{3-13}$$

$$k_{f3} = 7.1 \cdot 10^{10} \cdot e^{-\left(\frac{450}{T}\right)} \qquad k_{b3} = 1.7 \cdot 10^{11} \cdot e^{-\left(\frac{24560}{T}\right)} \tag{3-14}$$

As these rate constants are known, the net rate of formation of NO is given by the following expression:

$$\frac{d[NO]}{dt} = k_{f1}[O][N_2] + k_{f2}[N][O_2] + k_{f3}[N][OH] - k_{b1}[NO][N] \tag{3-15}$$
$$- k_{b2}[NO][O] - k_{b3}[NO][H]$$

Where [X] is the molar concentration of X. Since the activation energy for oxidation of N is small, a quasi-steady state can be considered and the molar concentration of N can be expressed as:

$$[N] = \frac{k_{f1}[O][N_2] + k_{b2}[NO][O] + k_{b3}[NO][H]}{k_{b1}[NO] + k_{f2}[O_2] + k_{f3}[OH]} \tag{3-16}$$

Substituting eq. (3-16) in eq. (3-15), the rate of formation of NO can be simplified:

$$\dot{\omega}_{NO_{x,therm}} = \frac{2AC - 2BD[NO]^2}{C + D[NO]} \tag{3-17}$$

Where:

$$A = k_{f1}[O][N_2]$$

$$B = k_{b2}[O] - k_{b3}[H]$$

$$C = k_{f2}[O_2] + k_{f3}[OH]$$ (3-18)

$$D = k_{b1}$$

The formation of nitric oxide can be predicted by this model knowing the local concentration of few species, which are well estimated by the Flamelet model.

3.8 Thermoacoustic Modelling Strategy

Basically, it is possible to assess thermoacoustic instabilities in two different ways: through a self-excited method or a flame response method. The first one provides a complete thermoacoustic analysis by modelling the flow phenomena in a single CFD simulation [2], but it is required to simulate the whole combustor geometry, including accurate acoustic conditions at compressor exit and turbine inlet for a large time domain. Any instabilities which occur in the flow will be amplified by the flame through a feedback loop and, if the flame amplification exceeds the acoustic losses, the oscillations will get bigger until they reach a limiting amplitude [2]. This method does not require external forcing to disturb the flow and introduce perturbations, for this reason is defined as self-excited method, the pressure oscillations are amplified through a feedback loop. The main issue associated with this method is that it requires an extremely high resolution LES or DNS simulations, which limits the possibility to implement this method for academic cases until computational resources improve [2]. A comparison between the two approaches is depicted in Figure 3.8.
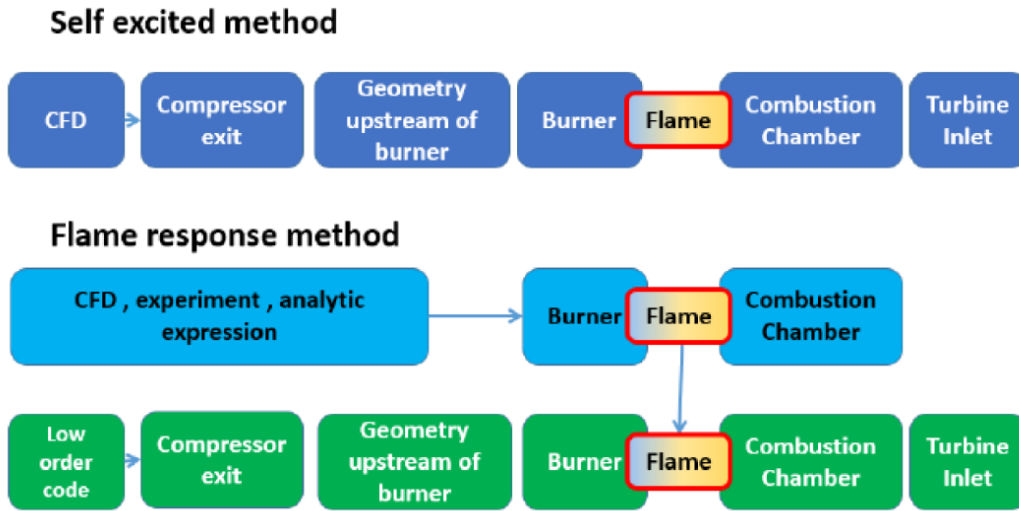
Figure 3.8: Representation of self-excited and flame response methods [35]

An alternative to the self-excited method is the flame response method, which requires much less computational costs. It allows to decouple the flame response and acoustic properties of the combustor. From acoustically forced LES simulations, it is possible to achieve the flame response, which is in the form of a transfer function, and relates the response of the unsteady heat release to perturbations in inlet flow. This transfer function can be a linear FTF model or non-linear FDF models. The Flame Transfer Function is defined as:

$$FTF(\omega) = \frac{Q'/\bar{Q}}{u'_{in}/\bar{u}_{in}}$$

(3-19)

The linear FTF represents the response of the unsteady heat release rate to small perturbations in the inlet flow velocity and it is a function of forcing frequency, with no dependence on the value of the fluctuating velocity.

The Flame Describing Function (FDF) model is not limited to small perturbations, but it can capture the non-linear effects present when the flame encounters larger perturbations. FDF is a function of both the forcing frequency and the magnitude of the inlet velocity perturbation and it is defined as:

56

$$FDF(\omega, |u'_{in}|) = \frac{Q'/\bar{Q}}{u'_{in}/\bar{u}_{in}}$$
<div align="right">(3-20)</div>

Once determined the flame response in the form of transfer function from numerical analysis, it is possible to achieve the acoustic response through a low-order combustor model. Combustor systems are modelled as a series of simpler subsystems (such as one-dimensional or annular ducts) and mathematical transfer function matrices are used to connect these lumped acoustic elements to each other [36]. This method enables to reduce significantly the computational cost since numerical simulations to simulate the acoustic behaviour of the whole combustion system are not requested anymore. In efforts to further reduce the computational expense of this method, studies using Unsteady Reynolds-Averaged Navier-Stokes (URANS) simulations as an alternative to LES have been performed [37]. FTFs obtained from URANS simulations has been found to be qualitatively similar to those obtained using LES, however with an underestimation of the amplification factor and phase lag [2].

The FTF can be measured experimentally by imposing small velocity fluctuations in the inlet flow and evaluating heat release fluctuations. Alternatively, it can be measured using time resolved CFD simulations. Due to the complexity of these methods, it is possible to calculate FTF using analytic formulations instead of the classic definition, which relates the response of the unsteady heat release to perturbations of the inlet velocity. Using this method, a time-varying simulation is not required and FTF can be determined using RANS simulations. Two different formulations are presented below:

- **Standard n-τ model**

$$FTF = n \cdot e^{-i\omega\tau}$$
<div align="right">(3-21)</div>

Where n is a proportionality constant and τ is the time delay between the inlet perturbation and the fluctuation in heat release. Thanks to this formulation, it will be possible to estimate FTF from RANS simulations deriving the time

delay. The standard n-τ model will overpredict high frequency oscillations and will therefore provide a conservative estimate for instabilities at high frequencies [2].

- **Modified n-τ model**

$$FTF = n \cdot \theta \cdot e^{-i\omega\tau} \qquad \textbf{(3-22)}$$

Where the θ term represents the influence of the time delay spread on the flame amplification and it is equal to:

$$\theta = \frac{\sin(\omega\Delta\tau)}{\omega\Delta\tau} \qquad \textbf{(3-23)}$$

In addition to the time delay, the time delay spread is also necessary to apply this analytic formulation, but the effect of reducing gain with frequency is represented [2].

4 Influence of Air Gate Shape Variation

In this section, the results achieved from the RANS simulations are reported and discussed in such a way to identify the physical phenomena occurring in the flow field and understand how the air gate shape variation influences the JICF and the micromix flame structure, in order to take advantage of this and improve the combustion performance parameters. For each configuration, two simulations have been run: a cold flow simulation, in which the air and the fuel streams do not react, and a reacting-flows simulation, in which the combustion takes place. The non-reacting analysis is necessary because it allows to capture the aerodynamic features of the JICF and the fuel-air mixing capabilities, without being affected by the combustion process, which alters the properties of the flow field.

The results are presented in terms of NO_x emissions, mixing properties, flame shape and position and time delay and, eventually, time delay spread, to estimate Flame Transfer Functions. A key trend for each of these performance parameters has been developed to assess the influence of the air gate shape.

4.1 Aerodynamic Features

First of all, the baseline configuration has been analysed and the main aerodynamic structures typical of a jet in cross-flow and a micromix flame have been identified. As clearly illustrated in Figure 4.1, the air stream passes throughout the air gate and deflects the hydrogen jet in the axial direction. As previously stated in Chapter 2, the jet penetration and trajectory are strictly dependent on the momentum flux ratio, which relates velocities and densities of the two streams. The momentum flux ratio is the same for all the different configurations because the air gate area and the operating conditions are kept constant in order to maintain the non-dimensional mass flow constant. Consequently, the mean velocity and the density are the same for the air stream. The calculated value is around 2.2, which is a relatively low value. It is reflected in the weak penetration of the jet, which is rapidly deflected and aligned in the cross-flow direction. For this reason, the reduction of the air gate height does not

represent a big limitation during the development of other air gate configurations because the risk of penetration within the inner recirculation vortex represents an issue for very low air gate height values. The inner recirculation vortex is generated downstream the air guiding panel, whereas the outer recirculation vortex downstream the injector plate. The micromix flame is stabilized between these two vortices within the shear layer.
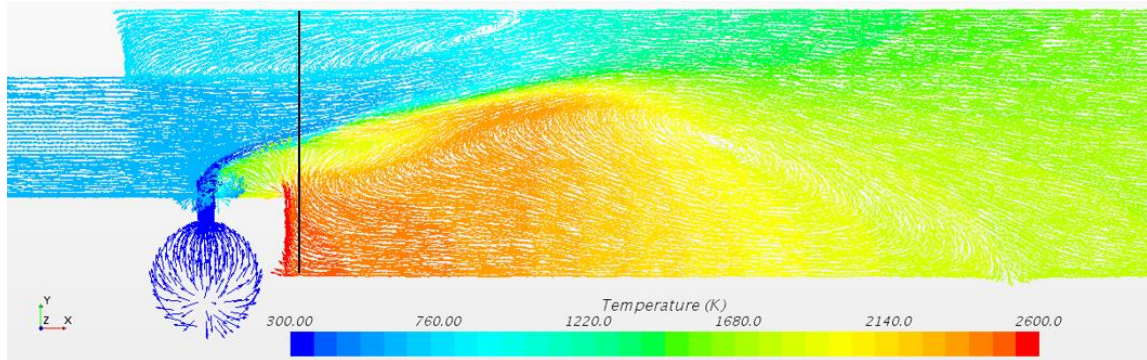
Figure 4.1: Vector plot with temperature contour at the symmetry plane

Figure 4.2 represents the vector plot of a section plane immediately downstream the injector plate. Its exact location is illustrated by the black line in Figure 4.1. This image allows the visualization of the counter-rotating vortex pair (CVP), typical of a jet in cross-flow structure. The formation of this structure is fundamental for the cross-flow entrainment in the far-field. The other vortical structures typical of a JICF, described in Section 2.2.1, are not captured by RANS simulation, probably because of the small scales of these turbulent phenomena and their unsteady behaviour. For this reason, the cross-flow entrainment in the near-field governed by these vortical structures could be slightly underestimated and, consequently, the mixing capabilities.
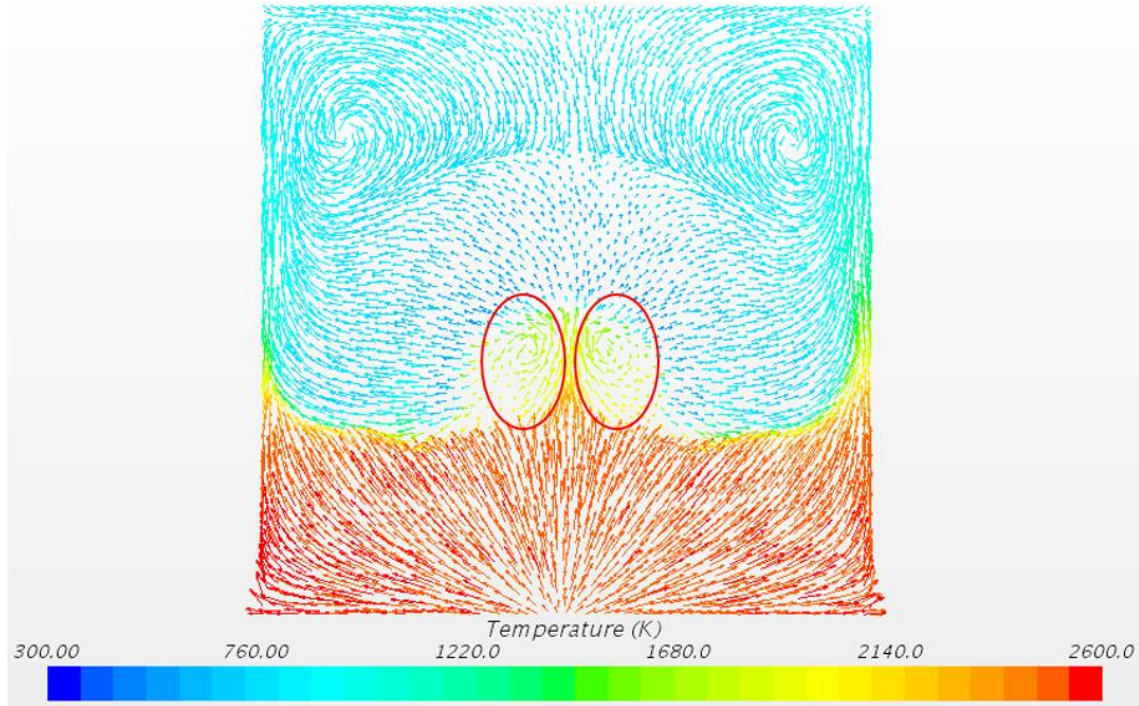
Figure 4.2: Vector plot with temperature contour at the section plane located in correspondence of the black line in Figure 4.1

4.2 Temperature Field

The temperature distribution within the computational domain assumes a fundamental role for two main reasons: firstly, it allows the identification of the flame shape and position and, secondly, it is able to provide a preliminary understanding of NO_x emissions because its formation mechanism is strictly related to the flame temperature.
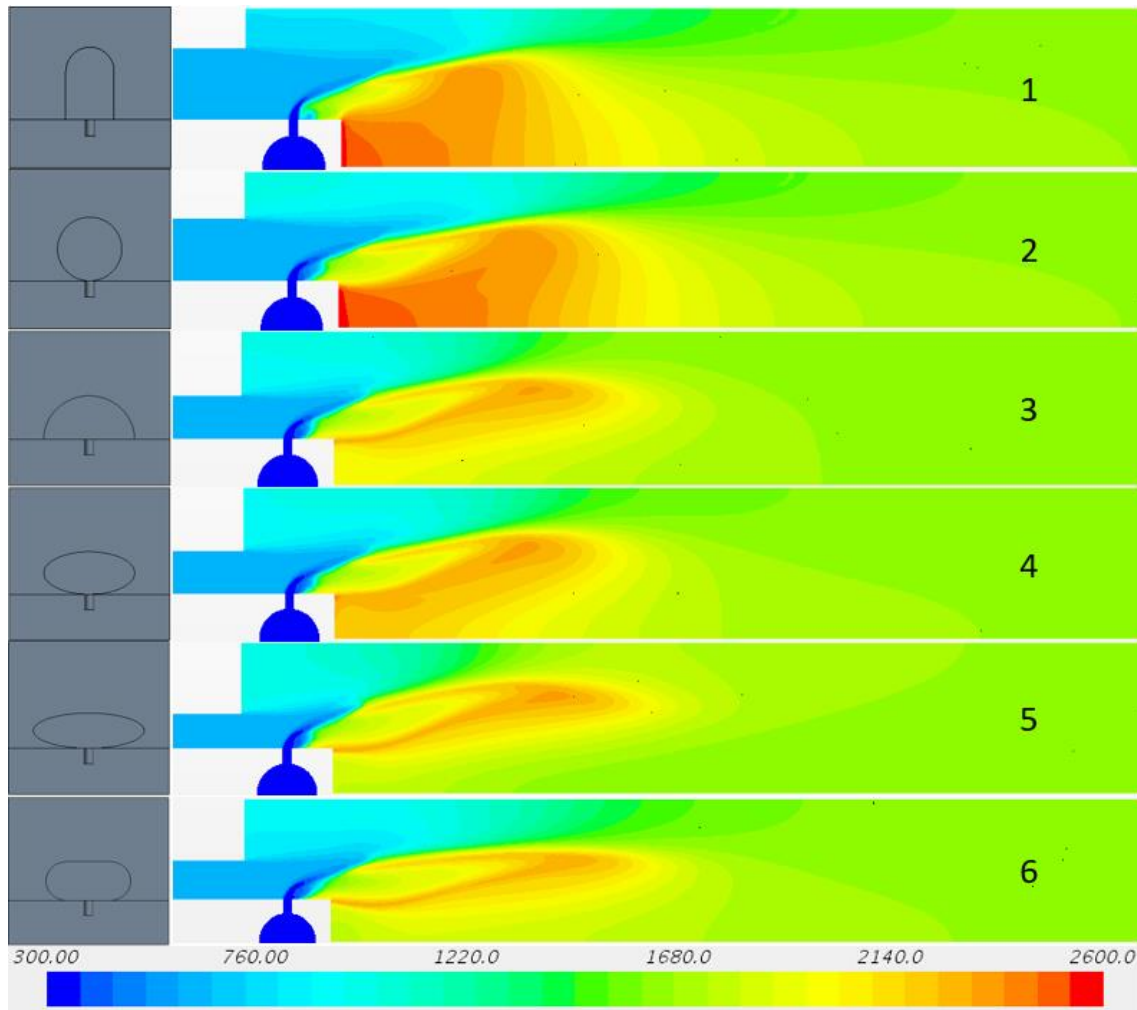
Figure 4.3: Temperature contours for 6 configurations characterized by different air gate shape at the symmetry plane

As shown in Figure 4.3, the 6 cases are characterized by significant differences. The temperature distribution for the first two cases reveals very high temperatures in the outer recirculation vortex, particularly close to the injector plate. It is extremely undesirable because these temperature values exceed the limit at which the dissociation starts and a significant production of NO_x could be expected. In addition, these temperature peaks are revealed in the recirculation zone: the hot stream is introduced and recirculates here, spending more time at very high temperature, which could drastically affect the NO_x production. Moreover, high temperatures in that region close to the injector plate must be avoided because it could significantly reduce the durability of the plate. The

injector plate is close to the hydrogen feed system and the heat transfer rate must be considered when designing the single injector and injector array.

Unlike the first two cases, configurations 3, 5 and 6 present a desirable temperature distribution, in which the temperature peak is located downstream the hydrogen flame, whereas the temperature in the recirculating vortices is significantly lower and, consequently, even the NO_x emissions are expected to be lower. The configuration 4 represents an intermediate case between the two different distributions described.
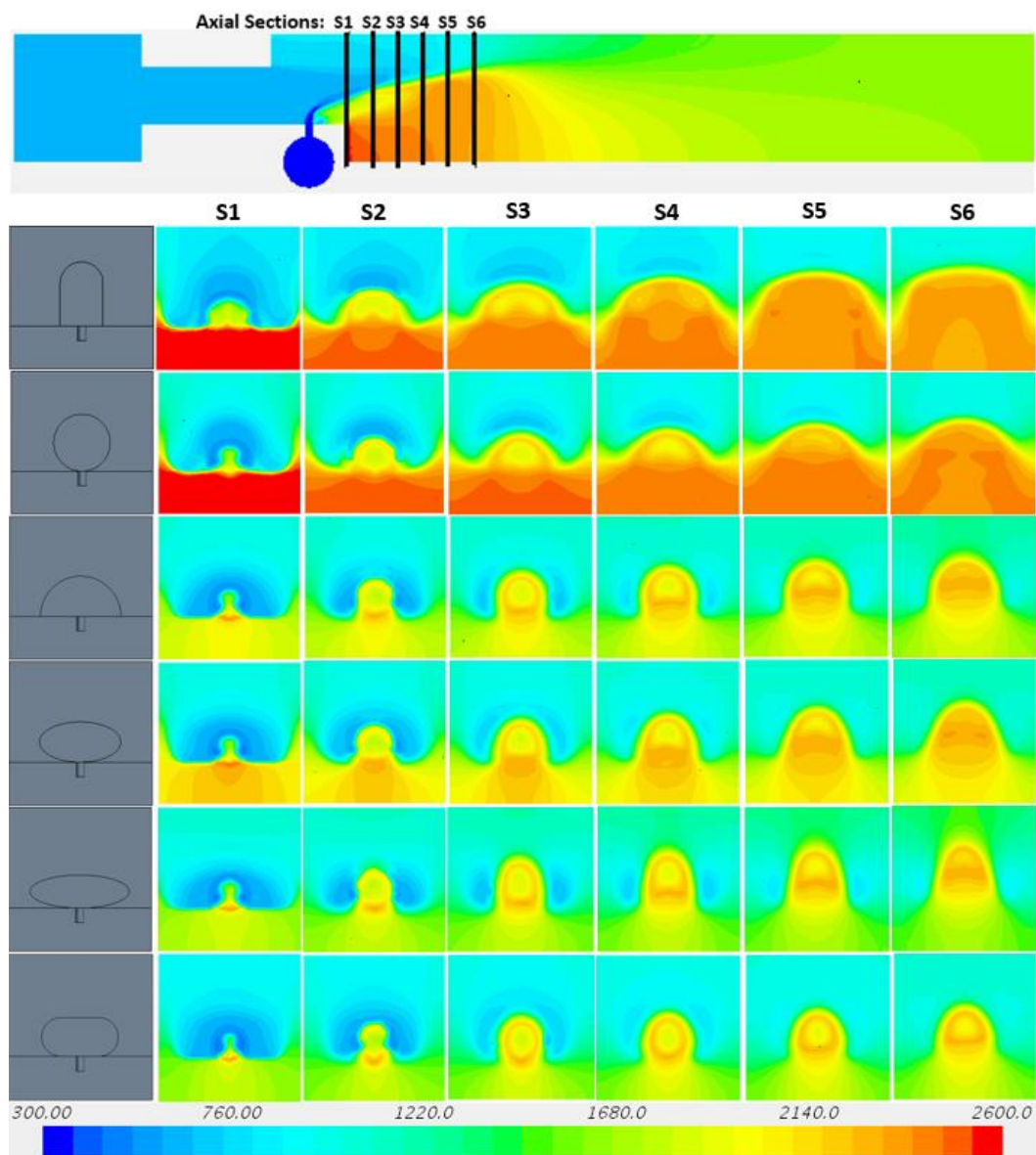
Figure 4.4: Temperature distribution at different axial sections for the 6 configurations

In Figure 4.4, the temperature distribution is represented at several axial sections. Their location throughout the domain is shown by the picture at the top. It emphasizes the occurrence of extremely high temperature in the outer recirculation vortex for the first two cases, particularly at section 1, which corresponds to the injector plate, where temperatures reach their peak of 2600 K. These temperatures are unacceptable and it is necessary to reduce them for the reasons explained before. In order to do this, it is essential to understand which are the main reasons of this very different behaviour.

4.3 Mixing Ability

In every combustion system based on diffusion flames, the mixing process is extremely relevant and affects the combustion efficiency in combination with the reaction process. Particularly in this combustion technology, in which the conventional flame is replaced by several micromix diffusion flames, the mixing assumes a primary role. For this reason, the JICF technique is employed in order to increase the fuel entrainment and enhance the fuel-air mixing. Moreover, the NO_x production is strictly related to the mixing process because a poor mixing is responsible of the presence of local hotspots where the mixture is at stoichiometric condition.

In the literature, several methods to quantify the mixing were found. In some cases, mixedness parameters were defined to achieve a value included between 0 and 1 for an axial section [29], [9]. Based on their applicability to this model, two different approaches were chosen. A first approach is derived from the Hornsby and Norster's paper [30], in which is suggested to estimate the degree of mixing through a statistical mixture distribution parameter such as the standard deviation. The mass flow weighted standard deviation of fuel distribution S were measured for several planar sections starting from the surface in correspondence of the injector plate. The standard deviation of fuel concentration is defined as follow:

$$S = \sqrt{\frac{\sum(c_i^2 \dot{m}_i)}{\sum \dot{m}_i} - \left(\frac{\sum c_i \dot{m}_i}{\sum \dot{m}_i}\right)^2}$$

(4-1)

Where c_i is the mass fraction of fuel at cell i and $\dot{m}_i$ is the mass flow through cell i. When air and fuel are perfectly mixed, this parameter is equal to 0. Since it is not a normalised parameter, the value of S for not perfectly mixed cases is dependent on the air-fuel ratio. Thus, a normalization is necessary in order to compare cases characterized by different equivalence ratios. The normalised standard deviation has been proposed by D. J. Abbott [45] and it is defined as:

$$S_N = \frac{S}{S_0} \tag{4-2}$$

Where S_0 is the value of S for fully un-mixed air and fuel:

$$S_0 = \sqrt{\left(\frac{1}{F+1}\right) - \left(\frac{1}{F+1}\right)^2} \tag{4-3}$$

F is the mass-based air-fuel ratio. A value for each axial section was calculated. The location of the planes is represented in Figure 4.5. The first plane is placed in correspondence of the injector plate, the second 1 mm later and the other four are separated of 2 mm.
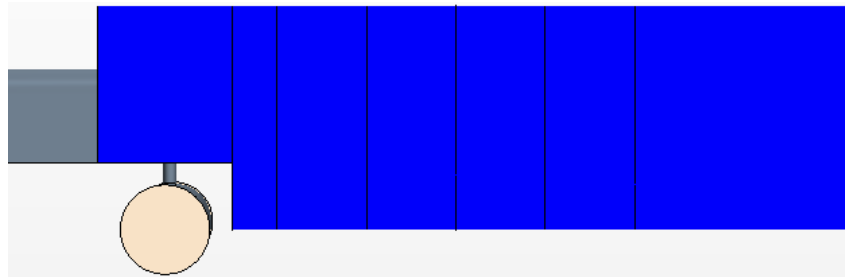
Figure 4.5: Location of axial sections where the standard deviation of fuel concentration was calculated

The other parameter used to estimate the mixing characteristics is the distribution of mole fraction of hydrogen along a line downstream the fuel injection. Some points were created at 2.5 mm from the hydrogen injector and their location is illustrated in Figure 4.6. In proximity of the recirculation vortices, the distance between the points was set to 0.5 mm, whereas in the shear layer between the vortices this distance was reduced to 0.1 mm because the flame is located there and the variation in mole fraction of hydrogen is significant. In this zone a higher

population of points is required to capture the effective fuel distribution. The fuel distributions achieved allow to extract two main information: the maximum mole fraction of hydrogen indicates the degree of mixing and the height of the maximum mole fraction denotes the jet penetration. In addition, the amount of hydrogen present in the recirculation vortices is quantified.

Figure 4.6: Location of points created to obtain the fuel distribution

In order to estimate the mixing capabilities of each single injector geometry, non-combusting simulations were run and the mixing parameters were calculated from them. This type of simulation, in which the reaction is not activated, is necessary to achieve a better prediction of the mixing characteristics and capture the mixture formation process because the combustion model could alter the aerodynamics of the flow field and affect the results. Additionally, in the combustion case the fuel is consumed, therefore it is not easy to distinguish between changes in fuel concentration due to mixing and those due to combustion.

The normalised standard deviation evolution is plotted in Figure 4.7 for the 6 cases characterised by different air gate shapes. It shows similar mixing characteristics for all the configurations, except for the first two cases, which provide a slightly better mixing. This could be explained because the baseline and the circular configurations are characterized by greater height. In this way, there is more air available in the injection direction to increase the entrainment of the fuel with the air. However, this is not a significant improvement in mixing capabilities.

NORMALISED STANDARD DEVIATION
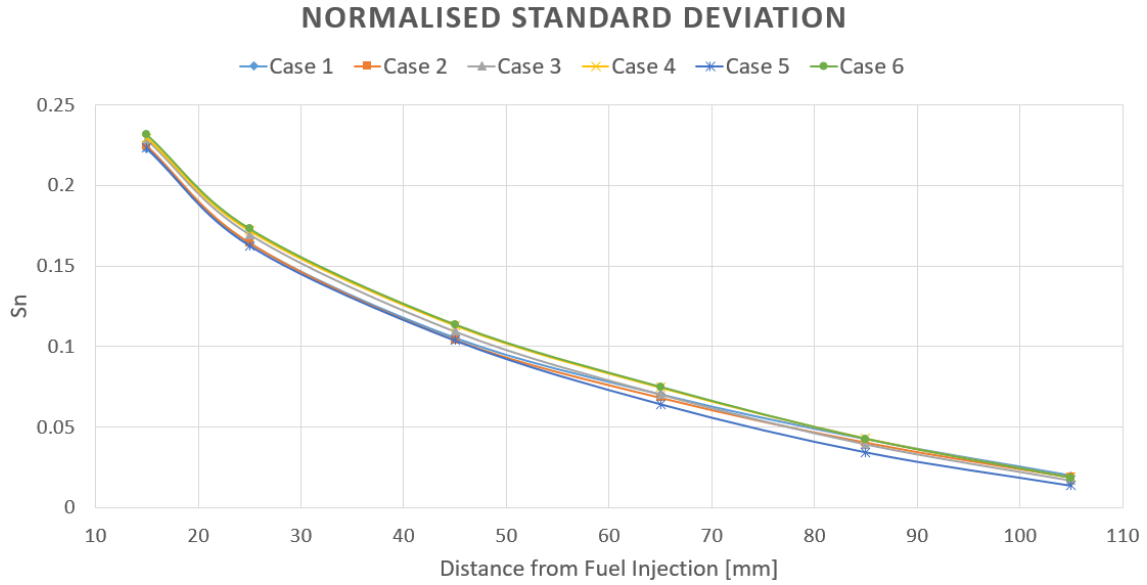
Figure 4.7: Normalised standard deviation of the fuel concentration for the 6 cases

In Figure 4.8, the distribution of mole fraction of hydrogen confirms the outcomes of the normalised standard deviation at the correspondent plane: the degree of mixing, which is related to the maximum mole fraction, is slightly better for the baseline and circular configurations. In addition, the fuel placement for these two air gate shapes is very similar in the recirculation vortices as well. Compared to the other configurations, they revealed a higher amount of fuel in the outer vortex, which could be a potential cause of the high temperatures there and lead to undesirable NO_x production. The degree of mixing and the fuel placement at this plane for all the other four configurations is similar everywhere, except for modest differences in the inner vortex. As expected, the jet penetration, displayed by the height of the maximum mole fraction, is the same for all the configurations because all of them are characterized by the same momentum flux ratio.
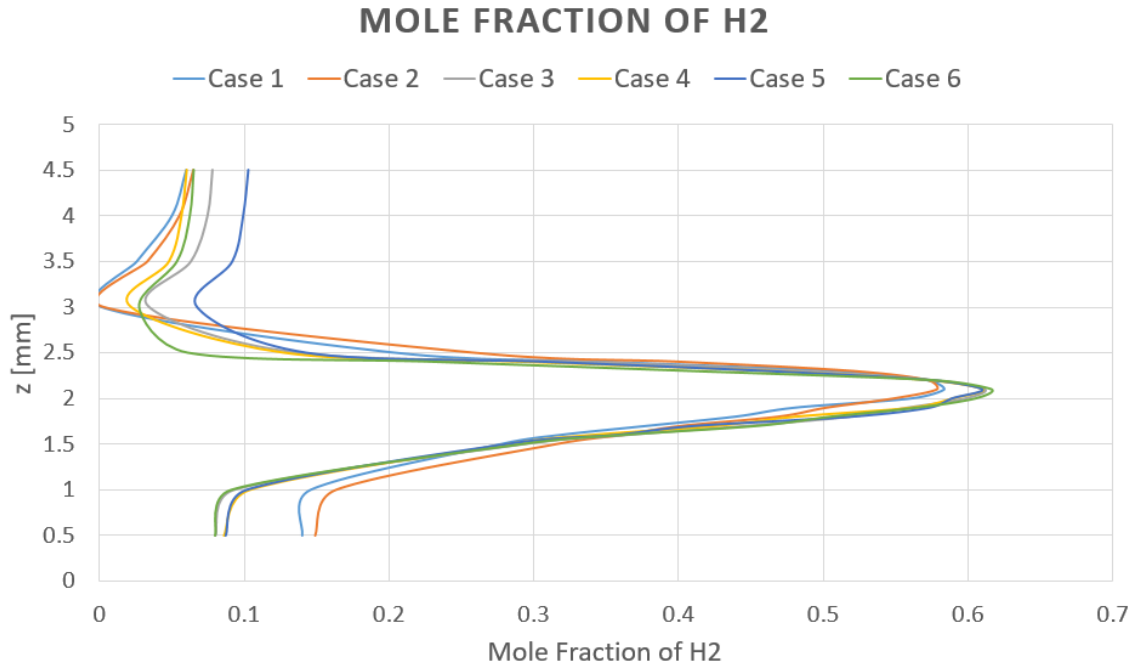
MOLE FRACTION OF H2

Figure 4.8: Mole fraction of H$_2$ along the line at 2.5 mm downstream the fuel injector

4.4 NO$_x$ Emissions

Each configuration is characterized by a different distribution of NO$_x$ within the computational domain, which affects the overall NO$_x$ emissions produced. This distribution is indicative of the location where NO$_x$ is mostly produced. Nevertheless, it is useful to find a quantitative evaluation of the production of NO$_x$. However, the values extracted from the simulations and used to compare the different configurations are not representative of the real NO$_x$ production capabilities of the injector because experimental tests have not been conducted yet and, thus, the numerical results have not been validated. In addition, the thermal NO$_x$ model available in STAR-CCM+ uses an additional equation to account for the NO formation, which is exclusively dependent on the temperature field and the local concentration of other species present in the computational domain. For this reason, an accurate prediction of the reacting flows behaviour is required to correctly estimate the formation of nitric oxide. Since RANS simulations represent a steady-state case and are unable to capture the occurrence of local hotspots within the domain, the NO$_x$ production tends to be underestimated due to the fact of being drastically influenced by the local flow

conditions. For this reason, the attention is not focussed on the absolute NO_x values, which are normalized relative to the baseline configuration, in order to develop a key trend and assess qualitatively the capabilities of different configurations.

The concentration of NO is measured using the definition of volumetric part per millions at the exit of the single injector geometry. The values obtained are corrected to account for the different oxygen concentrations. It allows to compare different concentrations based on the same basis. The correction calculates the NO_x values considering 15% of oxygen concentration.

$$C_r = C_m \cdot \frac{(20.9 - 15)}{(20.9 - \%O_2)} \tag{4-4}$$

Where C_m represents the NO_x concentration measured on a dry basis and C_r the corrected amount of pollutant. $\%O_2$ is the percentage of oxygen concentration at the outlet section. In order to obtain ppmV values, the corrected mass fraction of fuel has to be divided by the density to convert it in a volume fraction.

$$ppmV = C_r \cdot \frac{\rho_{mix}}{\rho_{H_2}} \cdot 10^6 \tag{4-5}$$

The value of the volumetric part per millions obtained for the baseline configuration is 228.5, which is significantly high. For the reasons already explained before, the amount of NO_x emissions for all the other configurations was normalised to this value in order to focus on trends and not on absolute values which are not validated and cannot be considered reliable. In the figure below, the NO_x distributions are illustrated. Unlike the temperature contours, in this case the scale is not the same for all the configurations. This can be explained in two ways: first of all, it is not possible to identify a maximum value for all the cases due to the considerable difference in NO_x produced. A single scale for all the cases would not be able to show relevant results. Secondly, the use of different scales allows to characterize the location of the maximum production of NO_x.
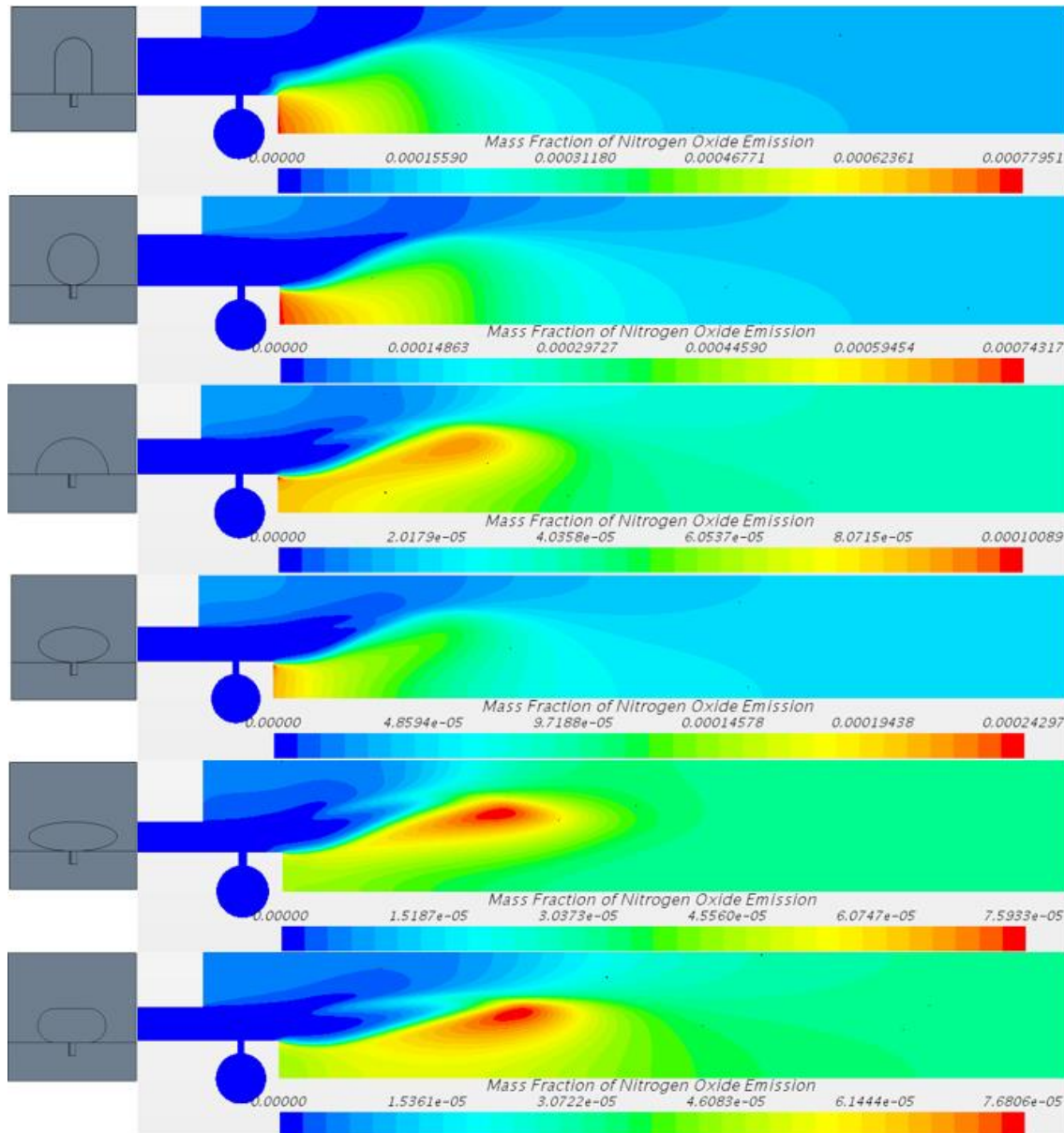
Figure 4.9: Contours of mass fraction of NO$_x$ emissions. Different scales have been used to identify the location of the maximum production of NO$_x$

The contours of mass fraction of NO$_x$ in Figure 4.9 revealed a distribution consistent with that found for the temperature, confirming the relationship between these quantities. The most desirable distributions are provided by configurations 3, 5 and 6, particularly the last two, in which the peak of NO$_x$ emission is located downstream the flame. Instead, the first two configurations showed their peaks within the outer recirculation vortex and, for the reasons already discussed, the NO$_x$ production is considerably higher than all the other geometries. The fourth represents an intermediate case because the peak was

found within the vortex, but the amount was significantly lower. Using the formulations described before, the mass flow weighted fraction of NO_x was measured at the outlet plane and the corrected value of volumetric part per millions calculated for each configuration. The normalised values are collected in the plots below. Unlike the injection angle, for the air gate shape there is not a unique parameter which characterizes its behaviour. For this purpose, two parameters have been defined: an aspect ratio between the air gate height and width and the location of the maximum width from the bottom surface of the gate.

Figure 4.10: Normalised values of NO_x emissions calculated at the exit for the 6 configurations in function of (a) the aspect ratio and (b) the distance of the maximum width from the bottom surface
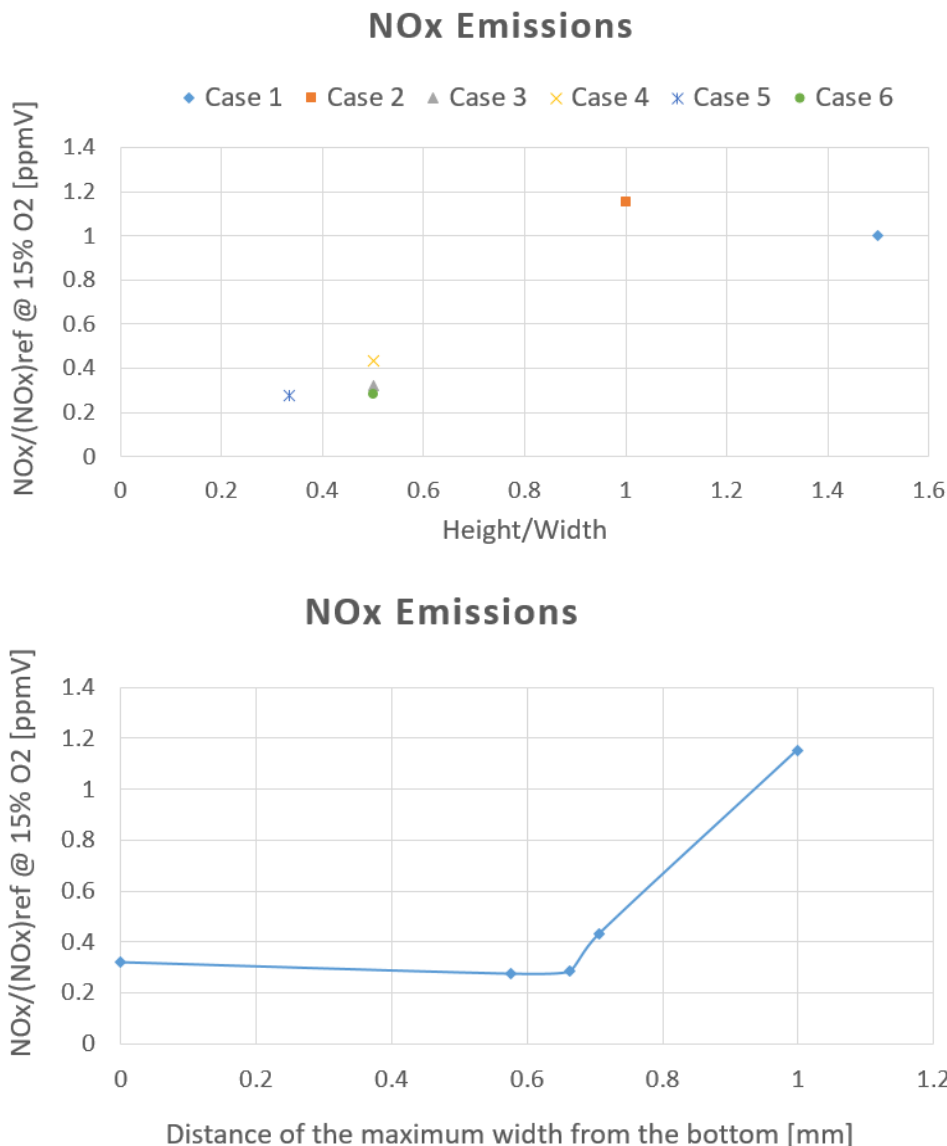
71

Figure 4.10 showed an increasing trend of NO_x emissions by moving along the axis: increasing the height and, consequently, reducing the width of the air gate has a negative impact, as well as moving the maximum width from the lower part of the air gate. It has led to consider that the NO_x produced is strictly related to the air gate shape. In this context, the mixing assumes a secondary role compared to the importance of the distribution of the air within the injection zone, which is the main key to reduce NO_x emissions. All the configurations are characterized by the same momentum flux ratio and, thus, the jet penetrates within the air stream with the same intensity. In this case, an equivalence ratio of 0.4 leads to a momentum flux ratio of around 2.2, which is relatively low. For this momentum flux ratio, a high air gate is not necessary because there is not the risk of a jet penetration within the inner recirculation vortex. Whereas, the benefits associated with an increased air gate width are relevant. A representation of the temperature distribution for two configurations representative of completely different behaviours (baseline and last configurations) at the axial section placed at 2.5 mm downstream the injector hole is provided in Figure 4.11.
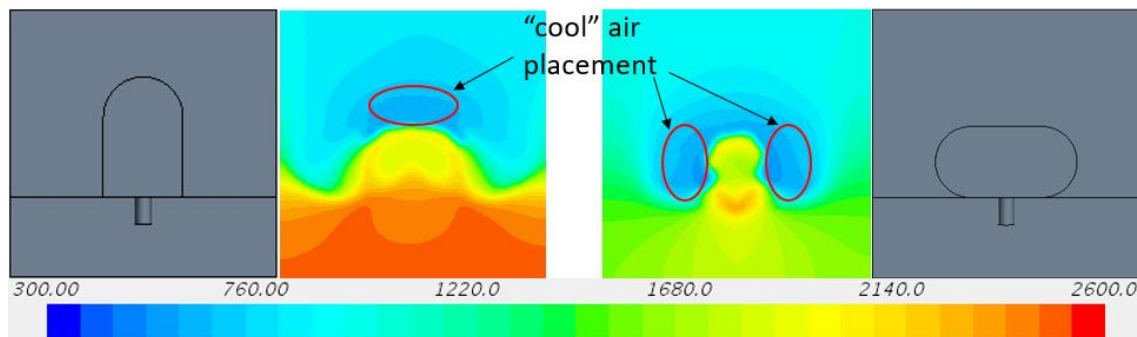
Figure 4.11: Distribution of cool air at the axial section placed at 2.5 mm downstream the injection hole for the configurations 1 and 6

The temperature distribution revealed that, in the baseline configuration, the air stream flowing from the lowest part of the gate reacts with the hydrogen jet and is recirculated within the outer vortex, causing a significant increase in temperature there. The air flowing from the upper part of the gate does not interact with the fuel stream, which has been already deflected, and remains relatively cool (about 600 K). This cool air is then recirculated in the inner vortex. Whereas, the other configuration takes advantage of this additional cool air

placing it at the sides of the fuel injector. In this way, the entrainment between the air and hydrogen streams is not affected considering that the mixing characteristics of the two configurations is similar, but the air placed laterally allows to surround the hot stream and cool the outer recirculation vortex.

In addition, a variation of the air gate height has a direct influence on the size of the inner recirculation vortex and it leads to a significant change in the aerodynamics of the reacting flow. A reduction of the air gate height causes the formation of a larger inner vortex and, due to the higher concentration of air in the lowest part, the outer vortex size is significantly reduced. It affects the flame position and shape, because the flame is now stabilized within a longer shear layer. This aerodynamic variation is clearly shown in Figure 4.12, where configuration 6 is compared with baseline (1). In conclusion, a longer flame is generated compared to the baseline configuration, but the benefits given by a smaller outer vortex, appropriately cooled by the lateral cool air, are evident in terms of NO_x emissions and temperatures close to the injector plate.
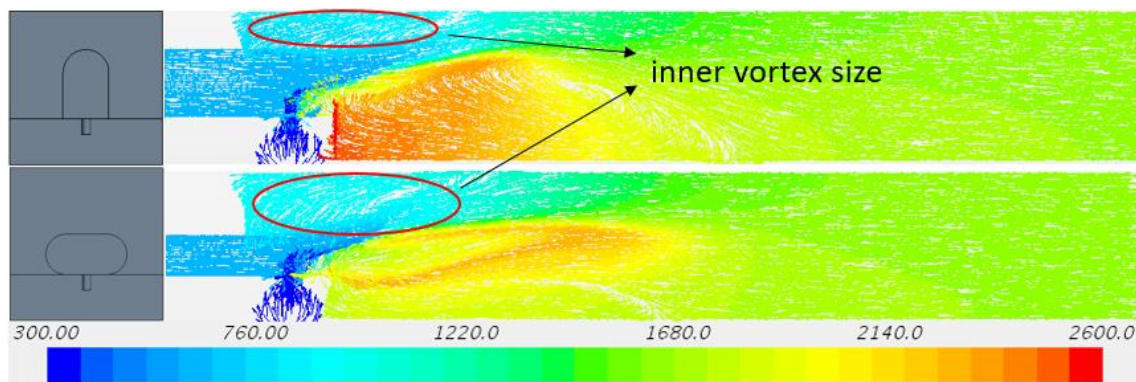

Figure 4.12: Temperature contours which illustrates the size of the inner vortex for configurations 1 and 6

4.5 Equivalence Ratio Study

The last configuration has shown interesting results in terms of NO_x emissions and temperature distribution. Nevertheless, a single equivalence ratio has been

considered in the previous study and the results could be significantly modified moving towards other equivalence ratios. The main effect of using different equivalence ratios is the variation of the momentum flux ratio because of a different fuel mass flow. In the Section 2.3, the importance of this parameter for a JICF configuration was explained, because a slight change in the momentum flux ratio could cause a big change in the injector properties. For this reason, two additional simulations with different equivalence ratio were run, in order to explore the capabilities of the model for a range of operating conditions: in the first, the value of the equivalence ratio was 0.3, in the other 0.5. Due to changes of momentum flux ratio, respectively equal to around 1.4 and 3.5, the two simulations have revealed a significant variation of the flow dynamics.
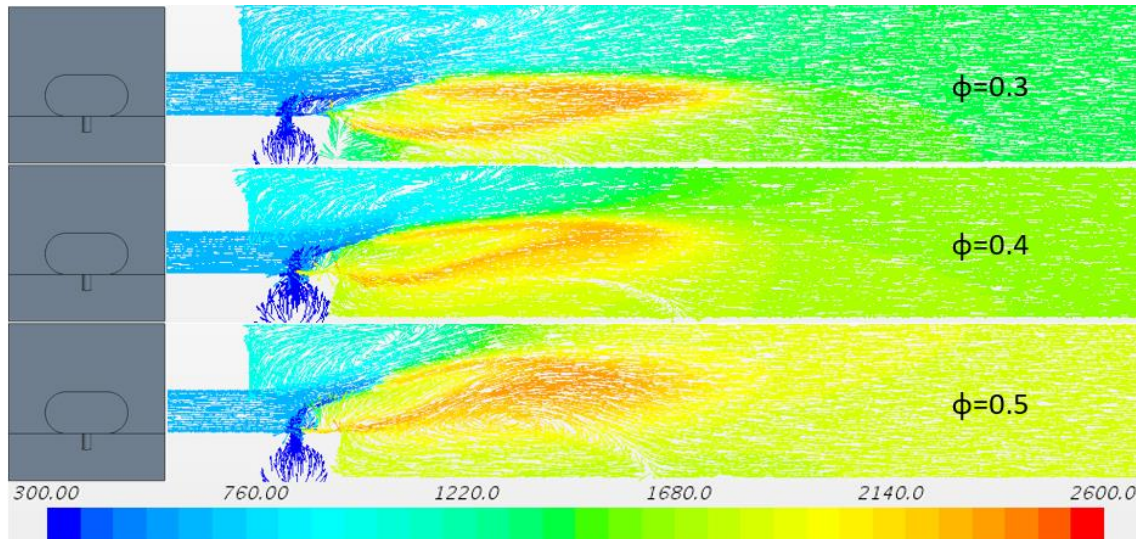
Figure 4.13: Temperature contours for the same configuration at different equivalence ratio

In Figure 4.13, the three cases are compared. The first case with the equivalence ratio of 0.3 is characterized by a weaker jet penetration. It affects the flame position and the size of both the recirculation vortices: the inner is enlarged, whereas the outer is considerably reduced. Due to this aerodynamic structure, the flame is moved down compared to the baseline configuration and it could lead to the flame merging, also considering the reduced size of the outer vortex. However, the temperatures within the outer vortex and particularly close to the injector plate are low. The case with the equivalence ratio of 0.5 showed opposite

74

results: due to the stronger jet penetration, the flame is moved up and the outer vortex is enlarged. For this reason, the risk of flame merging is not present anymore, but the temperature within the outer vortex is higher. The temperature is also high downstream the flame, but it was predictable due to the higher volumetric heat released and flame temperature characteristic of higher values of equivalence ratio.

The mixing characteristics of these configurations were compared using the parameters already described: the normalised standard deviation of the fuel concentration and the mole fraction of hydrogen.
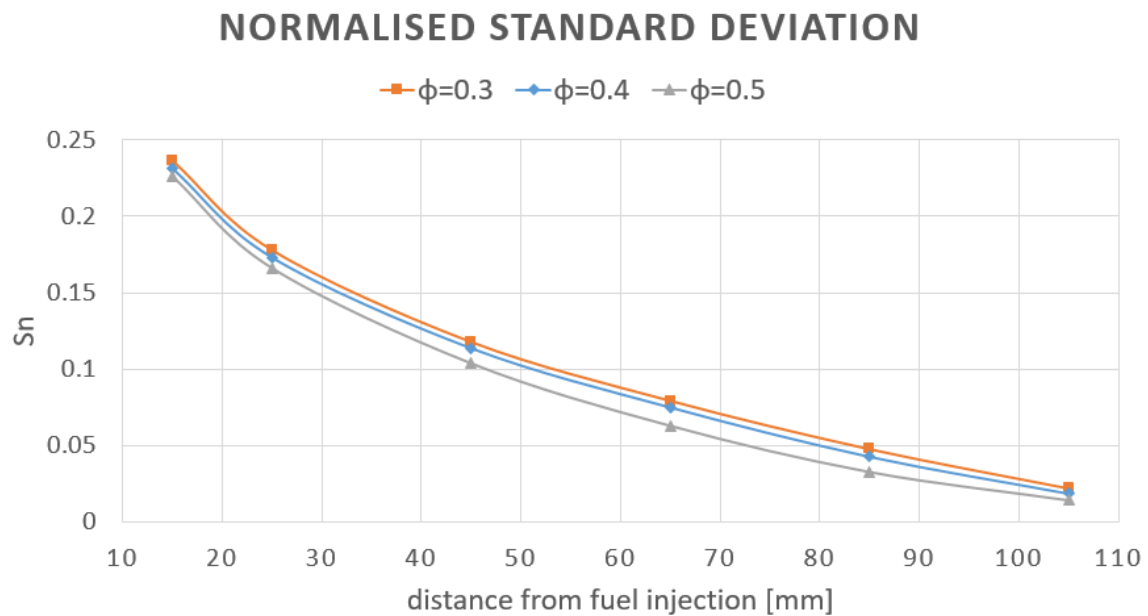
Figure 4.14: Normalised standard deviation evolution for three different equivalence ratios

In Figure 4.14, the evolution of normalised standard deviation revealed a consistent trend throughout the domain for all the sections: the greater the equivalence ratio, the better the mixing, which is reasonable due to higher amount of fuel available, higher jet velocity and, thus, greater penetration. The importance of the normalisation is particularly evident for this comparison, because the values of the standard deviation is a function of the mass-based air-fuel ratio. Without normalisation it would not be possible to make an appropriate comparison.
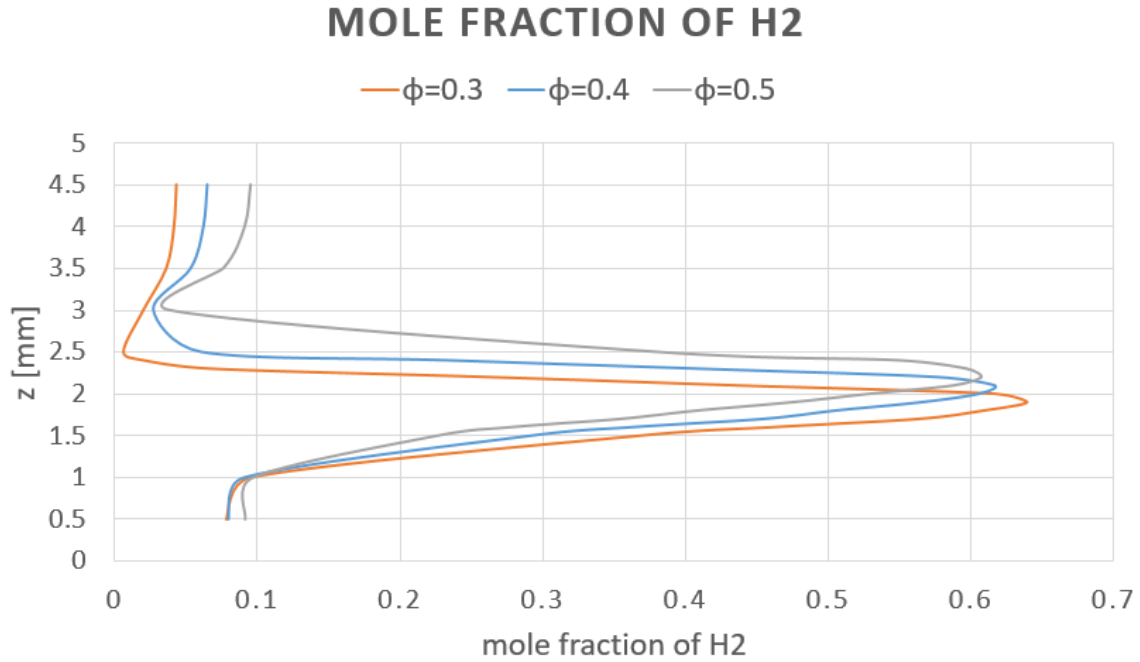
MOLE FRACTION OF H2

Figure 4.15: Distribution of mole fraction of hydrogen at the line at 2.5 mm downstream the injection hole

The fuel distribution at the line at 2.5 mm from the injector hole is illustrated in Figure 4.15. It confirms the behaviour described by the vector plot: due to the variation in the momentum flux ratio, the fuel jet penetrates more for the higher equivalence ratio and the maximum mole fraction is found in the upper zone, whereas for the lower equivalence ratio, the fuel penetration is weaker and the peak of fuel is moved down. The degree of mixing is also confirmed to be better for higher equivalence ratio and worse for lower equivalence ratio, based on the value of the maximum mole fraction.

In Figure 4.16, the distribution of NO_x production in the domain is represented. It revealed that, for all the three cases, the peak of NO_x is found downstream the flame and it increases with the equivalence ratio. The distribution is consistent with that of the temperature because, based on the flame position, the peak of NO_x is moved up or down. In the $\phi=0.3$ case, the temperature and, thus, the NO_x emission are significantly reduced within the outer vortex, in particular close to the injector plate.
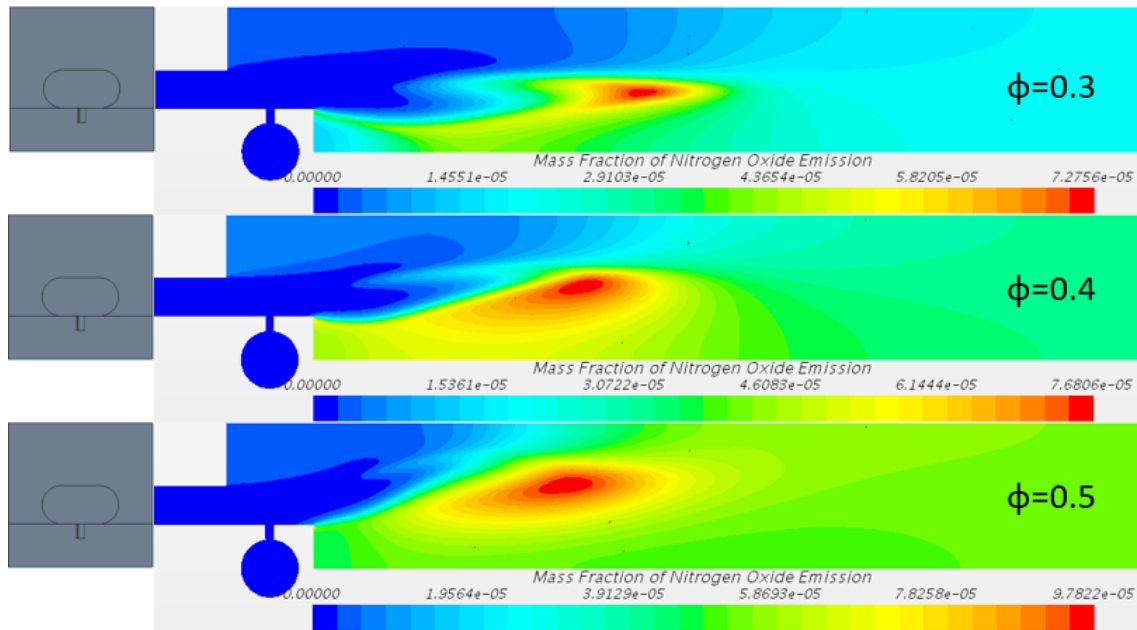
Figure 4.16: NO$_x$ emission distribution for a range of equivalence ratios

Normalised values of NO$_x$ emission at the outlet plane were calculated, one for each case, and gathered in the plot below. Particularly for the equivalence ratio study, the correction for the concentration of NO$_x$ is necessary to compare the values because the amount of oxygen at the exit is considerably different for the three cases: it is higher for ϕ=0.3 and lower for ϕ=0.5 due to the different amount of fuel available to mix with the air.

The trend of NO$_x$ emission shown in Figure 4.17 revealed that the NO$_x$ production is very similar for the cases with lower values of equivalence ratio, whereas ϕ=0.5 case exhibits a slight increase. However, it is acceptable, also considering the higher flame temperature associated with a higher value of equivalence ratio.
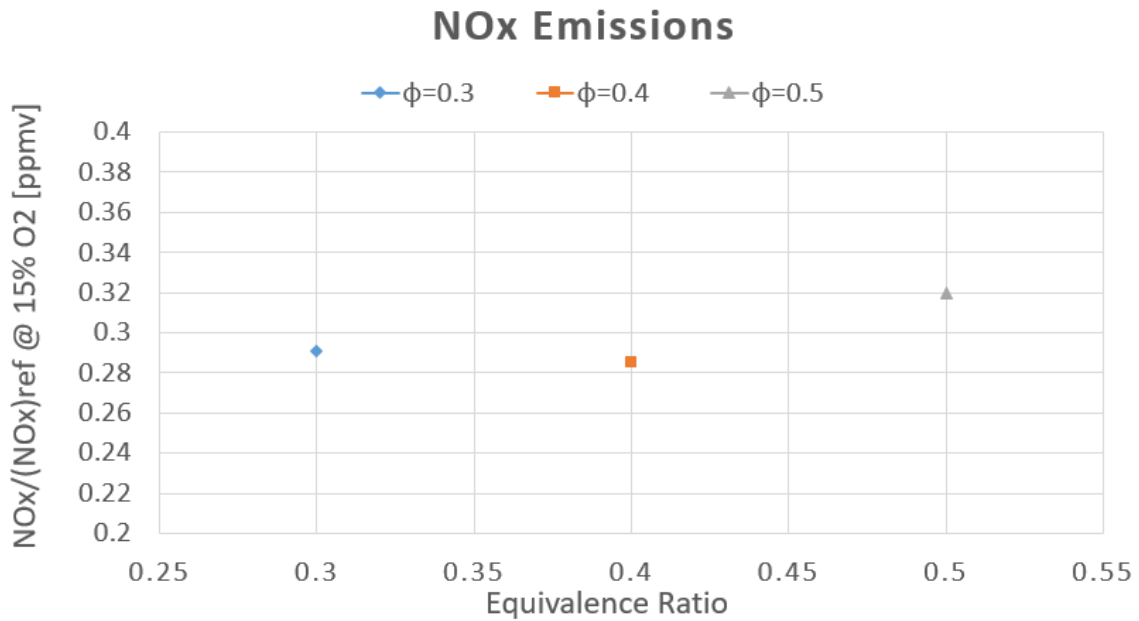
NOx Emissions

Figure 4.17: NO$_x$ emission trend for a range of equivalence ratio

This equivalence ratio study led to conclude that the air gate shape investigated provides still good results in terms of NO$_x$ emissions for a range of equivalence ratio included between 0.3 and 0.5. However, it would be beneficial to analyse other values of equivalence ratio in this range to achieve a more complete view of the trend and explore the feasibility to move towards lower equivalence ratio. Despite the results have shown good prediction of NO$_x$, it is necessary to underline the necessity of simulations on the whole injector array to investigate the interactions between flames. This aspect could be particularly critical for lower equivalence ratio, due to the extremely weak jet penetration, which leads to the formation of a small outer vortex to separate the flames and, consequently, and increased risk of flame merging, absolutely undesirable because it would significantly increase the NO$_x$ production.

4.6 Time Delay and FTF Estimation

As described in the previous section, it is possible to estimate FTF from time-averaged simulations by using alternative formulations. In this chapter, time delay and time delay spread are derived from RANS simulations in order to apply the standard n-τ and modified n-τ models and obtain a series of FTF. The main goal is not to achieve an accurate estimation of the flame response to acoustic perturbations because this approach is based on approximation, but to compare the results obtained for different air gate shapes, develop key trends of time delay and identify potential risks associated with some configurations. Two different methods have been used: the time for heat release to occur in the flame and the particle injection methods.

4.6.1 Time for Heat Release to Occur in the Flame Method

This method is based on the assumption that the main effect of the heat release is an increase in the flame velocity, which affects the system acoustics. The time delay can be estimated by calculating the time from the beginning to the conclusion of the heat release process [2]. Since the heat release rate is not a quantity directly available to determine in STAR-CCM+, an alternative approach is required to develop its evolution throughout the domain. Two alternative variables have been found to be related to the heat release rate: the temperature and the mass fraction of OH. The use of the mass fraction of OH has been proposed by A. Fogué Robles in his work [43]. The formation of OH is dependent on the temperature field because it is mostly produced at high temperatures. For this reason, it is generally employed to identify the flame shape and position.

$$\frac{Q'}{\overline{Q}} \propto \frac{OH'}{\overline{OH}} \qquad \qquad \textbf{(4-6)}$$

In order to develop the evolution of these two quantities throughout the domain, several planar sections were created starting from the plane immediately downstream the injector hole. The following planes are separated by 0.2 mm, close enough to generate an accurate distribution. The plane distribution is represented in Figure 4.18.

79
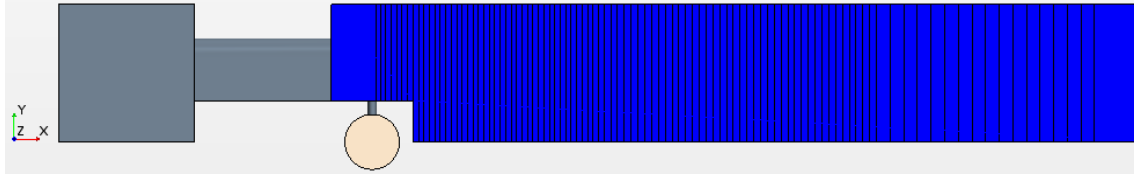
Figure 4.18: Series of axial sections created to evaluate the heat released rate distribution

The aim is to produce a temperature rise as that shown in Figure 4.19, in function of the mean time from fuel injection. It allows to determine easily the time delay by measuring the time from the beginning of the heat release process to its completion. In Figure 4.19, two different time delays are represented, which are extrapolated by the plot using two different approaches: the 80% rule and the maximum gradient method.
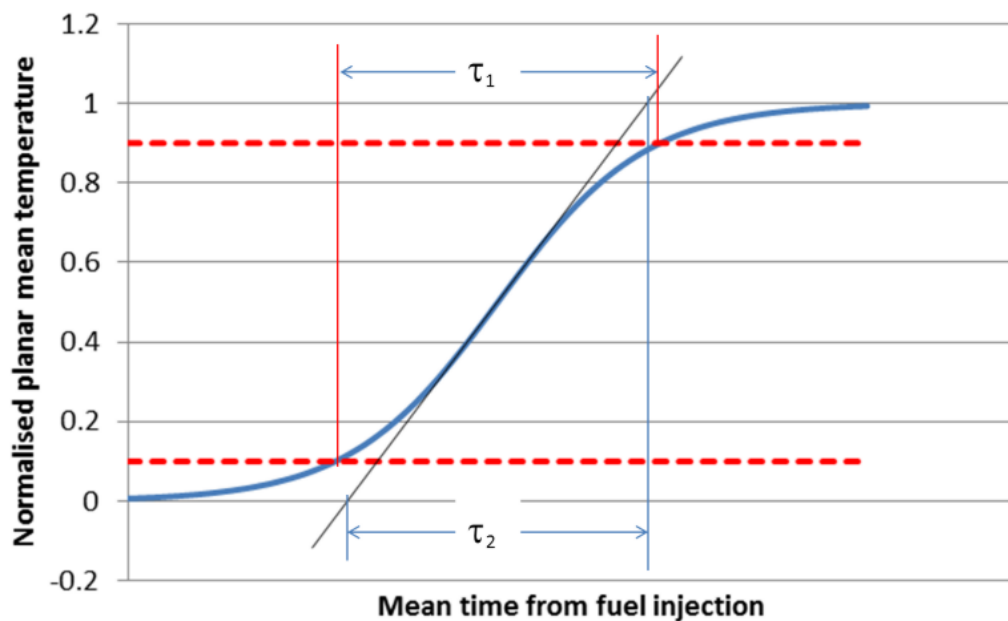
Figure 4.19: Typical planar mean temperature evolution as a function of the mean time from fuel injection [2]

- **80% Rule**

   This method assumes that most of the heat release occurs during the steady-state of the process, whereas, during the initial and the ending transient phases of the process, the rise is relatively weak and it has a negligible impact on the flame acoustic properties [2]. For this reason, exclusively the 80% in the middle is taken into account in the calculation

of the time delay. The 10% is an arbitrary estimation to identify the transient region, thus this value can be adapted relative to the particular case. T_1 in Figure 4.19 corresponds to the time delay calculated using this approach.

- **Maximum Gradient Method**

  This approach assumes that the maximum gradient is able to capture the most significant part of the flame where most of the heat release occurs. This method aims to reproduce an idealised form of the temperature rise [2]. However, this method is extremely sensitive to the distribution found. T_2 is the time delay which corresponds to this approach.

As already stated, the heat release process causes a rise in the flame speed and it has to be considered to calculate the time from the fuel injection for each plane because the velocity is not constant throughout the domain. For this reason, a value of axial velocity for each section was obtained from the simulation as area weighted mean. The area weighting is more appropriate than the mass flow weighting to estimate the axial velocity due to the presence of the recirculation vortices, where the presence of reverse flow drastically affects the estimation. Using a mass flow weighted mean, a decreasing trend of axial velocity was obtained, which is not consistent with the real behaviour. In addition, the absolute values of axial velocity were considerably overestimated by the mass flow weighted mean. The axial velocity evolution is represented in the figure below for the baseline configuration. Within the 1.5 mm downstream the injection hole, the velocity is subject to a rise as expected, whereas immediately later it rapidly decreases. It is due to the presence of the step which causes an increase in the area and, thus the reduction in axial velocity. Downstream the step, the area remains constant and the axial velocity continues to increase until a limit of around 26 m/s is reached. The variation of axial velocity is shown in Figure 4.20.
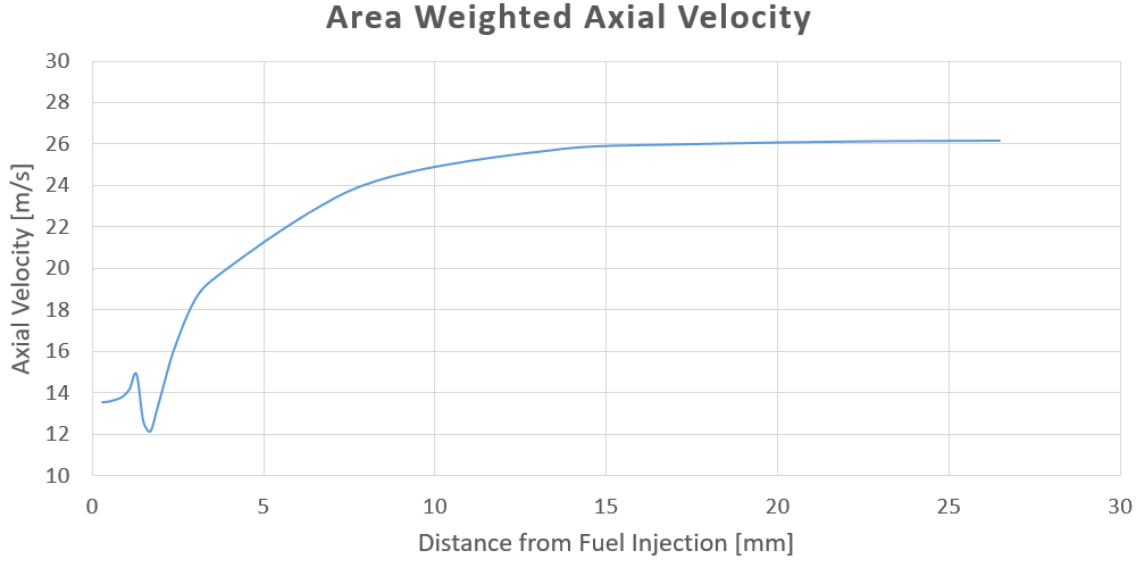
Figure 4.20: Area weighted axial velocity throughout the domain for the baseline configuration

The mean time from fuel injection was calculated considering the variation in axial velocity. To account for this effect, an iterative process was employed: the average axial velocity was calculated between two adjacent sections and the corresponding time step measured using the average velocity calculated and the distance between those sections. The final mean time from fuel injection is the sum of all the time steps.

$$v_m = \frac{v_i + v_{i+1}}{2}$$

$$t_i = \frac{x_{i+1} - x_i}{v_m}$$

(4-7)

$$T = \sum_{i=1}^{n} t_i$$

Where i is the section index and n is the total number of planar sections.

This iterative process allows to calculate a mean time from fuel injection for each configuration and plot the temperature and the mass fraction of OH for each configuration, as shown in Figure 4.21.
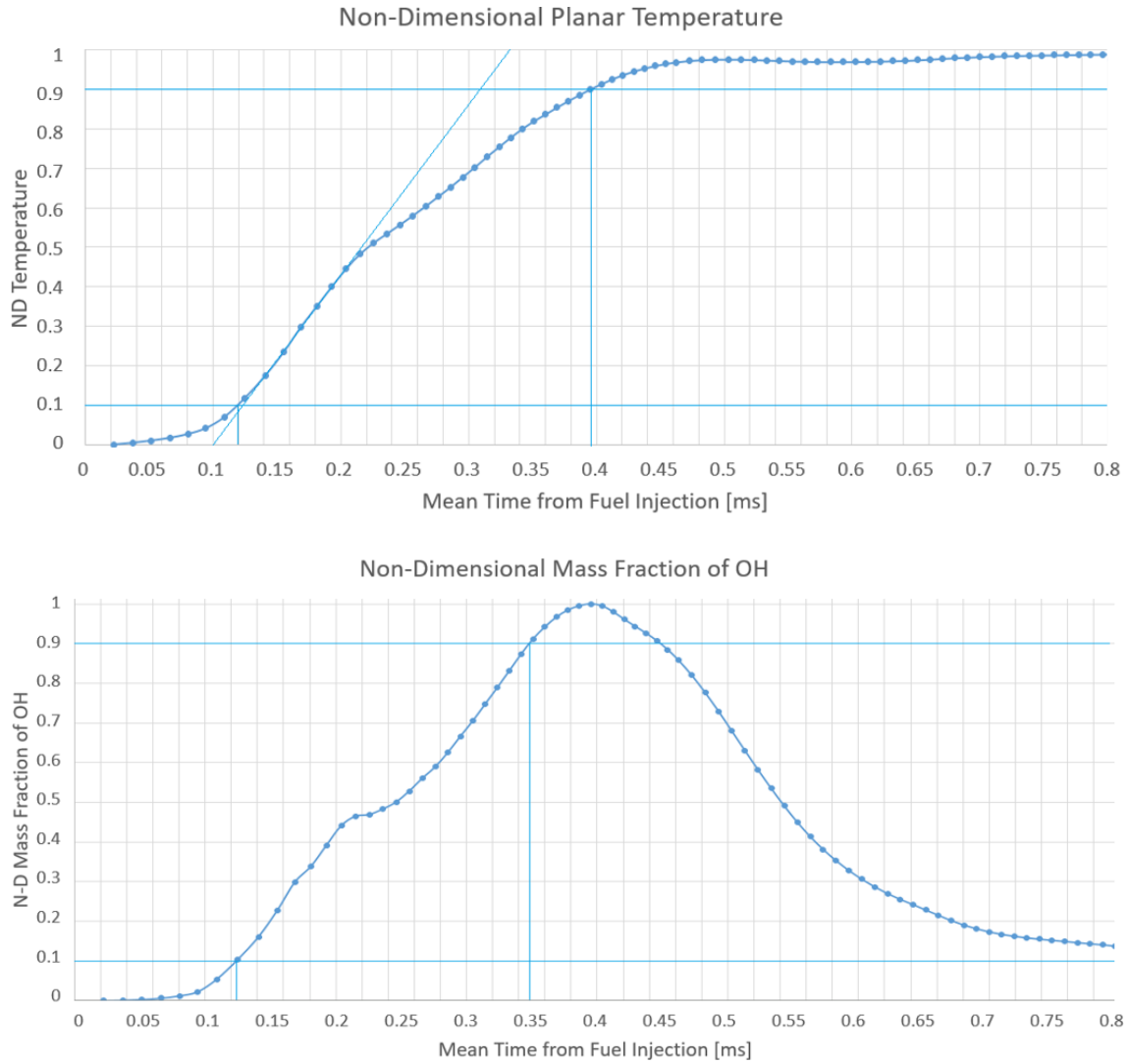
Figure 4.21: Non-dimensional planar temperature (a) and mass fraction of OH (b) distribution as a function of the mean time from fuel injection for the baseline configuration

All the values of time delay collected in Table 4.1 have been achieved using the 80% rule from the temperature and mass fraction of OH distributions and the maximum gradient method from the temperature plot for all the 6 cases. As shown in Figure 4.21(a), the maximum gradient method provides time delays shorter than the 80% rule because the temperature rise is characterized by two different gradients and the first, which is the greater, is the only one to be considered in the measurement of time delay. The trend of time delays shown

using the maximum gradient is not consistent compared to the other approaches because extremely dependant on the temperature distribution.

Time Delay [ms]	Case 1	Case 2	Case 3	Case 4	Case 5	Case 6
80% Rule (Temperature)	0.276	0.332	0.371	0.355	0.398	0.441
80% Rule (OH)	0.224	0.275	0.271	0.276	0.257	0.323
Maximum Gradient	0.232	0.193	0.201	0.188	0.196	0.233

Table 4.1: Collection of time delays for the 6 configurations using the 80% rule and the maximum gradient approaches

The time delays obtained using the 80% rule from both temperature and mass fraction of OH distributions are gathered in Figure 4.22. Although the two distributions provide values which differ by about 0.1 ms between them, the trends developed are consistent. The time delay is plotted as a function of the aspect ratio of the air gate. The configurations characterized by a low aspect ratio (cases 3, 4 and 5) exhibited similar values, particularly configurations 3 and 4 and are circled in the chart. Whereas, the other three configurations, in which the aspect ratio is gradually varied and the circular shape represents an intermediate configuration between the cases 1 and 6, both approaches revealed a decreasing trend, where the baseline configuration is characterized by the shortest time delay. Considering the aerodynamic features of the flow field and the flame length, it is absolutely reasonable to find the lowest value for this configuration due to its shorter flame and the heat release rate is mostly concentrated in a smaller region of the domain.
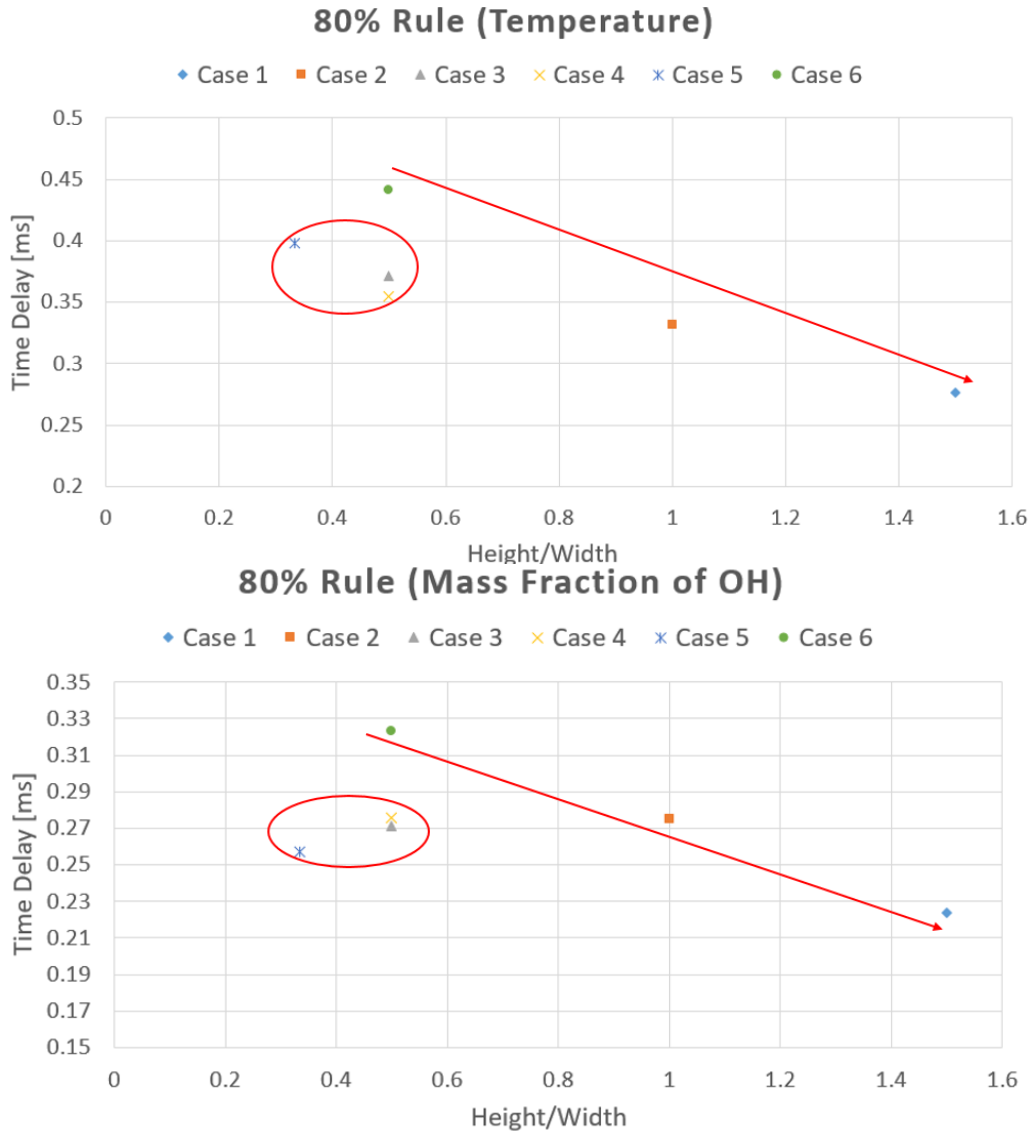
Figure 4.22: Time delay trends as function of the air gate aspect ratio using the 80% rule from the temperature (a) and mass fraction of OH (b) distribution

The calculation of time delay allows to apply the standard n-τ model, described in Section 3.8, to estimate the FTF. Since this is a preliminary study and the interest is focused on the comparison of the thermoacoustic behaviour of different geometries, the proportionality constant n was set to 1, which means that the gain tends to 1 as the frequency moves toward 0. Unlike the modified n-τ model employed later with the particle injection method, the standard approach assumes a constant gain, which is overestimated for high frequency values. The FTFs are illustrated in Figure 4.23.

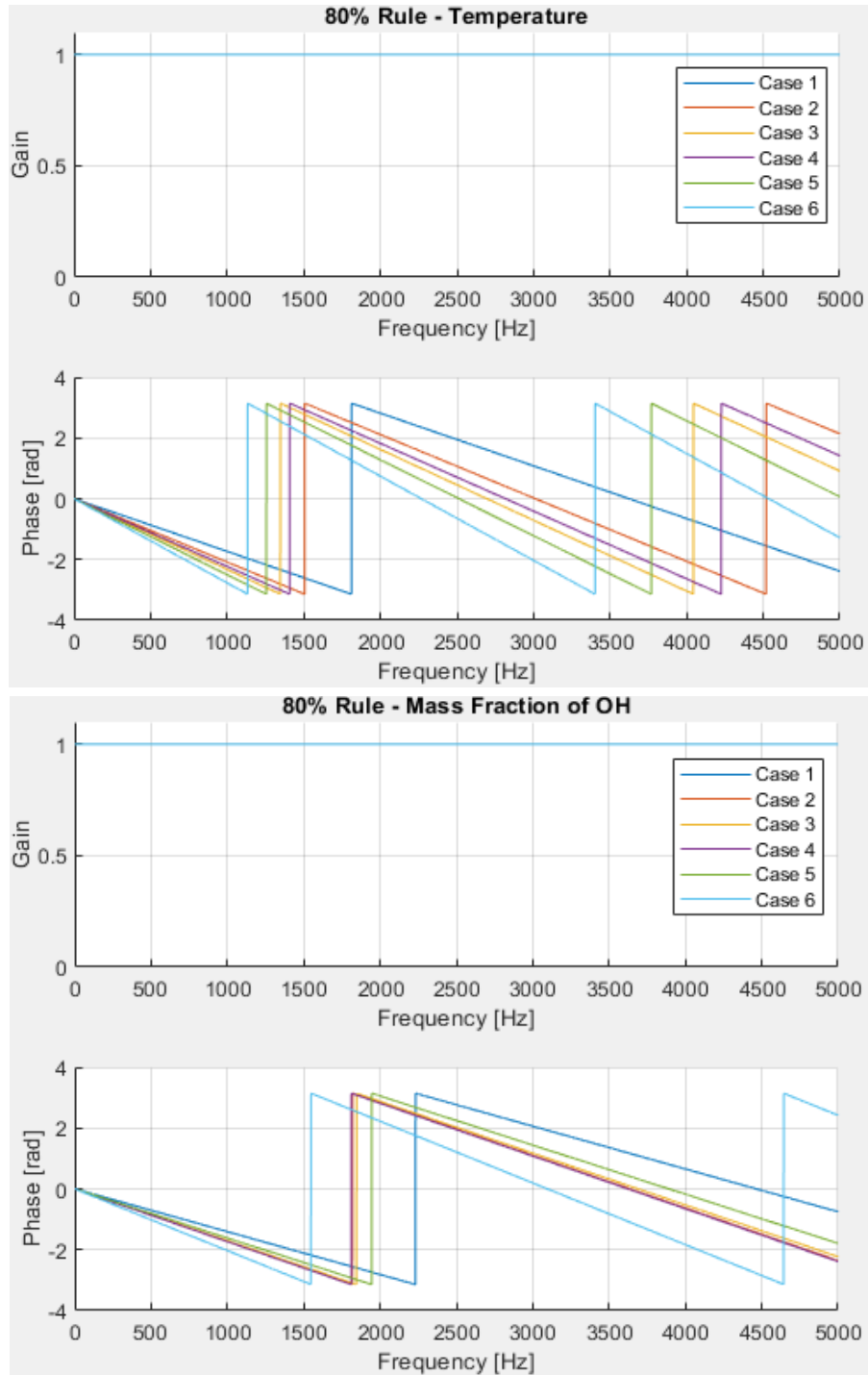**Figure 4.23: Series of FTF estimated using 80% rule from temperature and mass fraction of OH distributions**

Since the standard n-τ model provides a constant gain over the entire range of frequencies, the attention is focused exclusively on the variation in the phase. Its estimation is particularly important because it directly influences the interaction

between the acoustic field and the flame response, establishing whether it is constructive and produces a growth in pressure oscillations. Based on the time delay value, the phase is shifted with the frequency range: the higher the time delay, the faster the phase variation.

4.6.2 Particle Injection Method

This approach assumes that the time delay corresponds to the mean particle residence time from the fuel injection to the flame front. In order to apply this method, two additional requirements are demanded: the creation of a surface able to reproduce the flame front and the application of a model able to inject particles and accurately predict their track. In this way, this approach furnishes the possibility to calculate from RANS simulations the particles residence time necessary to reach the flame front. A big amount of data representative of the residence time for each particle injected is provided and it can be plotted in a histogram, which shows the distribution of the particle residence time. An example of distribution is depicted in Figure 4.24.
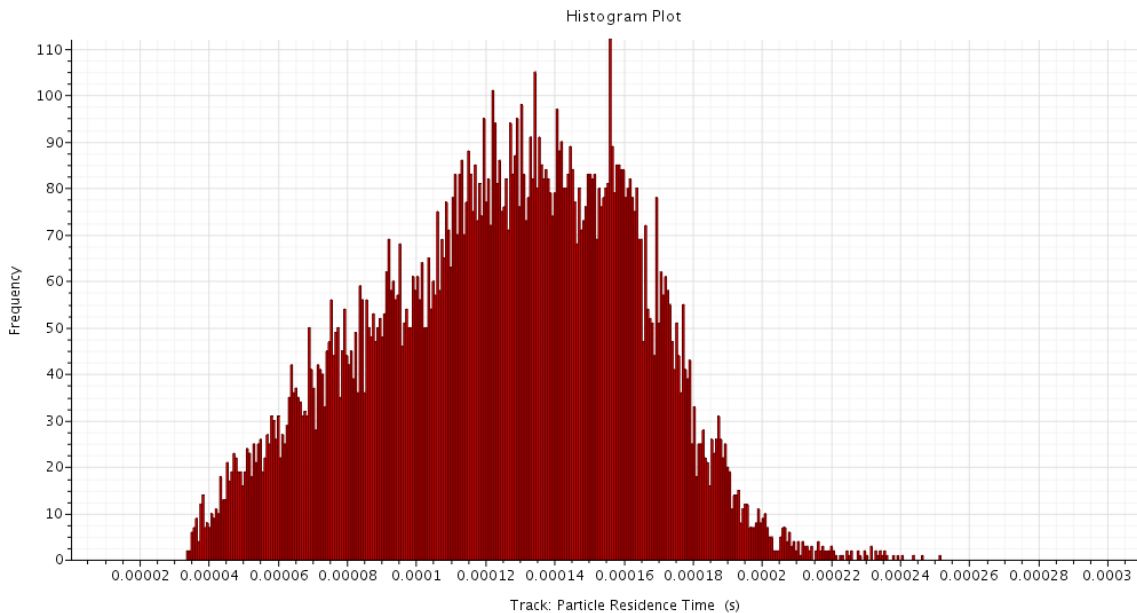

Figure 4.24: Particle residence time distribution for configuration 6

In order to obtain values of time delay from this distribution, the aim is to convert the sort of Gaussian "bell-shaped" function in a squared function, where the mean value corresponds to the time delay and the width of the squared distribution to the time delay spread. Therefore, the time delay and its spread can be estimated from this data distribution calculating respectively the average value and the standard deviation, which is a measure to quantify the amount of dispersion of data values.

In order to inject particles, a specific model available in STAR-CCM+, the Lagrangian Multiphase, is activated. This model makes a distinction between the continuous phase of the flow field and the dispersed phases of the particles. The conservation equations of mass, momentum and energy are solved for each particle in Lagrangian form, in such a way to calculate the trajectory of the individual particle [33]. The advantage of using the Langrangian approach in this case is that it is able to deliver the time delay distribution across predefined control surfaces, whereas the Eulerian approach can determine the time delay distribution in the whole computational domain [31]. STAR-CCM+ distinguishes between different kind of particles: material particles and massless particles. Massless particles are virtual particles, which are not associated to a mass and a volume, flowing with the continuous phase without interacting each other. In this case, massless particles were used because suitable to estimate turbulent diffusion of the continuous phase, the residence time of fluid in the continuous phase, or the mixing of fluid streams in the continuous phase [33]. A surface from which the particles are injected is required by the model. It was created close to the injector hole, as shown in Figure 4.25.
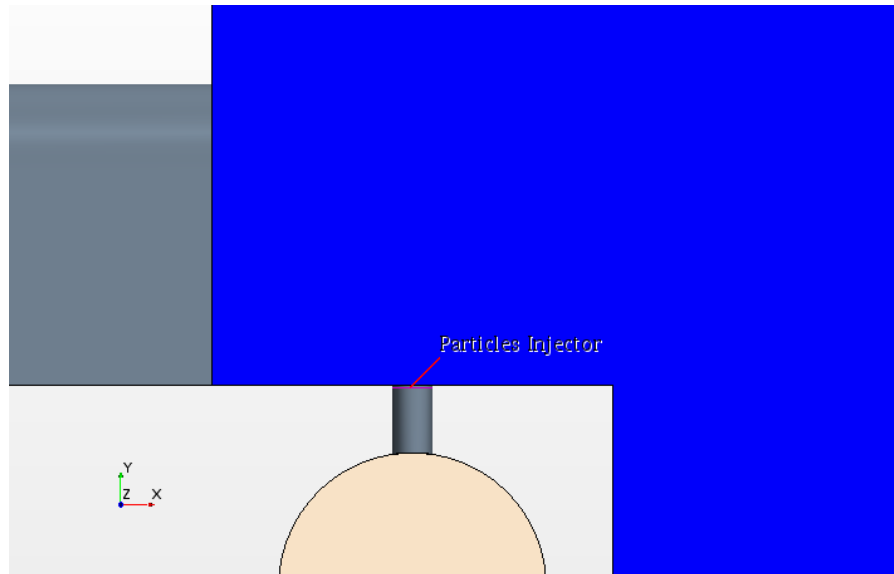
Figure 4.25: Location of the surface where the particles are injected

In order to create a surface representative of the flame front, several variables were taken into account. First of all, the progress variable was considered because it indicates the chemical state within a cell and describes the mixture development within the computational domain. This variable was used by J. McClure in his work [2] to visualize the flame front, choosing a value of 0.9, close to the burnt conditions. An iso-surface with the same progress variable value was created, but it was not representative of the flame front. In detail, the iso-surface was short compared to the flame length, particularly in the symmetry plane, where the combustion started immediately downstream the injector hole. This was mainly due to the high pressure, which reduces the flame front thickness and increases the temperature there and, consequently, the local flammability limits. Additionally, the FGM combustion model assumes fast chemistry, thus once the fuel and the oxidizer are mixed, the mixture burns. Alternatively, other variables were employed in the literature to reproduce the flame front. In the paper of W. Krebs et al. [31], the flame front was characterised by an iso-surface of the fuel concentration. In this case, an iso-surface on which the mass fraction of hydrogen is set to 0.005 has been selected. That value corresponds to the maximum production of OH and, therefore, where the maximum heat release occurs. The use of the maximum mass fraction of OH to determine an adequate value has been suggested by A. Fogué Robles [43]. However, the progress variable has

89

been used in his work to represent the flame front. In Figure 4.26, the iso-surface is superimposed on the contour of mass fraction of OH to highlight the correspondence between the chosen value of fuel concentration and the maximum production of OH.
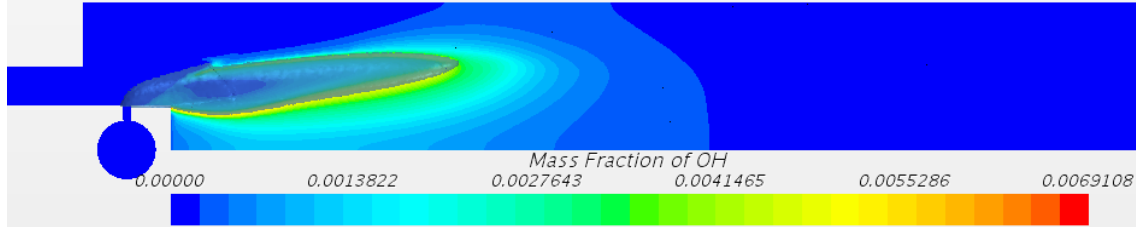

Figure 4.26: Iso-surface representative of the flame front superimposed on the contour of mass fraction of OH for case 6

The majority of the data achieved have revealed values significantly lower than those found using the 80% rule, but of the same order. Whereas, a small amount of values was characterized by residence time much higher, in the order of 2 or 3 ms. This behaviour is probably due to the fact that the particles escape when they encounter surfaces, but it is possible that few of them are recirculated within the recirculation vortices and enter again in the iso-surface. This is confirmed by the aerodynamic features of the different configurations: for the first two cases, characterised by bigger outer vortices, the amount of particles featured by very high residence time was significantly higher compared to the other configurations. For this reason, a data filtering is necessary in order to avoid these undesirable values of residence time compromising the measurement, particularly for the time delay spread. Since the majority of the data are comprised in the range between 0.05 and 0.25 ms, an arbitrary limit of 0.3 ms was selected to filter the data.

In Figure 4.27, the values of time delay and time delay spread using the particle injection method are plotted as a function of the aspect ratio. Despite the difference in absolute value compared to the previous approach is significant, the displayed trend is consistent. The geometries characterised by a low aspect ratio, particularly the cases 3 and 4, revealed similar values and are grouped in the red circle. The case 5 showed a slightly higher value due to its longer flame. The configuration 6 is featured by the highest value of time delay, which is consistent

with the behaviour already detected by the other approach. The only difference is the absence of the decreasing trend between configurations 1, 2 and 6 due to the unexpected value revealed for the baseline configuration. The typical short flame of this configuration would suggest a lower time delay, but it is possible that the aerodynamic properties of the flow field influences the particles trajectory in such a way to produce a wide data distribution representative of different particles behaviours. The wider data distribution is confirmed by the time delay spread of the first two configurations, significantly greater compared to the other cases.
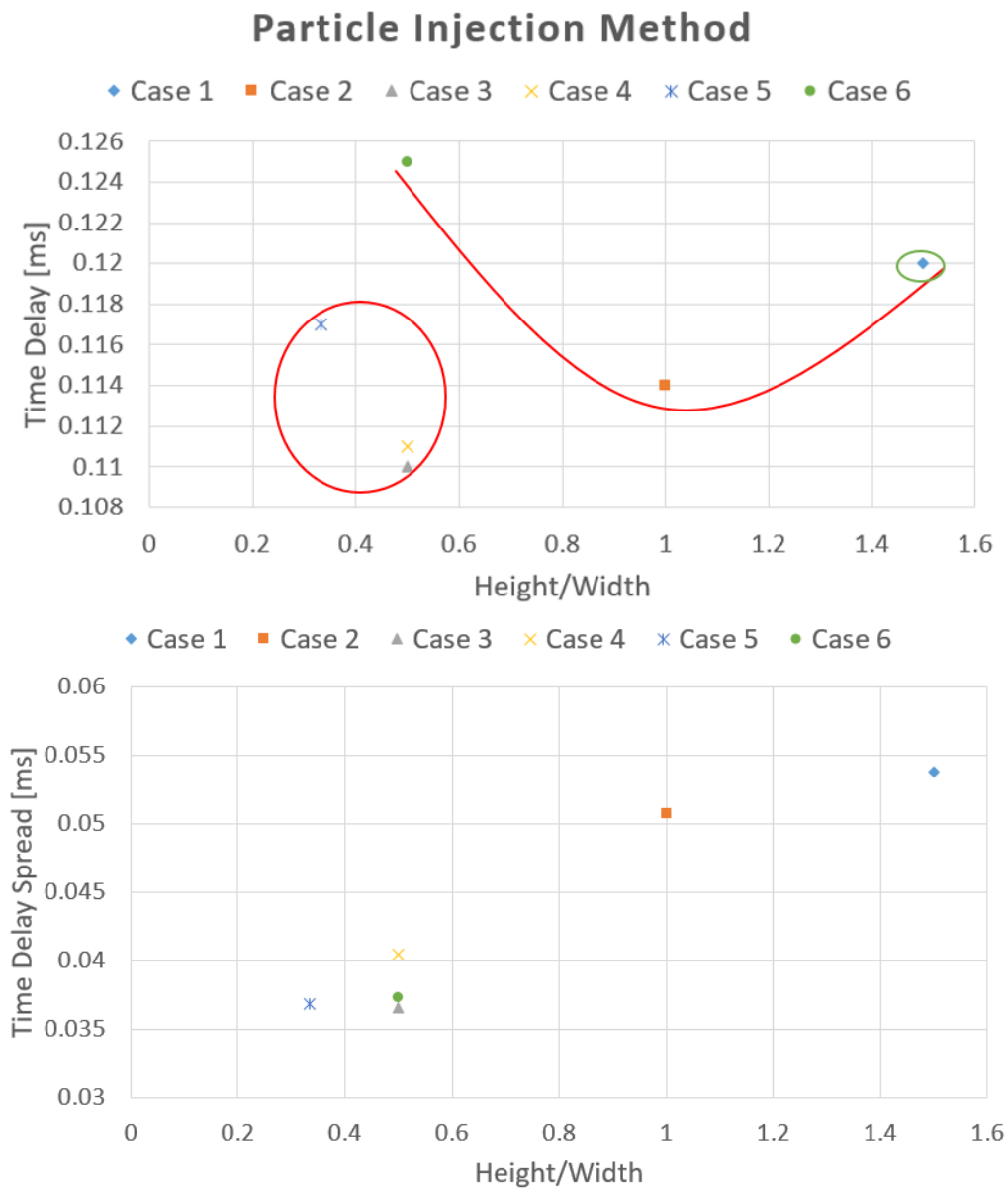

Figure 4.27: Time delay (a) and time delay spread (b) as a function of the aspect ratio obtained using the particle injection method

The estimation of both time delay and time delay spread allows the possibility to apply the modified n-τ model. The FTFs are gathered in Figure 4.28. The advantage of using this method is the introduction of the damping effect of the gain for high frequency values. However, the gain is weakly damped and it reaches a small reduction (25%) for very high frequency (5000 Hz). Unlike the time for heat release to occur approach, the particle injection method does not produce relevant variations in terms of gain and phase, particularly for the range of interest, included between 0 and 2000 Hz. The differences between different configurations begin to be appreciable for very high frequencies, where the phase of the FTFs shows a divergence.

The application of this approach led to conclude that the mean time necessary to reach the flame front is related to the flame length and, in particular for this operating condition characterized by high pressure and flame speed, a variation in the air gate shape, keeping the area constant, is insignificant.
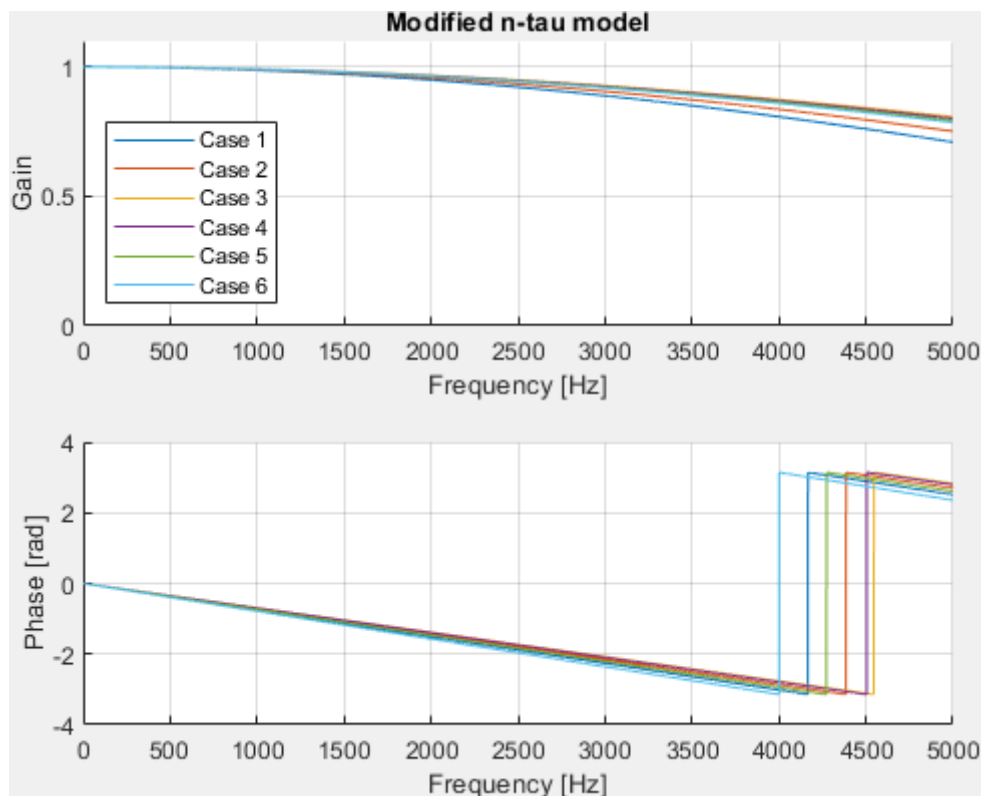
Figure 4.28: Series of FTF estimated using the particle injection approach for the 6 air gate shapes

5 Influence of Hydrogen Injector Angle Variation

In this section, the effects of varying the injection angle are investigated, looking at the advantages and disadvantages associated with the upwind and downwind injection. The results are presented following the same order of Chapter 4 and expressed in terms of temperature distribution, mixing characteristics, NO_x production and FTFs. In Figure 5.1, the four cases analysed are gathered. In this study, negative angles are associated to downwind injection and positive values to upwind injection. The choice of these values is limited by the single injector geometry: for the upwind injection, angles higher than 15º are not realizable due to the presence of the injector plate. Since the hydrogen pipe and injector are rotated as a unique body around a rotational axis placed in correspondence of the injector hole, the proximity of the hydrogen feed system to the injector plate has to be accounted as a drawback and a heat transfer analysis is necessary to quantify the amount of heat released by the injector plate.

Figure 5.1: Illustration of the 4 cases analysed to assess the influence of injection angle variation

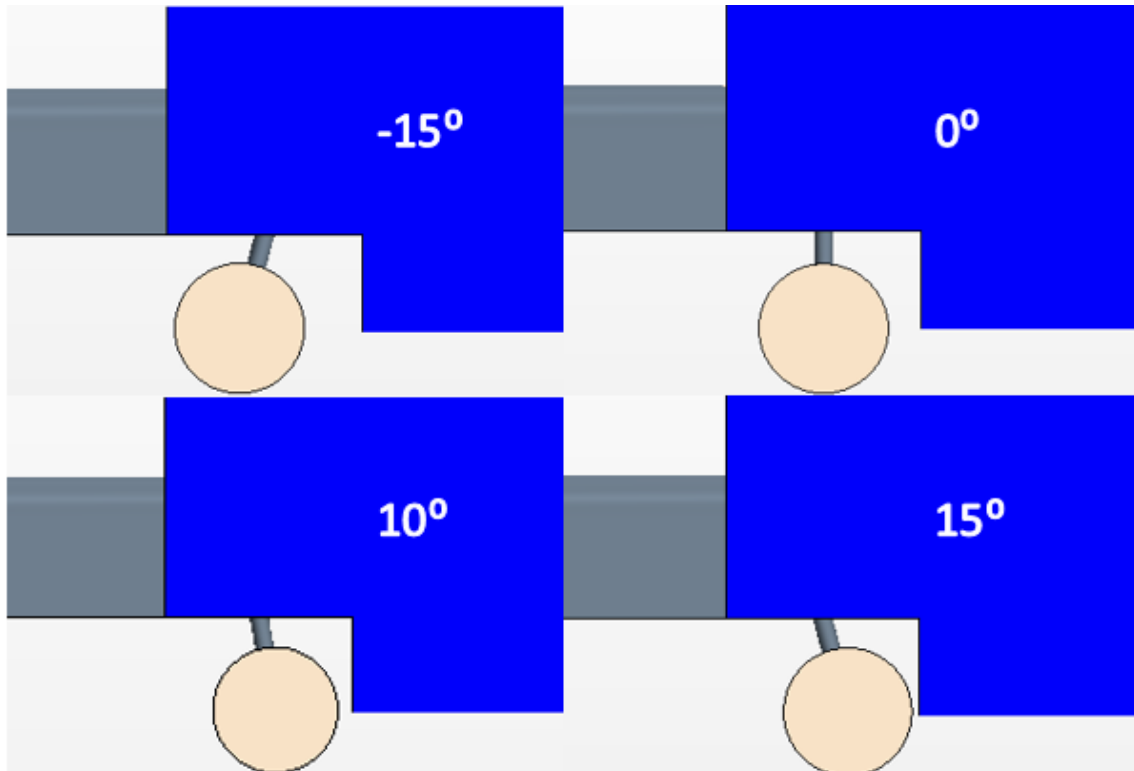## 5.1 Aerodynamic Features and Temperature Field

In Figure 5.2, the temperature distributions are depicted. In this study, the air gate shape is the same for all the configurations and, thus, the air distribution does not influence the JICF behaviour. Therefore, the temperature distribution is similar to that already described for the baseline configuration and the temperature peak is close to the injector plate.
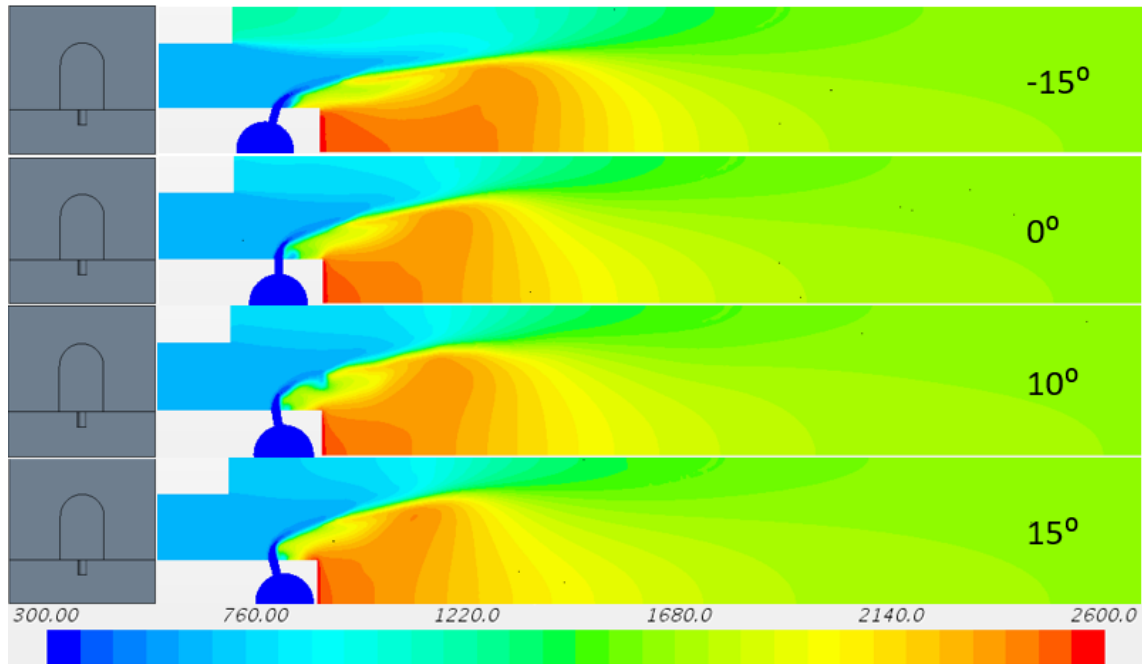
Figure 5.2: Contours of temperature for the configurations characterized by different injection angles at the symmetry plane

The influence of the injection angle variation regards more the flame position and length. In the case of the downwind injection, despite the hydrogen is injected with the same intensity, the jet penetrates less and is deflected earlier than the upwind injection because the fuel stream is partially directed in the air stream direction. Whereas, when the fuel is injected upwind, the jet penetrates partially in the opposite flow direction and it needs more space to deflect. Therefore, the jet follows a different trajectory to diffuse within the flow field. In addition, the upwind injection, due to its trajectory, creates a stagnation region immediately downstream the injector hole, which allows the mixture from the outer vortex to enter. Therefore, the outer vortex itself is enlarged and the flame is moved up.

The aerodynamic structures of the flow field for the downwind and upwind injection are compared in Figure 5.3, in which it is shown how the size and position of the recirculation vortices affect the flame position and length.
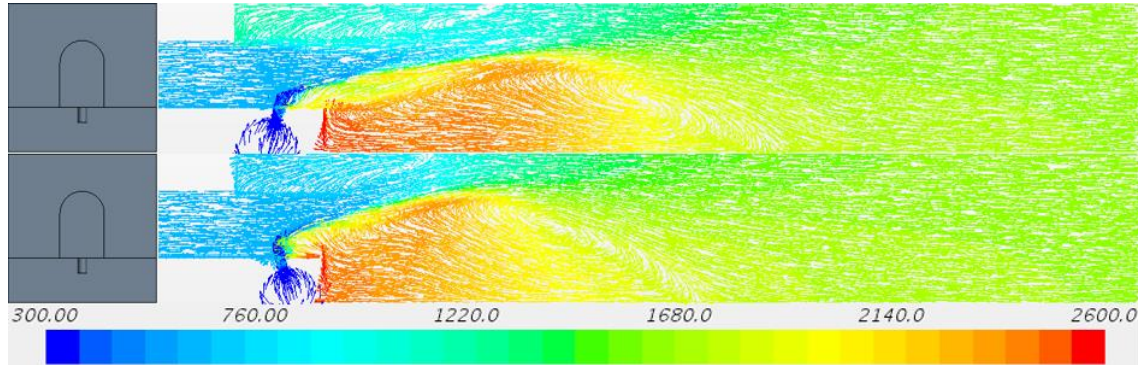
Figure 5.3: Aerodynamic structure of the flow field for (a) downwind and (b) upwind injection

5.2 Mixing Capability

The mixing characteristics are analysed using the parameters described in the previous chapter: the normalised standard deviation of fuel concentration and the distribution of mole fraction of hydrogen along a vertical line.

The normalised standard deviation is calculated for 6 planar sections and its distribution is illustrated in Figure 5.4. As expected, the best mixing is provided by the upwind injection, whereas the downwind injection is characterised by worse mixing ability. It is explained by the aerodynamic features of the flow field: in the upwind injection, the jet is directed in the opposite flow direction, thus the entrainment with the air is enhanced and the mixing process begins immediately upstream the injector hole. The distribution revealed a significant improvement in the mixing between the baseline and the upwind injection configurations, whereas the difference between 10 and 15 degrees configurations is modest. Therefore, even a small injector angle variation provides better characteristics in terms of mixing.
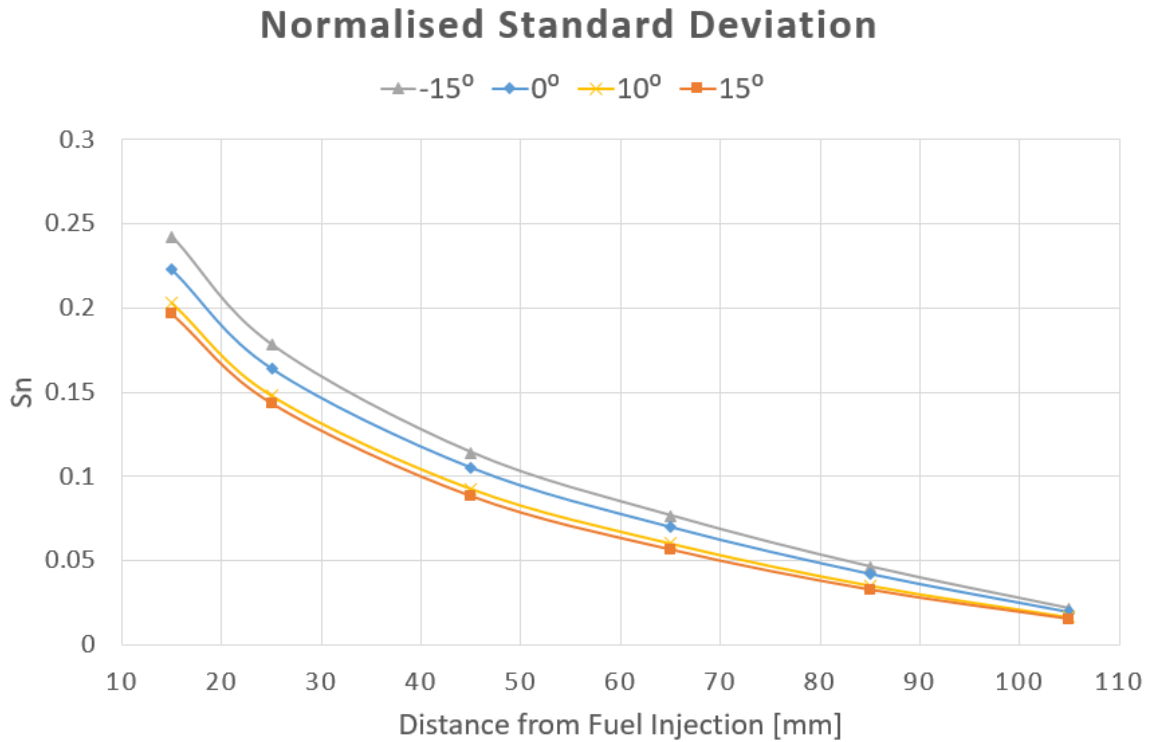
Figure 5.4: Distribution of the normalised standard deviation

The distribution of fuel along the vertical line placed at 2.5 mm downstream the injector hole, illustrated in Figure 5.5, confirms the results obtained using the standard deviation: the maximum mole fraction for the upwind injection is lower, which identifies a greater degree of dispersion. Also the distribution is consistent with the behaviour described: the downwind injection concentrates most of the fuel downstream the injector hole, whereas the downwind injection diffuses part of the fuel in the upper region due to the jet trajectory and the larger outer vortex. Unlike the air gate shape variation, in which the mixing process does not affect a lot the combustion performance, in this case it plays an important role in order to reduce the NO_x emissions.
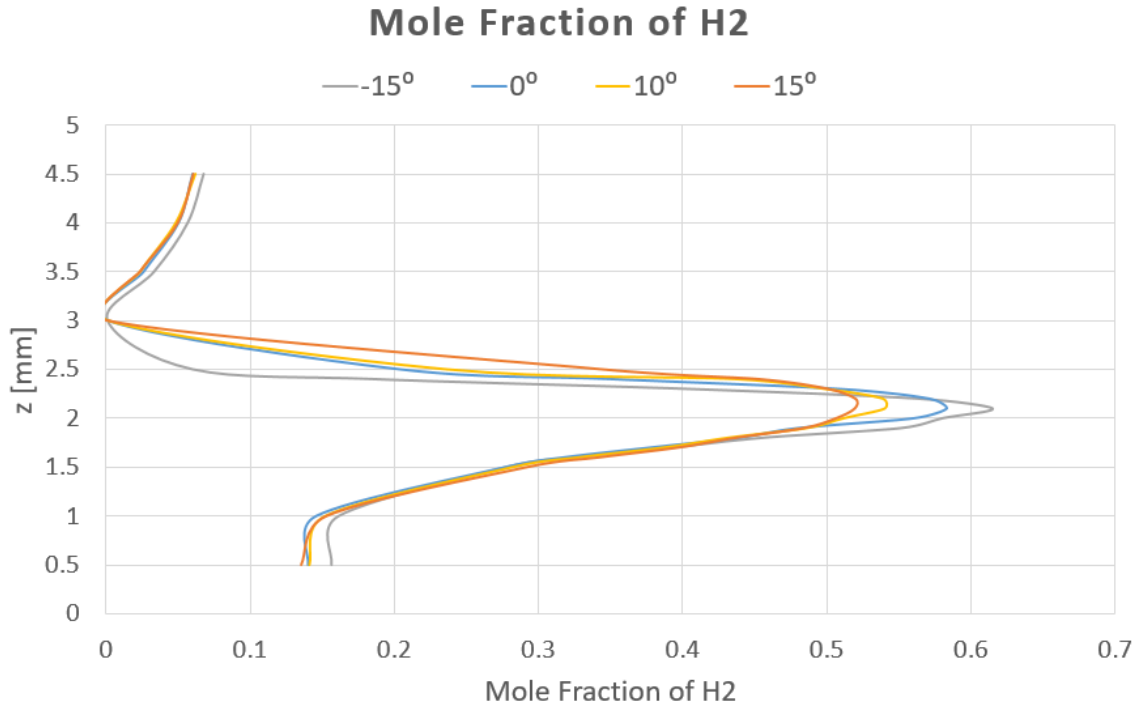
Mole Fraction of H2

Figure 5.5: Mole fraction of H$_2$ along the vertical line for the 4 cases with different injection angle

5.3 NO$_x$ Emissions

The contours of NO$_x$ emissions are provided in Figure 5.6. The distributions of NO$_x$ production are similar and consistent with the temperature distribution: the peak is found within the outer vortex, close to the injector plate, where the highest temperatures are revealed. Nevertheless, a gradually reduction in NO$_x$ emissions is associated to the transition from the downwind injection to the upwind injection. The normalised values have been calculated and collected in the chart in Figure 5.7.
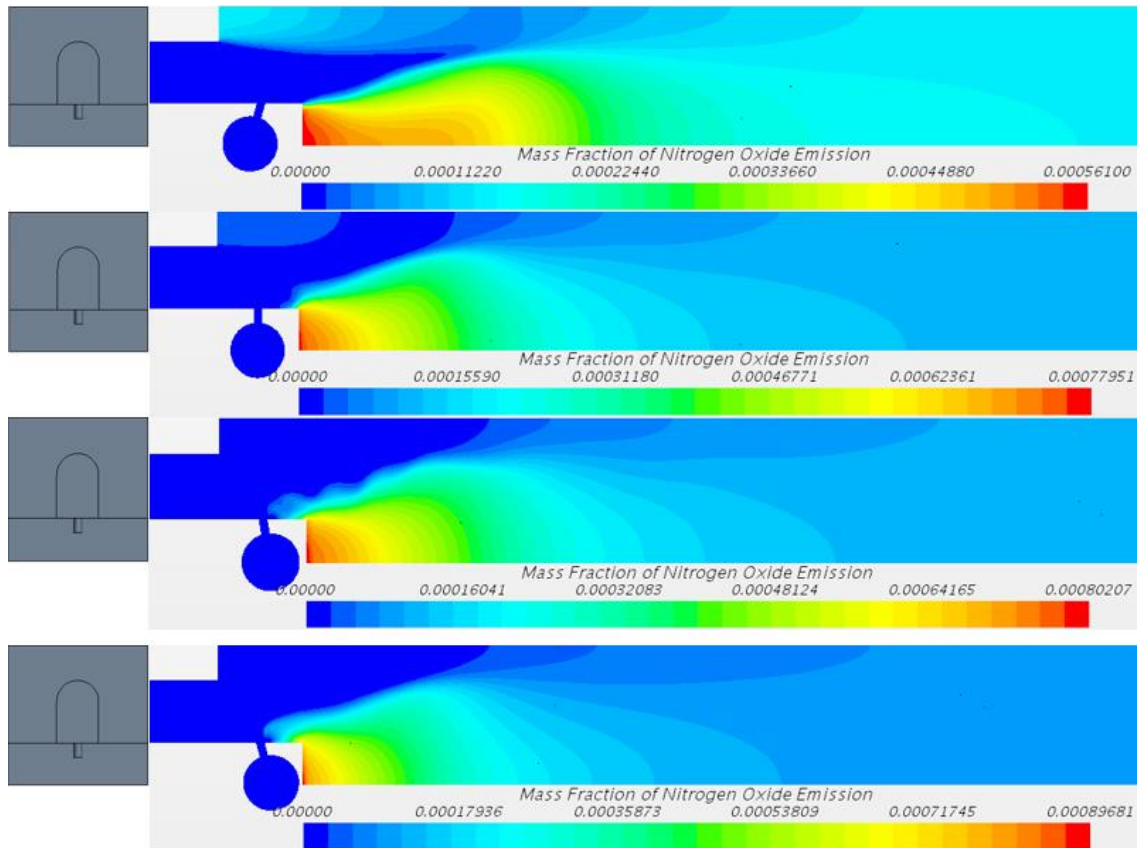
Figure 5.6: Contours of NO$_x$ emissions for the 4 cases characterised by different injection angles
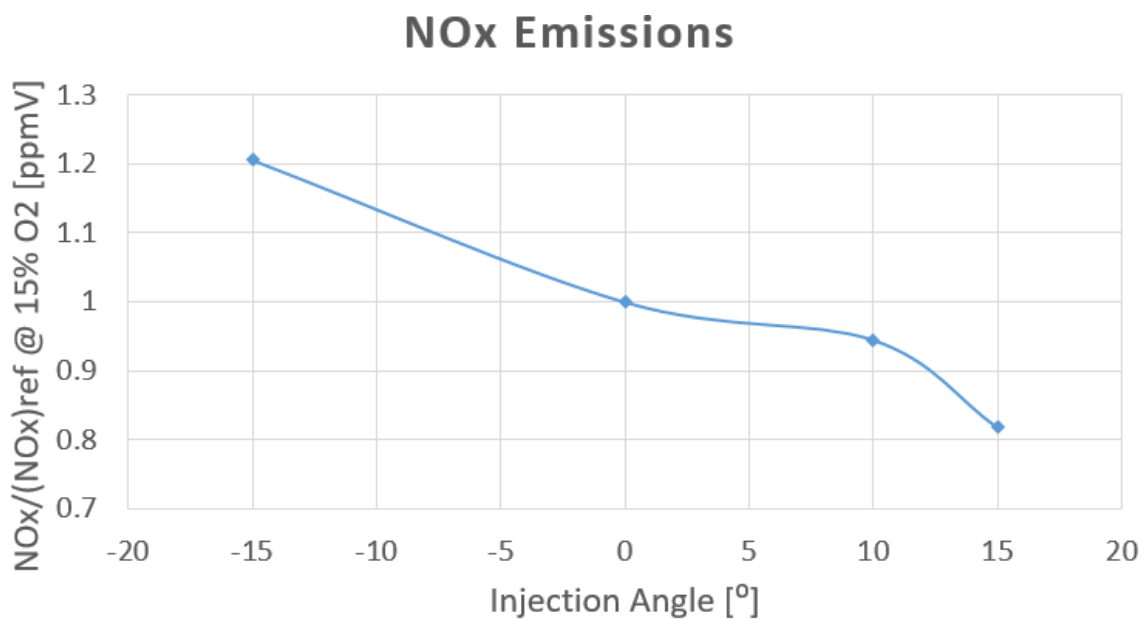
Figure 5.7: Normalised NO$_x$ emissions as a function of the injection angle

98

5.4 Time Delay and FTF Estimation

The aim of this section is to analyse the flame response to injection angle variations in terms of time delay. The achievement of these values will be necessary to estimate and deliver a series of FTFs. The comparison between them will allow to identify potential variations in the acoustic properties of the flame. The approaches employed are already explained in the previous chapter: the 80% rule and the particle injection method. In this way, it will be possible to carry out a trend comparison between the different approaches used and identify potential inaccuracies associated with an approach.

| Time Delay [mgs]	-15º	0º	10º	15º
80% Rule (Temperature)	0.384	0.276	0.265	0.246
80% Rule (OH)	0.327	0.224	0.208	0.196
Maximum Gradient	0.178	0.232	0.187	0.205

Table 5.1: Collection of time delays for the 4 cases using the 80% rule and the maximum gradient approaches

The 80% rule has been applied to both temperature and mass fraction of OH distributions, whereas the maximum gradient method only to the temperature distributions. The values obtained from these approaches are collected in Table 5.1 and plotted in Figure 5.8 as a function of the injection angle. Despite the absolute values achieved using the 80% rule differ, the trends develop in the same way. In particular, a significantly decreasing trend has been found moving from the downwind injection to the normal condition, whereas a rotation of the injector angle in the upwind direction provides a slight decrease in time delay. This behaviour can be explained observing the flames length in Figure 5.2: the downwind injection delivers a longer flame, which reflects in a temperature distribution shifted downstream compared to the distribution found in the other cases. Instead, the upwind injection provides a flame similar to that found in the

99

baseline configuration, but slightly shorter and tilted upwards. However, the temperature distribution revealed higher values compared to the mass fraction of OH distribution. As already noticed, the maximum gradient method shows different absolute values and, especially, different trends. This is due to its high sensibility to the temperature distribution and an ideal constant slope is required to achieve relevant results.
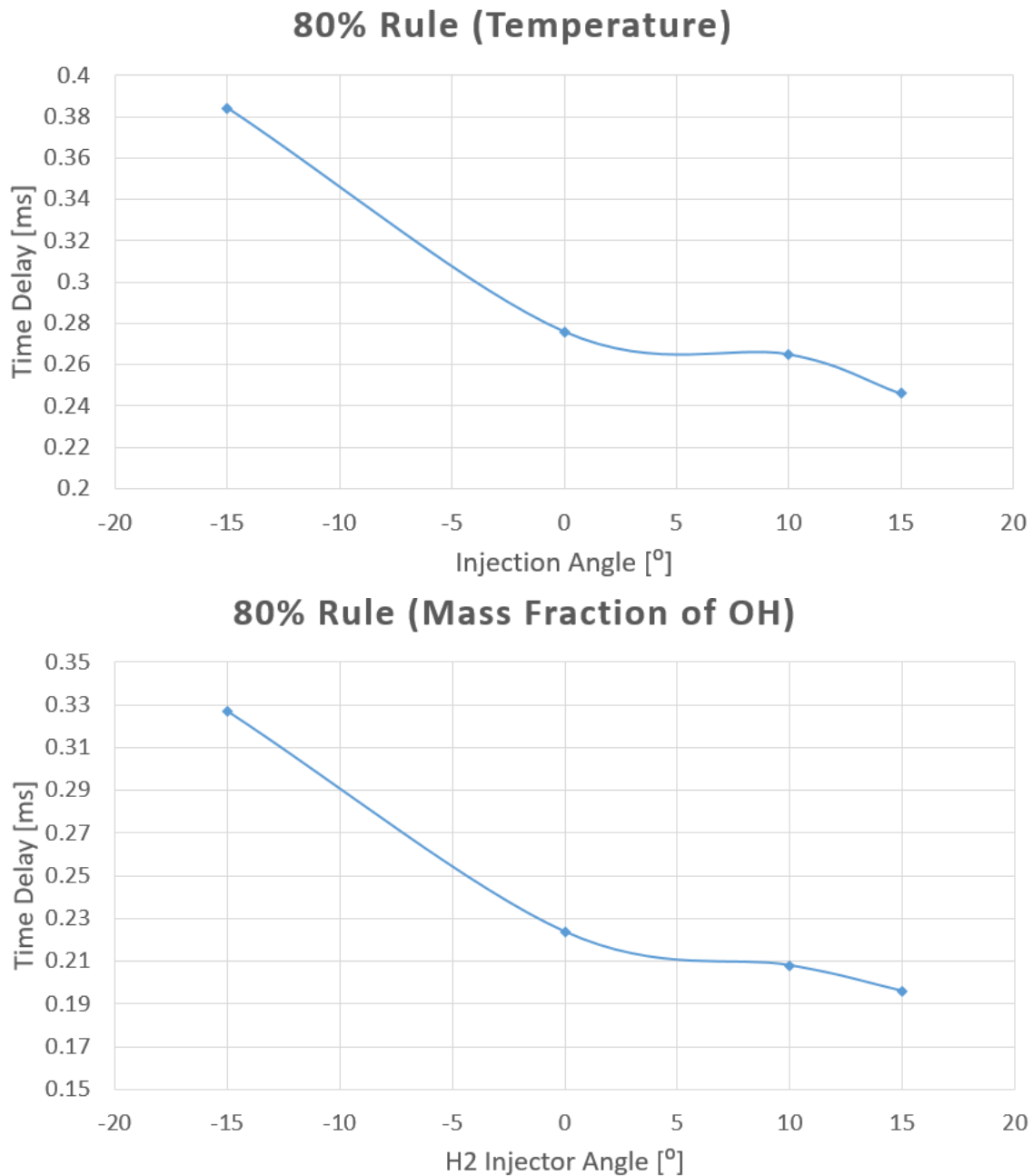

Figure 5.8: Time delay trends as function of the injection angle using the 80% rule from the temperature (a) and mass fraction of OH (b) distribution
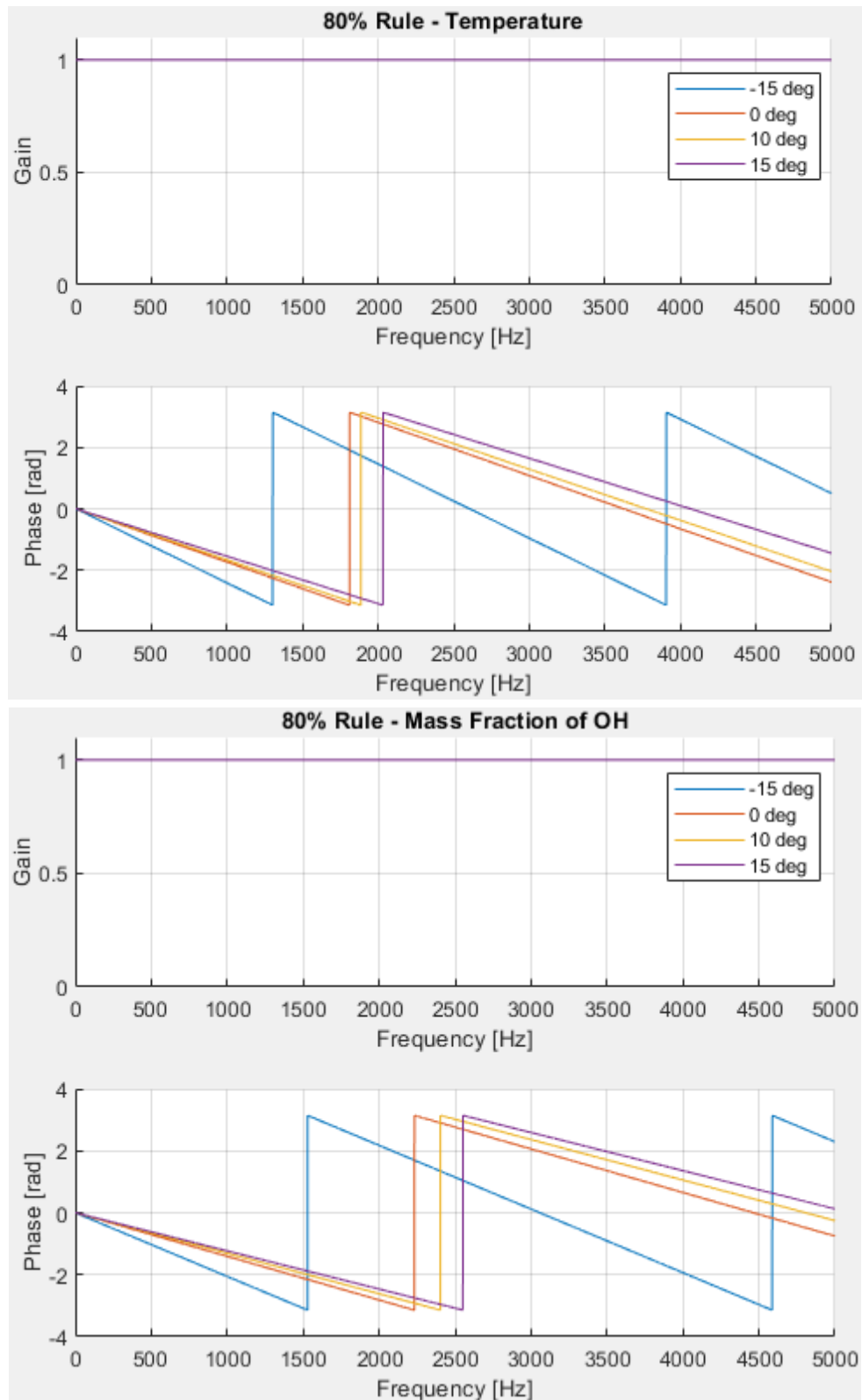
Figure 5.9: Series of FTF estimated using 80% rule from temperature and mass fraction of OH distributions

The values of time delays collected in Table 5.1 have been implemented using the standard n-τ model to obtain a series of FTFs depicted in Figure 5.9. The gain of this function is constant and equals to 1 because the proportionality constant n was assumed equal to 1 in order to satisfy the condition of a unitary gain as the frequency tends to 0. The differences are shown in the phase chart: the main variation is revealed by the downwind injection, which is characterized by a faster transition and the peak is moved towards lower frequencies (around 1500 Hz). This configuration could be more prone to thermoacoustic instabilities, but an evaluation regarding this potential risk is impossible without coupling the flame response to the acoustic field of the whole combustion system.

The particle injection method has been applied in the same way described in Chapter 4. The trend developed using this approach is illustrated in Figure 5.10.

Particle Injection Method
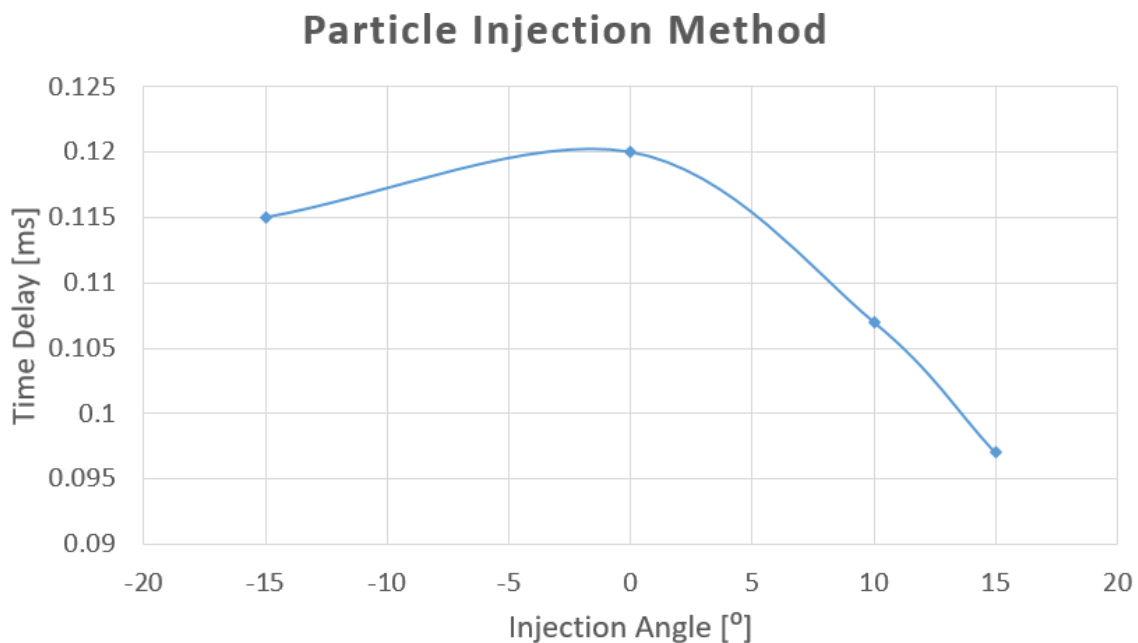
Figure 5.10: Time delay trend as a function of the injection angle obtained using the particle injection method

The trend shown is different compared to that found using the 80% rule, especially for the behaviour of the downwind injection. Due to the worse mixing provided by this configuration, a higher amount of fuel has been found in the outer

vortex. It was partially detected by the distribution of fuel along the vertical line placed at 2.5 mm downstream the injector hole shown in Figure 5.5. Nevertheless, this behaviour is emphasised in proximity of surfaces parallel to the symmetry plane. This increased amount of fuel within the outer vortex significantly influences the shape of the iso-surface, which is deformed including a bigger volume, represented in Figure 5.11. However, the illustration confirms that the iso-surface profile corresponds to the maximum amount of OH and, thus, to the maximum heat release rate.
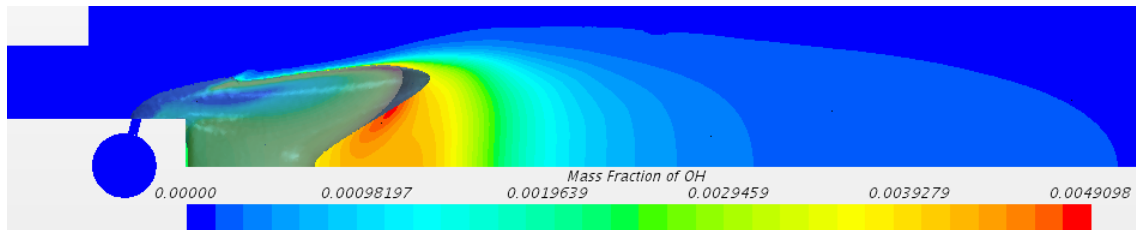
Figure 5.11: Iso-surface representative of the flame front superimposed on the contour of mass fraction of OH for the downwind injection

The shape of the iso-surface will inevitably influence the distribution of particles residence time and the value of time delay. However, a series of FTFs has been achieved employing the values of time delay and time delay spread in the modified n-τ model. As displayed in Figure 5.12, due to the shorter time delays, the FTFs are subject to modest variations. The gain is weakly damped and this effect is visible only for very high frequencies. The same behaviour has been revealed by the phase chart, in which the trend for different injection modes is very similar and some appreciable discrepancies are displayed only in the region of high frequencies.
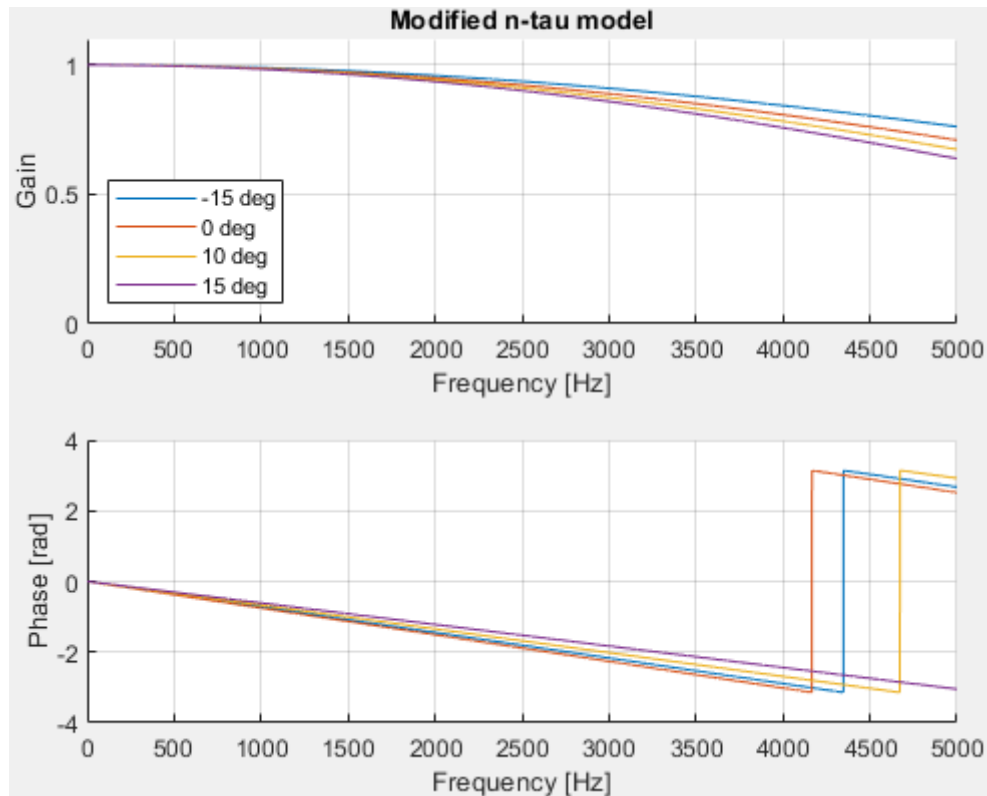
Figure 5.12: Series of FTFs achieved using the modified n-τ model

5.5 Combined Effect

In the previous sections, the influences of the air gate shape and the injection angle variations have been investigated separately. The aim of this section is to assess whether the benefits associated with each parameter are amplified or not when combining their effects. To do this, the most promising air gate geometry in terms of NO_x emissions has been choose. Both the last two configurations have shown interesting results, but the geometry 6 was selected due to its ease of manufacturing compared to the other one (considering conventional methods) and, thus, the possibility to introduce it in real applications. This configuration has been combined with both downwind and upwind injection.

First of all, the effect of the downstream injection was investigated. The temperature and the mass fraction of NO_x distributions are respectively illustrated in Figure 5.13 and Figure 5.14. The aerodynamic structures of the flow field are

characterized by similar recirculating vortices in terms of size and position. Therefore, a similarity has been revealed also in the temperature distribution. Nevertheless, the downwind injection is associated with a worse mixing compared to the normal injection. It causes a slightly longer flame, but finer. It is an effect of the downwind injection, in which the fuel jet is partially injected in the air stream direction.
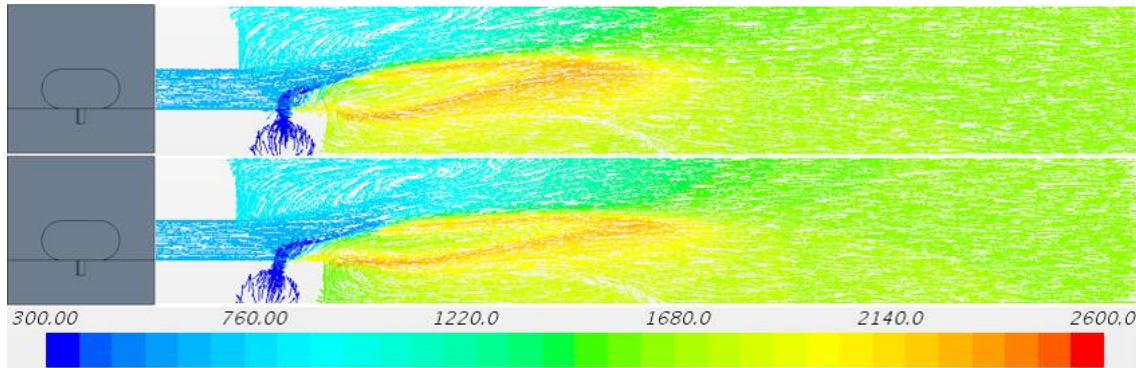
Figure 5.13: Temperature contours for the configuration 6 combined with (a) normal injection and (b) downwind injection

However, the longer flame does not affect the NO_x production because the peak has been found in the same position downstream the flame, just shifted of few mm due to the different flame length. The NO_x values are calculated using the same approach at the outlet plane and normalised relative to the baseline configuration.
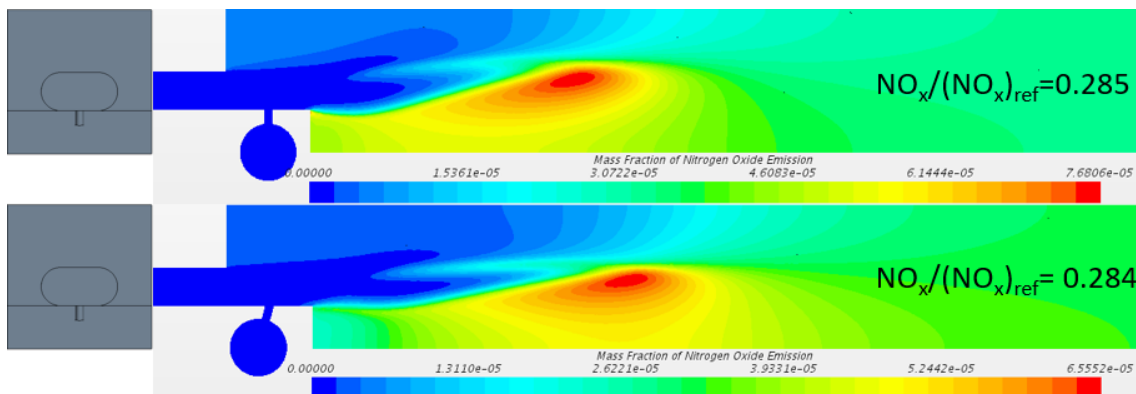
Figure 5.14: Contours of mass fraction of NO_x for the configuration 6 combined with (a) normal injection and (b) downwind injection

Therefore, this simulation has led to conclude that the downwind injection does not affect positively the NO_x emissions. Whereas, we would expect to significantly reduce the NO_x production by combining the beneficial effects of the last air gate geometry developed and the upwind injection. Nevertheless, the results achieved are reported in Figure 5.15 and Figure 5.16 and do not meet the expectations. The aerodynamic flow field illustrated in Figure 5.15 shows the typical behaviour associated with the upwind injection: the flame is shorter and tilted upwards compared to that found using normal injection. This is mainly due to the jet trajectory and the bigger outer vortex. Due to this structure, higher temperatures have been detected in the outer recirculation vortex.
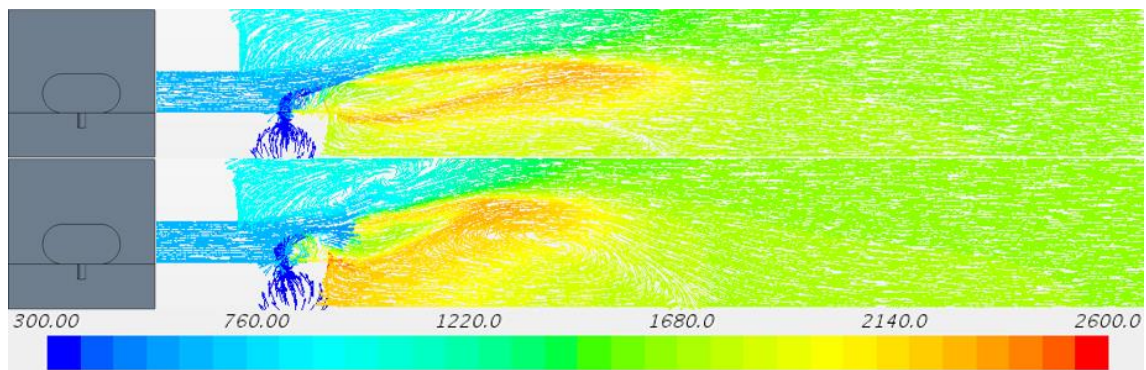
Figure 5.15: Temperature contour and aerodynamic structure of the flow field combining the upwind injection and the geometry 6

The distribution of NO_x is illustrated in Figure 5.16 and reveals that most of the NO_x is produced within the outer vortex, especially in proximity of the corner, where the peak has been identified.
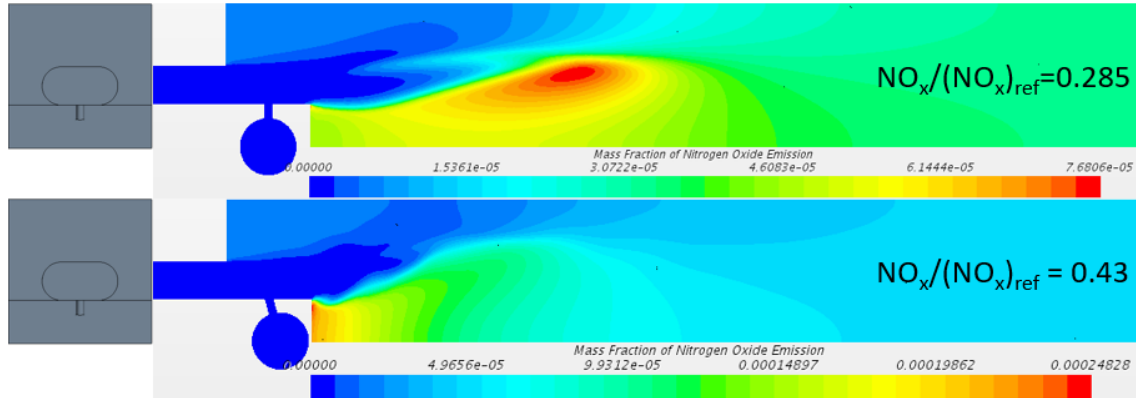
Figure 5.16: Contours of mass fraction of NO$_x$ for the configuration 6 combined with (a) normal injection and (b) upwind injection

This analysis leads to conclude that it is not necessary true that the beneficial effects of two geometric parameters are summarized when combined.

Nevertheless, it is necessary to mention that the resulting flow quantities have revealed some fluctuations and the solution is not completely stable. It is confirmed by the residuals, which are one or two orders higher than those found for the other simulations. Therefore, a more accurate analysis is required.

6 Conclusions

The present research work represents a preliminary numerical investigation, whose purpose is to analyse the impact of geometric variations on hydrogen micromix combustion performance in terms of NO_x emissions, mixing properties and time delays. Several research works have been conducted in Cranfield University in order to develop a micromix combustor for aero engines applications. Nevertheless, the majority of this work has been done using commercial CFD codes, such as Ansys Fluent and Simcenter STAR-CCM+. A large number of simulations have been run, taking advantage of different level of computational complexity, applying different operating conditions and investigating the behaviour of the single injector geometry and the injector array. Nevertheless, due to the computational nature of this work, the results obtained need to be validated by experimental work.

In particular, the aim of the present work does not rely on quantitative results, but is based on a qualitative understanding of the phenomena occurring when geometric parameters are varied, in order to develop key trends of performance relative to the baseline configuration. Following, a brief summary of the assumptions and limitations is provided.

- Due to the high computational power required by more complex turbulence models, a RANS approach has been employed for all the simulations. Due to its time-averaged nature, unsteady behaviours of the flame are not captured. It represents a limitation for two main reasons: firstly, the occurrence of local hotspots is not detected. They are one of the main sources of NO_x production and, therefore, an accurate prediction cannot be carried out. Secondly, the heat release fluctuations cannot be revealed and alternative approaches are necessary to estimate the flame response to velocity inlet perturbations.
- Due to the high computational cost associated with complex chemistry mechanisms, a reduced hydrogen combustion mechanism has been employed. Despite the accuracy of the chemistry mechanism, it is still a simplification, particularly considering the complexity of hydrogen

combustion, characterized by fast chemistry and high reactivity and diffusivity.

- The main assumption of the Flamelet model is the fast chemistry, therefore the combustion process takes place within a thin layer. Additionally, the FGM model is unable to accurately predict non-equilibrium effects. It represents a further limitation to achieve reliable values of NO_x emissions.

- In order to estimate FTF from RANS simulations, two analytical formulations have been employed: the standard and the modified n-τ models. Although they provide the possibility to estimate FTF extracting data from RANS simulations, they represent an approximation, especially the standard model, which assumes a constant gain also for very high frequencies. Additionally, these approaches have been widely used for conventional combustors, but have not yet been validated for micromix combustion system.

- Two different approaches have been used to calculate time delay from RANS simulations: the time for heat release to occur and the particle injection methods. The first is based on the assumption that the main impact of the heat release is an increase of the flame speed, which affects the system acoustic. However, due to the presence of the recirculating vortices, the increase of velocity can be subject to inaccuracies.

- The particle injection method employs the Lagrangian multiphase model to inject particles and calculate their residence time necessary to reach the flame front. It assumes that the mean residence time corresponds to the time delay and the standard deviation of the distribution to the spread. The transition from the Gaussian distribution to a squared distribution represents a simplification.

- Another challenge associated with this method is the creation of an iso-surface able to model the flame front. Due to the high-pressure conditions and the FGM combustion model, the flame front thickness is significantly reduced and the combustion begins immediately downstream the injector hole. Therefore, the progress variable has been revealed unsuitable to properly model the flame front. Alternatively, the concentration of fuel

corresponding to the maximum concentration of OH has been applied. However, due to the different flow dynamics shown by the investigated configurations, this quantity is not always able to model the flame front, which is enlarged including regions within the outer vortex.

Influence of Air Gate Shape Variation

Firstly, the impact of air gate shape variation on combustion performance has been investigated. Due to the high-pressure condition, very high values of temperature have been found, therefore it is essential to modify the flow dynamics in such a way to achieve a desirable temperature distribution within the domain in order to minimise NO_x emissions. The baseline configuration has revealed the peak of temperature within the outer recirculation vortex. This condition is extremely undesirable, due to the long residence time spent at such high temperatures. After analysing several air gate geometries, it was concluded that enlarging the width and, at the same time, shortening the height of the air gate lead to significant benefits in terms of temperature distribution and NO_x production. It is mainly due to a better distribution of the incoming air. The FAR considered, which leads to an equivalence ratio equal to 0.4, is characterized by a weak jet penetration, therefore the height can be reduced enough without approaching the risk of fuel penetration within the inner recirculation vortex. Whereas, enlarging the air gate and distributing more air at the bottom of the air gate is beneficial because the fuel jet is constantly surrounded by relatively cool air, which is then introduced within the outer vortex and allows to cool the temperature there. The analysis of the fuel mixing revealed that such a variation of the air gate shape has a limited impact on the mixing ability of the investigated geometries. Therefore, the key to deliver a good temperature profile is the distribution of the incoming air flow. However, it is necessary to consider the impact of this variation on the flow structure and the flame shape, which can influence the acoustic properties of the flame. The trend of time delay is well-described by the 80% rule: the more the aspect ratio (height/width) is reduced, the longer the flame and the greater the time delay. Nevertheless, this approach tends to overestimate the particles residence time. Instead, the values predicted

by the particle injection method are considerably lower and suggest that the acoustic properties of the flames differ only for very high frequencies.

An equivalence ratio study has been conducted in order to assess the behaviour of the most promising geometry in terms of NO_x emissions for a range of equivalence ratios. Despite the change in the momentum flux ratio associated with different equivalence ratios, which causes a different jet penetration, the low NO_x ability is not affected. However, the aerodynamic structure of the flow field and the flame position are considerably modified. Although it does not represent a problem for the single injector geometry, it is necessary to monitor its behaviour in an injector array to account for flames interaction. Especially for lower equivalence ratios, the size of the outer recirculation vortex is reduced, the flame is moved downwards and the risk of flame merging needs to be assessed.

Influence of Hydrogen Injector Angle Variation

The second geometry parameter to be investigated was the hydrogen injector angle. The main impact of the upwind injection is the enhanced fuel mixing, because the fuel jet is partially injected in the opposite direction of the air stream and, therefore, the mixing length is increased and the fuel mixing is enhanced. It is reflected in a shorter flame and lower NO_x emissions. Nevertheless, the different jet trajectory has an impact on the aerodynamic structure of the flow field and the flame position: the outer recirculation vortex is enlarged and it can favour the introduction of hot stream within it. This behaviour has been detected when combining the beneficial effects of upwind injection and the air gate shape characterized by lower aspect ratio, in which the temperature peak has been found within the outer vortex. Instead, the downwind injection, due to a worse mixing, delivers a significantly longer flame compared to the other injection cases.

In terms of thermoacoustic instabilities, the main variation is associated with the downwind injection because of its longer flame, whereas the other cases have a similar flame. This change affects the acoustic properties of the flame, providing higher time delays.

7 Suggestions for Further Work

Improvement of Parametric Analysis

In this research work, simplified RANS simulations of a single injector geometry have been performed to provide a general understanding of the main flow phenomena occurring when varying design parameters. The results achieved from this numerical investigation will be useful to support the down-selection of promising designs in terms of mixing and emission characteristics for the experimental evaluation. Nevertheless, due to the limitations of the simplified model explained in Chapter 6, the key trends delivered can be affected by several inaccuracies and the absolute values, particularly for NO_x emissions, cannot be considered reliable. Therefore, it is suggested to carry out a more accurate LES analysis, more appropriate than RANS to capture the occurrence of local hotspots and predict NO_x. Additionally, numerous correlations are available in the literature to estimate parameters from other quantities. Although this approach is an approximation, it represents an alternative approach and it could be beneficial to compare results achieved from different methods to have a clear idea of the flow phenomena. However, it is important to consider that most of them are developed for specific combustion systems and cannot be applied for hydrogen micromix flames.

Due to the interesting results shown, some promising single injector designs have been selected. Nevertheless, the simulations have been carried out for a specific pressure (15 bar) and a restricted range of equivalence ratios. The analysis needs to be extended to a wider range of boundary conditions, in order to explore the design capabilities to operate at different conditions and, eventually, its limitations. In Figure 3.5, a set of operating conditions of interest is represented and it can be considered as a guidance for the investigation.

In the present work, two design parameters have been analysed: the air gate shape and the injection angle. Due to the importance of the JICF to enhance the fuel mixing, a further exploration of the impact of other geometric variations on performance parameters is suggested. The main design parameters of a single

injector design are gathered in Figure 1.3, however the number of parameters can be further extended.

A single injector analysis has been performed in this work. However, an injector array analysis is required to investigate the impact of flame interaction on NO_x emissions. This analysis is particularly required for low equivalence ratios, due to the weak jet penetration, which causes the flame to move downwards and the outer recirculating vortex to shrink.

Improvement of Thermoacoustic Analysis

Two analytical formulations have been used in this work, however a large number of other formulations characterized by increasing complexity are available in the literature. It would be interesting to estimate FTFs using other formulations and compare them with standard and modified n-τ models.

The analytical formulations used have been widely validated for conventional combustion systems, but they have not yet been employed to hydrogen micromix flames. Therefore, an experimental validation of this approach is required to assess their applicability.

Due to the high-pressure conditions and the considerable variety of flame behaviour shown by different configurations, a significant difficulty was found in identifying a unique value of fuel concentration able to reproduce the flame front. In order to accurately apply the particle injection method, it is suggested to find an alternative way to represent the flame front.

However, due to the unsteady nature of these phenomena, a RANS analysis can be used to preliminary estimate FTF. The use of time-varying simulations, such as URANS or LES, is suggested to investigate the impact of geometric variations on the acoustic flame properties. In this way, it will be possible to achieve a series of non-linear FDFs by imposing sinusoidal inlet velocity for a range of forcing frequencies.

Once achieved an accurate estimation of FTF, based on experimental and analytical results, it will be worth assessing the thermoacoustic instabilities by

coupling the flame response to the acoustic field of the combustion system using OSCILOS or other similar codes.

Experimental Validation

The CFD approach represents a powerful tool to explore the behaviour of the flow dynamics and improve the quality of the design. However, experimental results are necessary to validate the results provided by simulations and understand if they are representative and reliable. Therefore, the experimental work is recommended for the following reasons:

- Perform single injector experiments to validate the results achieved from RANS simulations and verify the occurrence of the flow dynamics detected by this investigation study. It will enable to determine the validity of the developed key trends of NO_x and fuel mixing.
- Perform measurements of flame acoustic properties and validate the results obtained from RANS simulations
- Compare different approaches used to estimate time delay from RANS simulations and establish the most appropriate one to model the micromix flame response

REFERENCES

[1] Nalianda, D., Sun, X., Wang, L., Li, Y.-G., Liu, Y. and Sethi, V. (2017) 'Review of modern low emissions combustion technologies for aero gas turbine engines', *Progress in Aerospace Sciences*. Elsevier Ltd, 94(August), pp. 12–45. doi: 10.1016/j.paerosci.2017.08.001.

[2] Jonathan McClure (2018) *Preliminary Thermoacoustic Risk Assessment for Hydrogen Micromix Combustion Systems using CFD*, *MSc Thesis*.

[3] Haj Ayed, A., Kusterer, K., Funke, H. H. W., Keinz, J., Striegan, C. and Bohn, D. (2015) 'Experimental and numerical investigations of the dry-low-NO x hydrogen micromix combustion chamber of an industrial gas turbine', *Propulsion and Power Research*. Elsevier, 4(3), pp. 123–131. doi: 10.1016/j.jppr.2015.07.005.

[4] Heinz G. KLUG, R. F. and Civil (no date d) 'CRYOPLANE: Hydrogen Fuelled Aircraft Status and Challenges'. doi: 10.1080/23311843.2016.1139434.

[5] Haj Ayed, A., Kusterer, K., Funke, H. H. W., Keinz, J., Striegan, C. and Bohn, D. (2015) 'Improvement study for the dry-low-NO x hydrogen micromix combustion technology', *Propulsion and Power Research*. Elsevier, 4(3), pp. 132–140. doi: 10.1016/j.jppr.2015.07.003.

[6] Ayed, A. H. (2017) 'Numerical Characterization and Development of the Dry Low NOx High Hydrogen Content Fuel Micromix Combustion for Gas Turbine Applications', *PhD Thesis*.

[7] A. Haj Ayed, K. Kusterer, H. H.-W. Funke, J. Keinz, M. Kazari, J. Kitajima, A. Horikawa, K. Okada, D. B. (2014) 'Numerical Study on Increased Energy Density for the DLN Micromix Hydrogen Combustion Principle', pp. 1–12.

[8] Ayed, A. H., Kusterer, K., Funke, H. H. W., Keinz, J. and Bohn, D. (2017) 'CFD based exploration of the dry-low-NO x hydrogen micromix combustion technology at increased energy densities', *Propulsion and Power Research*. Elsevier B.V., 6(1), pp. 15–24. doi: 10.1016/j.jppr.2017.01.005.

[9] Wegner, B., Huai, Y. and Sadiki, A. (2004) 'Comparative study of turbulent mixing in jet in cross-flow configurations using LES', *International Journal of Heat and Fluid Flow*, 25(5), pp. 767–775. doi: 10.1016/j.ijheatfluidflow.2004.05.015.

[10] New, T. H., Lim, T. T. and Luo, S. C. (2006) 'Effects of jet velocity profiles on a round jet in cross-flow', *Experiments in Fluids*, 40(6), pp. 859–875. doi: 10.1007/s00348-006-0124-y.

[11] Plesniak, M. W. and Cusano, D. M. (2005) 'Scalar mixing in a confined rectangular jet in crossflow', *Journal of Fluid Mechanics*, 524, pp. 1–45. doi: 10.1017/S0022112004001132.

[12] Noble, D. R., Dubsky, S., Periagaram, K., Sullivan, R., Jones, M., Seitzman, J. and Lieuwen, T. (2011) 'Imaging of a Reacting Fuel Jet in 6 Atm Vitiated Cross-Flow', *7th US National Combustion Meeting of the Combustion Institute*, (2).

[13] Murthy, P. (2011) 'Numerical Study of Hydrogen Micromix Combustors for Aero Gas Turbine Engines', *MSc Thesis*.

[14] Karakurt, A. (2012) 'Parametric Investigation of Combustion Characteristics of a Hydrogen Micromix Combustor Concept', *MSc Thesis*.

[15] Degroote, A. J. G. (2013) 'Assessment of the Feasibility of Controlling the Outlet Temperature Distribution of a Novel Micromix Combustor', *MSc Thesis*.

[16] Asanitthong, S. (2014) 'Outlet Temperature Distribution Control and Heat Transfer Calculation for a Hydrogen Micromix Combustor', *MSc Thesis*.

[17] Matthieu Petit de Bantel (2014) 'Comparison Study of Combustion Models for a Conceptual Hydrogen Micromix Combustor', *MSc Thesis*.

[18] Sabín, R. (2016) 'Comparative Performance Study of CFD Species Models for Hydrogen Micromix Combustion', *MSc Thesis*.

[19] Abdallah, R. Ben (2017) 'Ultra-low NOx Micromix Hydrogen Combustion System: -Preliminary Design and Performance Assessment of Novel Injectors Using RANS and LES CFD', *MSc Thesis*.

[20] Babazzi, G. (2018) 'Turbulence-Chemistry Interaction Study for a Hydrogen

Micromix Combustion System', *MSc Thesis*.

[21] Gollahalli, S. R. and Pardiwalla, D. (2002) 'Comparison of the Flame Characteristics of Turbulent Circular and Elliptic Jets in a Crossflow', *Journal of Energy Resources Technology*, 124(3), p. 197. doi: 10.1115/1.1488170.

[22] B. A. Haven; M. Kurosaka (1997) 'Kidney and anti-kidney vortices in crossflow jets', *Journal of Fluid Mechanics*. Cranfield University, 352, pp. 27–64. doi: 10.1017/S0022112097007271.

[23] Kandakure, M. T., Patkar, V. C., Patwardhan, A. W. and Patwardhan, J. A. (2009) 'Mixing with jets in cross-flow', *Industrial and Engineering Chemistry Research*, 48(14), pp. 6820–6829. doi: 10.1021/ie801863a.

[24] Veynante, D. and Vervisch, L. (2002) 'Turbulent combustion modeling', *Progress in Energy and Combustion Science*, 28(3), pp. 193–266. doi: 10.1016/S0360-1285(01)00017-X.

[25] Peters, N. (1986) 'Laminar Flamelet Concepts in Turbulent Combustion', *21st Symp. (Int.) on Combustion, The Combustion Institute*, pp. 1231–1250.

[26] Lieuwen, T., Torres, H., Johnson, C. and Zinn, B. T. (1999) 'A Mechanism of Combustion Instability in Lean Premixed Gas Turbine Combustors', *Volume 2: Coal, Biomass and Alternative Fuels; Combustion and Fuels; Oil and Gas Applications; Cycle Innovations*, (April 2015), p. V002T02A001. doi: 10.1115/99-GT-003.

[27] Peric, M. and Ferguson, S. (no date aa) 'The advantage of polyhedral meshes'.

[28] Veynante, Denis; Poinsot, T. (no date ab) 'Theoretical and Numerical Combustion'.

[29] Fric, T. F. (2008) 'Skewed shear-layer mixing within a duct', *AIAA Journal*, 34(4), pp. 847–849. doi: 10.2514/3.13150.

[30] Hornsby, C. and Norster, E. R. (1997) 'Application of CFD to DLN Combustion', p. V002T06A053. doi: 10.1115/97-gt-371.

[31] Krebs, W., Flohr, P., Prade, B. and Hoffmann, S. (2002) 'Thermoacoustic stability chart for high-intensity gas turbine combustion systems', *Combustion Science and Technology*, 174(7), pp. 99–128. doi: 10.1080/00102200208984089.

[33] STAR-CCM+ Tutorial Guide

[34] Baulch, D. L., Drysdall, D. D., Horne, D. G., and Lloyd, A. C. (1973) 'Evaluated Kinetic Data for High Temperature Reactions', vols. 1-3. Butterworth.

[35] D.J. Abbott. Lecture Notes – Dynamics in Gas Turbine Combustors, Cranfield University, 2018.

[36] L. Rofi, G. Campa, V. Anisimov, F. Dacc, E. Bertolotto, E. Gottardo, and F. Bonzani. Numerical Procedure for the Investigation of Combustion Dynamics in Industrial Gas Turbines: LES, RANS and Thermoacoustics. In ASME Turbo Expo 2015: Turbine Technical Conference and Exposition, Montreal, Canada, 2018.

[37] V. L. Zimont and V. Battaglia. Joint RANS/LES Approach to Premixed Flame Modelling in the Context of the TFC Combustion Model. Flow, Turbulence and Combustion, 77:305–331, 2006.

[38] A. H. Lefebvre and D. R. Ballal. Gas Turbine Combustion: Alternative Fuels and Emissions. CRC Press, Boca Raton, Florida, 3rd edition, 2010.

[39] E. M. Goodger and S. O. T. Ogaji. Fuels & Combustion in Heat Engines. Cranfield University Press, Cranfield, U.K., 2011.

[40] J. Brand, S. Sampath, F. Shum, R.L. Bayt, J. Cohen. Potential Use of Hydrogen in Air Propulsion. In AIAA/ICAS International Air and Space Symposium and Exposition: The Next 100 Years, Dayton, Ohio, 2003.

[41] C. J. Marek, T. D. Smith, and K. Kundu. Low Emission Hydrogen Combustors for Gas Turbines Using Lean Direct Injection. In 41st AIAA/ASME/SAE/ASEE Joint Propulsion Conference & Exhibit, Tucson, Arizona, 2005.

[42] P. Gauthier. Lecture Notes – Introduction to Combustors for Aero-Derivative Engines and Large Industrial Gas Turbines, Cranfield University, 2018.

[43] Alvaro Fogué Robles, Dynamics of H_2-Micromix Arrays Using CFD, MSc Thesis, Cranfield University, 2019.

[44] Marcos Lòpez Juàrez, CFD Evaluation of Flame Characteristics and Emissions of H_2 Micromix Combustor Injectors, MSc Thesis, Cranfield University, 2019.

[45] D. J. Abbott, Personal Correspondance, 2019.

[46] https://www.enableh2.eu/about/